

Nitrile-Substituted 2-(Oxazolinyl)-Phenols: Minimalistic Excited-State Intramolecular Proton Transfer (ESIPT)-Based Fluorophores

Supporting Information

Dominik Göbel,^a Daniel Duvinage,^b Tim Stauch,^{*c,d,e} Boris J. Nachtsheim^{*a}

^a Institute for Organic and Analytical Chemistry, University of Bremen, Leobener Straße NW2,
D-28359 Bremen, Germany

^b Institute for Inorganic and Crystallographic Chemistry, University of Bremen, Leobener Straße NW2,
D- 28359 Bremen, Germany

^c Institute for Physical and Theoretical Chemistry, University of Bremen, Leobener Straße NW2,
D- 28359 Bremen, Germany

^d Bremen Center for Computational Materials Science, University of Bremen, Am Fallturm 1,
D-28359 Bremen, Germany

^e MAPEX Center for Materials and Processes, University of Bremen, Bibliothekstraße 1,
D-28359 Bremen, Germany

*Corresponding authors: nachtsheim@uni-bremen.de, tstauch@uni-bremen.de

Table of Content

1 General Information	1
2 Experimental Procedures	4
2.1 Preparation of Metalation Agents	4
2.1.1 Preparation of the Reagent <i>i</i>PrMgCl·LiCl	4
2.1.2 Preparation of the Reagent TMPMgCl·LiCl.....	4
2.2 Procedures for Oxazoline Syntheses.....	5
2.2.1 General Procedure for the Oxazoline Synthesis from the Corresponding Aldehyde (GP 1)	5
2.2.2 2-(4,4-Dimethyl-4,5-dihydrooxazol-2-yl)benzonitrile (1-Oxa)	5
2.2.3 3-(4,4-Dimethyl-4,5-dihydrooxazol-2-yl)benzonitrile (2-Oxa)	6
2.2.4 4-(4,4-Dimethyl-4,5-dihydrooxazol-2-yl)benzonitrile (3-Oxa)	7
2.3 Procedures for <i>ortho</i>-Hydroxylations.....	7
2.3.1 General Procedure for the <i>ortho</i>-Hydroxylation of 2-Aryloxazolines (GP 2).....	7
2.3.2 2-(4,4-Dimethyl-4,5-dihydrooxazol-2-yl)-3-hydroxybenzonitrile (1-CN).....	8
2.3.3 3-(4,4-Dimethyl-4,5-dihydrooxazol-2-yl)-4-hydroxybenzonitrile (2-CN) and 3-(4,4-Dimethyl-4,5-dihydrooxazol-2-yl)-2-hydroxybenzonitrile (4-CN).....	9
2.3.4 4-(4,4-Dimethyl-4,5-dihydrooxazol-2-yl)-3-hydroxybenzonitrile (3-CN).....	10
2.4 Detailed Large-Scale Procedures.....	11
2.4.1 Decagram Preparation of 1-Oxa.....	11
2.4.2 Decagram Preparation of 1-CN	11
3 Optical Properties	14
3.1 2-(4,4-Dimethyl-4,5-dihydrooxazol-2-yl)-3-hydroxybenzonitrile (1-CN)	14
3.1.1 Absorption and Emission Properties in Solution and Solid-State	14
3.1.2 Temperature-Dependent Emission.....	25
3.1.3 Emission Properties in Doped PMMA Films.....	27
3.2 3-(4,4-Dimethyl-4,5-dihydrooxazol-2-yl)-4-hydroxybenzonitrile (2-CN)	28
3.2.1 Absorption and Emission Properties in Solution and Solid-State	28
3.2.2 Temperature-Dependent Emission.....	38
3.3 4-(4,4-Dimethyl-4,5-dihydrooxazol-2-yl)-3-hydroxybenzonitrile (3-CN)	40

3.3.1	Absorption and Emission Properties in Solution and Solid-State	40
3.3.2	Temperature-Dependent Emission.....	50
3.4	3-(4,4-Dimethyl-4,5-dihydrooxazol-2-yl)-2-hydroxybenzonitrile (4-CN)	52
3.4.1	Absorption and Emission Properties in Solution and Solid-State	52
3.4.2	Temperature-Dependent Emission.....	62
3.5	Photophysical Data of 1-CN, 2-CN, 3-CN and 4-CN	64
3.6	Photographs of Luminophores.....	65
3.6.1	Images of 1-CN.....	65
3.6.2	Images of 2-CN.....	66
3.6.3	Images of 3-CN.....	67
3.6.4	Images of 4-CN.....	68
4	Crystal Structures	69
4.1	2-(4,4-Dimethyl-4,5-dihydrooxazol-2-yl)-3-hydroxybenzonitrile (1-CN)	69
4.1.1	Crystal Data for 1-CN.....	69
4.1.2	Crystal Packing Views of 1-CN.....	73
4.1.3	Intermolecular Contacts in Crystal Lattice of 1-CN.....	77
4.1.4	Intermolecular π - π -Interactions in Crystal Lattice of 1-CN.....	78
4.2	3-(4,4-Dimethyl-4,5-dihydrooxazol-2-yl)-4-hydroxybenzonitrile (2-CN)	79
4.2.1	Crystal Data for 2-CN.....	79
4.2.2	Crystal Packing Views of 2-CN.....	85
4.2.3	Intermolecular Contacts in Crystal Lattice of 2-CN.....	89
4.2.4	Intermolecular π - π -Interactions in Crystal Lattice of 2-CN	90
4.3	4-(4,4-Dimethyl-4,5-dihydrooxazol-2-yl)-3-hydroxybenzonitrile (3-CN)	91
4.3.1	Crystal Data for 3-CN.....	91
4.3.2	Crystal Packing Views of 3-CN.....	95
4.3.3	Intermolecular Contacts in Crystal Lattice of 3-CN.....	100
4.3.4	Intermolecular π - π -Interactions in Crystal Lattice of 3-CN	101
5	Cartesian Coordinates of Optimized Structures	102
6	NBO Analysis.....	110
7	TGA and DSC.....	111

8	References	113
9	NMR-Spectra.....	114

1 General Information

Unless otherwise noted, all reactions were carried out under a nitrogen atmosphere using standard *Schlenk* techniques. All chemicals were purchased from commercial suppliers and either used as received or purified according to *Purification of Common Laboratory Chemicals*.¹ Anhydrous tetrahydrofuran (THF) was obtained from an *inert* PS-MD-6 solvent purification system. All other solvents were dried using standard methods.¹ Yields refer to isolated yields of compounds estimated to be > 95 % pure as determined by ¹H-NMR spectroscopy.

Thin layer chromatography was performed on fluorescence indicator marked precoated silica gel 60 plates (*Macherey-Nagel*, ALUGRAM Xtra SIL G/UV₂₅₄) and visualized by UV light (254 nm/366 nm). Flash column chromatography was performed on silica gel (0.040 – 0.063 mm) with the solvents given in the procedures. Abbreviations for solvents used: CH = cyclohexane, EE = ethyl acetate. Retention factors were determined at chamber saturation at 25 °C. Developments were carried out between 3.0 – 3.5 cm. If not otherwise stated, crude products were adsorbed on silica gel (up to twice the amount of crude product mass) prior to purification by flash column chromatography.

NMR spectra were recorded on a *Bruker* Avance Neo 600 MHz spectrometer with BBO probe head and a *Bruker* Avance Neo 600 MHz spectrometer with TXI probe head at 23 °C. Chemical shifts for ¹H-NMR spectra are reported as δ (parts per million) relative to the residual proton signal of CDCl₃ at 7.26 ppm (s) and C₆D₆ at 7.16 ppm (s). Chemical shifts for ¹³C-NMR spectra are reported as δ (parts per million) relative to the signal of CDCl₃ at 77.0 ppm (t) and C₆D₆ at 128.1 ppm (t). The following abbreviations are used to describe splitting patterns: br. = broad, s = singlet, d = doublet, dd = doublet of doublets, t = triplet, td = triplet of doublets. Coupling constants J are given in Hertz.

APCI mass spectra were recorded on an *Advion* Expression CMS^L via ASAP probe or direct inlet. High resolution (HR) ESI mass spectra were recorded on a *Bruker* Impact II. All Signals are reported with the quotient from mass to charge m/z.

IR spectra were recorded on a *Nicolet* Thermo iS10 scientific spectrometer with a diamond ATR unit. The absorption bands are reported in cm⁻¹ with indicated relative intensities: s (strong, 0 – 33 % T); m (medium, 34 – 66 % T), w (weak, 67 – 100 % T), and br (broad).

Melting points of solids, compounds that solidified after chromatography, were measured on a *Büchi* M-5600 Melting Point apparatus and are uncorrected. The measurements were performed with a heating rate of 5 °C/min and the melting points are reported in °C.

If not otherwise noted, solvents were removed on a *Büchi* Rotavapor R-300 with 40 °C water bath temperature.

Absorption measurements were performed either using a *Shimadzu* UV-2700 UV-Vis spectrophotometer. Emission measurements were performed using an *Edinburgh Instruments* FLS 1000 photoluminescence spectrometer. Absolute quantum yields were measured using an *Edinburgh Instruments* integrating sphere. TCSPC measurements were performed using a fast response MCP-PMT detector on the FLS 1000 and a 376 nm *Edinburgh Instruments* EPL Laser as excitation source with 10 – 20 MHz repetition rate and 80 ps pulse width. Furthermore, TCSPC measurements were performed using the *Horiba* FluoroHub coupled with the *Horiba* Fluoromax-4 spectrometer. A NanoLED by *Horiba* was used as excitation source with 254 nm wavelength with 5 MHz repetition rate and pulse width of 1.2 ns. Temperature dependent-fluorescence measurements were carried out using an *Edinburgh Instruments* FLS 1000 spectrometer equipped with an *Oxford Instruments* Optistat-CF cryostat cooled with liquid nitrogen. Unless otherwise noted, all measurements were performed at 22 °C room temperature in Quartz Cuvettes with 10 mm path length by *Hellma Analytics*. CIE 1931 chromaticity coordinates were generated from the respective photoluminescence spectra using the *Edinburgh Instruments* software Fluoracle.

Nanoparticles formed during Aggregation-Induced Emission Enhancement (AIEE) experiments were analyzed in respect of their size using a *Malvern Zetasizer Nano ZSP* with a 633 nm laser.

Simultaneous Thermogravimetric Analysis (TGA) and Differential Scanning Calorimetry (DSC) measurement was carried out on a Mettler Toledo TGA/DSC 3+ STAR^e system (and SDT Q600 Thermal Gravimetric Analyzer) using 1.85 to 6.63 mg of compounds under a constant flow of nitrogen gas (20 mL/min). The temperature of oven was held at 298 K for 1 minute, then heated from 298 K (25 °C) to 673 K (400 °C) with a heating rate of 10 K per minute. A reference (empty crucible) was run prior to measurement.

Single crystals were grown as described in the experimental procedures. Intensity data of suitable crystals were collected on a *Bruker* Venture D8 diffractometer at 100 K with Mo-K α (0.71073 Å) radiation. All structures were solved by direct methods and refined based on F² by use of the SHELX program package as implemented in Olex2.² All non-hydrogen atoms were refined using anisotropic displacement parameters. Hydrogen atoms attached to carbon atoms were included in geometrically calculated positions using a rigid model. Crystal and refinement data are collected in Tables S2-S19. Figures were created using Diamond from *Crystal Impact*. Crystallographic data for the structural analyses have been deposited with the Cambridge Crystallographic Data Centre. Copies of this

information may be obtained free of charge from The Director, CCDC, 12 Union Road, Cambridge CB2 1EZ, UK (Fax: +44-1223-336033; e-mail: deposit@ccdc.cam.ac.uk or <http://www.ccdc.cam.ac.uk>).

All calculations were performed with the Orca 4.2.0 program package.³ Ground state (S_0) geometries of the keto tautomers of all investigated molecules were optimized with Density Functional Theory⁴ at the B97⁵/cc-pVDZ⁶ level of theory. The integration grid was adjusted with the Orca options GRIDX5, GRID5 and NoFinalGrid. Tight convergence criteria for the self-consistent field and geometry optimizations were enforced throughout (options TightSCF and TightOPT). In the case of **1-CN**, a constraint of the N-H bond length (1.08 Å) was necessary to avoid the generation of the enol tautomer. Geometry optimizations in the first electronically excited singlet state (S_1) were carried out with Time-Dependent Density Functional Theory (TDDFT)⁷ at the same level of theory as in the S_0 state.

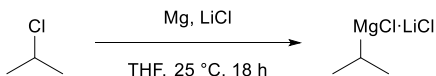
In the case of **4-CN**, default convergence criteria of the geometry optimization as well as a maximum step size of 0.01 a.u. were applied to avoid the creation to the enol tautomer in the S_1 state. In all cases, the lack of imaginary frequencies confirmed that the calculated stationary points are indeed true minima on the respective potential energy surface. The RIJCOSX integration scheme⁸ was used to accelerate all calculations. Based on the calculated geometries and Hessian matrices, fluorescence spectra were calculated with Orca's Excited State Dynamics (ESD) module. A product of Gaussian and Lorentzian curves was used (VOIGT line shape) and the line width parameters of each type of curve were adjusted to 200 cm⁻¹. Vibronic coupling was allowed in all calculations. The S_1 states were characterized using Natural Transition Orbitals (NTOs).⁹ The NTOs were visualized with the VMD 1.9.3 program package,¹⁰ where the isovalues in the orbital representations were adjusted to 0.05 and -0.05.

Photographs of experimental setup and flasks were taken with a *Canon* EOS 700D and a *Canon* EFS 18–55 mm lens. For close-up photographs of solid samples, a *Sigma* 105 mm F2.8 EX DG OS HSM lens was used.

2 Experimental Procedures

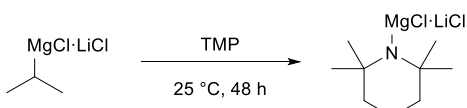
2.1 Preparation of Metalation Agents

2.1.1 Preparation of the Reagent $i\text{PrMgCl}\cdot\text{LiCl}$



A slightly modified literature procedure was used.¹¹ LiCl (4.24 g, 100 mmol, 1.00 eq) was placed in a heat gun-dried and nitrogen-flushed *Schlenk* flask and heated *in vacuo* at 140°C by heat gun for five hours. Magnesium turnings (2.67 g, 110 mmol, 1.10 eq) were placed in another heat gun-dried and nitrogen-flushed *Schlenk* flask and the dried LiCl and anhydrous THF (50 mL) were added. 2-Chloropropane (9.14 mL, 100 mmol, 1.00 eq) in anhydrous THF (50 mL) was slowly added at 25°C through a dropping funnel. After approximately 1/5 of addition the mixture was slightly warmed with a heat gun until the reaction started (within ten minutes). When the reaction started the remaining solution was added dropwise and stirring was continued for 18 hours. After complete addition the temperature of the mixture rose until it started to boil. To remove excess of magnesium the grey solution was cannulated to another heat gun-dried and nitrogen-flushed *Schlenk* flask. The Grignard reagent was titrated¹² prior to use against I_2 (0.50 – 0.60 mmol) in anhydrous THF (2 mL) at 0°C which resulted in a conversion of 92 – 96 %. Color change from dark violet to pale brown indicated the end of the titration.

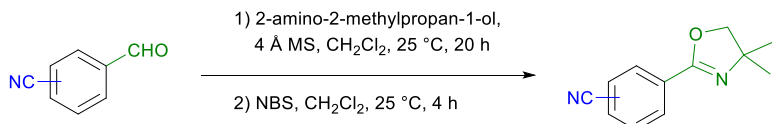
2.1.2 Preparation of the Reagent $\text{TMPMgCl}\cdot\text{LiCl}$



A slightly modified literature procedure was used.¹³ A heat gun-dried and nitrogen-flushed *Schlenk* flask was charged with freshly titrated $i\text{PrMgCl}\cdot\text{LiCl}$ (75.0 mL, 90.0 mmol, 1.00 eq, 1.20 M). Freshly distilled TMP (16.0 mL, 94.5 mmol, 1.05 eq) was added through a rubber septum to the vigorously stirred Grignard solution *via* syringe pump (0.5 mL/min) at 25°C . The reaction mixture was stirred at 25°C for 48 hours, while the solution turned dark green. The base was titrated¹⁴ prior to use against benzoic acid (122 mg, 1.00 mmol) using (4-phenylazo)diphenylamine (3 mg) as indicator in anhydrous THF (2.00 mL) at 0°C which resulted in a conversion of 96 – 99 %. Color change from orange to dark violet indicated the end of the titration.

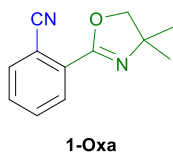
2.2 Procedures for Oxazoline Syntheses

2.2.1 General Procedure for the Oxazoline Synthesis from the Corresponding Aldehyde (GP 1)



A modified literature procedure was used.¹⁵ A round bottom flask, equipped with a magnetic stirring bar and a rubber septum, was charged with aldehyde (1.00 eq) and CH_2Cl_2 (0.25 M). Then 2-amino-2-methylpropan-1-ol (1.50 eq) and 4 Å MS (1.0 g/1.5 mmol aldehyde) were added successively. Due to the waxy nature of the 2-amino-2-methylpropan-1-ol at 25 °C and for a better handling, the bottle containing 2-amino-2-methylpropan-1-ol was placed in a 40 °C water bath until the reagent was melted and simple transfer *via* syringe was possible. After slowly stirring (100 – 200 rpm) for the indicated time at 25 °C NBS (1.50 eq) was added in one portion and rapid stirring was continued for the indicated time at 25 °C. Then all solids were filtered off and washed with CH_2Cl_2 . The organic phase was subjected to aqueous workup, dried over anhydrous Na_2SO_4 , filtered and concentrated under reduced pressure on a rotary evaporator. Purification of the crude product was conducted by flash column chromatography using the given eluent.

2.2.2 2-(4,4-Dimethyl-4,5-dihydrooxazol-2-yl)benzonitrile (1-Oxa)

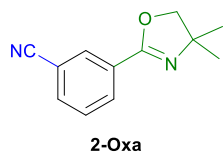


Prepared according to **GP 1** from 2-formylbenzonitrile (1.31 g, 10.0 mmol, 1.00 eq) in CH_2Cl_2 (40 mL, 0.25 M) and 2-amino-2-methylpropan-1-ol (1.34 g, 1.43 mL, 15.0 mmol, 1.50 eq) and 4 Å MS (10.0 g). Stirring for 20 h and addition of NBS (2.67 g, 15.0 mmol, 1.50 eq) was followed by stirring for four more hours. After filtration the organic phase was washed with saturated NaHCO_3 solution (3×50 mL). The combined aqueous phases were extracted with CH_2Cl_2 (2×50 mL). All organic phases were washed with saturated NaS_2O_3 solution (50 mL) and the aqueous phase was extracted with CH_2Cl_2 (2×50 mL). Purification by flash column chromatography (SiO_2 , CH:EE 10:1 v:v) afforded **1-Oxa** (1.88 g, 9.39 mmol, 93 %) as a slightly yellow solid.

$\mathbf{R}_f = 0.10$ (SiO_2 , CH:EE 10:1 v:v). **Mp.:** 58 – 60 °C. **$^1\text{H-NMR}$ (601 MHz, CDCl_3):** $\delta = 8.04$ (d, $^3J_{\text{HH}} = 7.9$ Hz, 1H), 7.76 (d, $^3J_{\text{HH}} = 7.7$ Hz, 1H), 7.62 (td, $^3J_{\text{HH}} = 7.7$ Hz, $^4J_{\text{HH}} = 1.3$ Hz, 1H), 7.55 (td, $^3J_{\text{HH}} = 7.7$ Hz, $^4J_{\text{HH}} = 1.3$ Hz, 1H), 4.20 (s, 2H), 1.42 (s, 6H) ppm. **$^{13}\text{C}\{\text{H}\}-\text{NMR}$ (151 MHz, CDCl_3):** $\delta =$

159.9, 134.6, 132.5, 131.1, 130.8, 130.3, 117.9, 111.9, 79.9, 68.4, 28.4 (2x) ppm. **IR (ATR, neat):** $\tilde{\nu}$ = 2969 (m), 2930 (w), 2895 (w), 2869 (w), 2226 (w), 1731 (w), 1652 (m), 1593 (m), 1578 (w), 1494 (m), 1482 (w), 1463 (w), 1438 (m), 1380 (w), 1352 (m), 1316 (m), 1289 (m), 1272 (m), 1247 (w), 1210 (w), 1181 (m), 1122 (w), 1047 (s), 990 (m), 965 (m), 919 (m), 888 (w), 864 (w), 817 (w), 775 (s), 746 (s), 676 (s), 659 (m). **MS (APCI):** m/z = 201.1 [C₁₂H₁₂N₂O+H]⁺. **HR-MS (ESI):** calculated for C₁₂H₁₃N₂O⁺ [M+H]⁺: m/z = 201.10224, found: 201.10216 (Dev.: -0.08 mu; -0.40 ppm); calculated for C₁₂H₁₂N₂NaO⁺ [M+Na]⁺: m/z = 223.08418, found: 223.08413 (Dev.: -0.05 mu; -0.22 ppm). The analytical data are in accordance with the literature.¹⁶

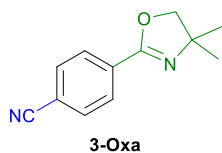
2.2.3 3-(4,4-Dimethyl-4,5-dihydrooxazol-2-yl)benzonitrile (2-Oxa)



Prepared according to **GP 1** from 3-formylbenzonitrile (1.31 g, 10.0 mmol, 1.00 eq) in CH₂Cl₂ (40 mL, 0.25 M) and 2-amino-2-methylpropan-1-ol (1.34 g, 1.43 mL, 15.0 mmol, 1.50 eq) and 4 Å MS (10.0 g). Stirring for 20 h and addition of NBS (2.67 g, 15.0 mmol, 1.50 eq) was followed by stirring for four more hours. After filtration the organic phase was washed with saturated NaHCO₃ solution (3 × 50 mL). The combined aqueous phases were extracted with CH₂Cl₂ (2 × 50 mL). All organic phases were washed with saturated NaS₂O₃ solution (50 mL) and the aqueous phase was extracted with CH₂Cl₂ (2 × 50 mL). Purification by flash column chromatography (SiO₂, CH:EE 10:1 v:v) afforded **2-Oxa** (1.62 g, 8.09 mmol, 81 %) as a colorless liquid. Upon standing at -10 °C the liquid solidified to form a colorless solid.

R_f = 0.09 (SiO₂, CH:EE 10:1 v:v). **¹H-NMR (601 MHz, CDCl₃):** δ = 8.24 (s, 1H), 8.16 (d, ³J_{HH} = 7.9 Hz, 1H), 7.74 (d, ³J_{HH} = 7.7 Hz, 1H), 7.52 (t, ³J_{HH} = 7.8 Hz, 1H), 4.14 (s, 2H), 1.39 (s, 6H) ppm. **¹³C{¹H}-NMR (151 MHz, CDCl₃):** δ = 160.3, 134.4, 132.4, 132.0, 129.6, 129.4, 118.2, 112.9, 79.6, 68.1, 28.5 (2x) ppm. **IR (ATR, neat):** $\tilde{\nu}$ = 3074 (w), 2969 (m), 2930 (w), 2896 (w), 2231 (m), 1737 (w), 1651 (s), 1601 (w), 1578 (w), 1476 (w), 1463 (w), 1437 (w), 1418 (w), 1384 (w), 1354 (m), 1314 (m), 1247 (w), 1190 (m), 1166 (m), 1080 (m), 1071 (m), 1058 (m), 1017 (w), 989 (w), 968 (s), 925 (m), 888 (w), 845 (w), 807 (m), 765 (w), 741 (w), 716 (s), 682 (m). **MS (APCI):** m/z = 201.1 [C₁₂H₁₂N₂O+H]⁺. **HR-MS (ESI):** calculated for C₁₂H₁₃N₂O⁺ [M+H]⁺: m/z = 201.10224, found: 201.10217 (Dev.: -0.07 mu; -0.34 ppm); calculated for C₁₂H₁₂N₂NaO⁺ [M+Na]⁺: m/z = 223.08418, found: 223.08425 (Dev.: 0.07 mu; 0.31 ppm). The analytical data are in accordance with the literature.¹⁶

2.2.4 4-(4,4-Dimethyl-4,5-dihydrooxazol-2-yl)benzonitrile (3-Oxa)

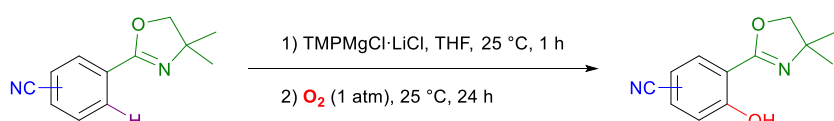


Prepared according to **GP 1** from 4-formylbenzonitrile (1.31 g, 10.0 mmol, 1.00 eq) in CH₂Cl₂ (40 mL, 0.25 M) and 2-amino-2-methylpropan-1-ol (1.34 g, 1.43 mL, 15.0 mmol, 1.50 eq) and 4 Å MS (10.0 g). Stirring for 20 h and addition of NBS (2.67 g, 15.0 mmol, 1.50 eq) was followed by stirring for four more hours. After filtration the organic phase was washed with saturated NaHCO₃ solution (3 × 50 mL). The combined aqueous phases were extracted with CH₂Cl₂ (2 × 50 mL). All organic phases were washed with saturated NaS₂O₃ solution (50 mL) and the aqueous phase was extracted with CH₂Cl₂ (2 × 50 mL). Purification by flash column chromatography (SiO₂, CH:EE 10:1 v:v) afforded **3-Oxa** (1.88 g, 9.39 mmol, 94 %) as a colorless solid.

R_f = 0.10 (SiO₂, CH:EE 10:1 v:v). **Mp.:** 105 – 107 °C. **¹H-NMR (601 MHz, CDCl₃):** δ = 8.03 (d, ³J_{HH} = 8.0 Hz, 2H), 7.69 (d, ³J_{HH} = 8.0 Hz, 2H), 4.14 (s, 2H), 1.39 (s, 6H) ppm. **¹³C{¹H}-NMR (151 MHz, CDCl₃):** δ = 160.6, 132.4, 132.2 (2x), 128.9 (2x), 118.5, 114.7, 79.6, 68.2, 28.5 (2x) ppm. **IR (ATR, neat):** $\tilde{\nu}$ = 3044 (w), 2973 (m), 2935 (w), 2907 (w), 2874 (w), 2286 (w), 2229 (m), 1929 (w), 1641 (s), 1610 (m), 1564 (w), 1503 (w), 1478 (w), 1461 (m), 1408 (m), 1382 (m), 1356 (s), 1320 (m), 1310 (m), 1293 (m), 1250 (w), 1219 (w), 1184 (m), 1111 (w), 1071 (s), 1017 (m), 986 (w), 950 (s), 924 (m), 873 (w), 844 (s), 830 (m), 822 (m), 771 (w), 741 (m), 675 (s). **MS (APCI):** m/z = 201.1 [C₁₂H₁₂N₂O+H]⁺. The analytical data are in accordance with the literature.¹⁷

2.3 Procedures for *ortho*-Hydroxylations

2.3.1 General Procedure for the *ortho*-Hydroxylation of 2-Aryloxazolines (GP 2)

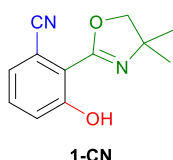


A reported procedure was used.¹⁸ A heat gun-dried and nitrogen-flushed *Schlenk* tube, equipped with a magnetic stirring bar and a rubber septum, was charged with 2-aryloxazoline (1.00 eq) and anhydrous THF (0.4 M) was added. Dropwise addition of TMPPMgCl·LiCl (3.00 eq, in THF) *via* syringe through the rubber septum at 25 °C was followed by stirring for the indicated time under the same conditions, while the mixture discolored dark red/brown. Then the nitrogen atmosphere was replaced by an oxygen atmosphere by flushing the reaction system using an oxygen filled balloon and the mixture was stirred for an additional 24 hours at 25 °C. The clear, pale red to yellow, mixture was subjected to aqueous

workup and the organic layer was dried over anhydrous Na₂SO₄, filtered and concentrated under reduced pressure on a rotary evaporator. Purification of the crude product was conducted by flash column chromatography using the given eluent.

The hydroxylation can be also performed using air as oxygen source – this leads to slightly reduced yield due to reduced partial pressure of oxygen.¹⁸

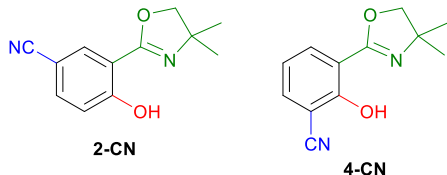
2.3.2 2-(4,4-Dimethyl-4,5-dihydrooxazol-2-yl)-3-hydroxybenzonitrile (**1-CN**)



Prepared according to **GP 2** from **1-Oxa** (100 mg, 500 µmol, 1.00 eq) in THF (1.25 mL, 0.4 M) and TMPMgCl·LiCl (1.25 mL, 1.50 mmol, 3.00 eq, 1.20 M in THF). Stirring for one hour was followed by flushing with oxygen and stirring for another 24 hours. Saturated NH₄Cl solution (10 mL), water (10 mL) and CH₂Cl₂ (20 mL) were added and the phases were separated. The aqueous phase was extracted with CH₂Cl₂ (4 × 20 mL). Purification by flash column chromatography (SiO₂, CH:EE 20:1 v:v) afforded **1-CN** (101 mg, 467 µmol, 93 %) as a colorless solid. Single crystals suitable for X-ray analysis were grown from CH₂Cl₂ solution by slow solvent evaporation. Also, suitable crystals were obtained from very slow diffusion of a cyclohexane layer into a CH₂Cl₂ solution of **1-CN** and concomitant slow solvent evaporation.

R_f = 0.10 (SiO₂, CH:EE 20:1 v:v). **Mp.:** 170 – 172 °C. **¹H-NMR (601 MHz, CDCl₃):** δ = 13.25 (s, 1H), 7.41 (dd, ³J_{HH} = 8.4 Hz, ³J_{HH} = 7.6 Hz, 1H), 7.27 (dd, ³J_{HH} = 7.5 Hz, ⁴J_{HH} = 1.2 Hz, 1H), 7.25 (dd, ³J_{HH} = 8.5 Hz, ⁴J_{HH} = 1.2 Hz, 1H), 4.26 (s, 2H), 1.43 (s, 6H) ppm. **¹H-NMR (600 MHz, C₆D₆):** δ = 13.43 (s, 1H), 6.96 (dd, ³J_{HH} = 8.5 Hz, ⁴J_{HH} = 0.9 Hz, 1H), 6.77 (dd, ³J_{HH} = 7.5 Hz, ⁴J_{HH} = 1.0 Hz, 1H), 6.60 (dd, ³J_{HH} = 8.5 Hz, ³J_{HH} = 7.5 Hz, 1H), 3.48 (s, 2H), 0.80 (s, 6H) ppm. **¹³C{¹H}-NMR (151 MHz, CDCl₃):** δ = 162.5, 161.3, 132.7, 126.2, 122.4, 118.2, 111.2, 111.1, 79.4, 66.9, 28.5 (2x) ppm. **¹³C{¹H}-NMR (151 MHz, C₆D₆):** δ = 162.9, 161.8, 132.7, 126.0, 121.9, 118.0, 112.0, 111.2, 78.8, 66.3, 27.7 (2x) ppm. **IR (ATR, neat):** $\tilde{\nu}$ = 2969 (w), 2930 (w), 2230 (w), 1627 (m), 1596 (w), 1572 (w), 1491 (m), 1466 (w), 1453 (m), 1378 (w), 1362 (w), 1331 (m), 1320 (m), 1268 (s), 1204 (m), 1184 (m), 1164 (m), 1100 (m), 1065 (m), 993 (w), 977 (w), 948 (s), 888 (w), 876 (w), 833 (m), 800 (s), 755 (w), 683 (m) cm⁻¹. **MS (APCI):** m/z = 217.1 [C₁₂H₁₂N₂O₂+H]⁺. **HR-MS (ESI):** calculated for C₁₂H₁₃N₂O₂⁺ [M+H]⁺: m/z = 217.09715, found: 217.09713 (Dev.: -0.03 mu; -0.13 ppm); calculated for C₁₂H₁₂N₂NaO₂⁺ [M+Na]⁺: m/z = 239.07910, found: 239.07902 (Dev.: -0.08 mu; -0.32 ppm). The analytical data are in accordance with the literature.¹⁸

2.3.3 3-(4,4-Dimethyl-4,5-dihydrooxazol-2-yl)-4-hydroxybenzonitrile (**2-CN**) and 3-(4,4-Dimethyl-4,5-dihydrooxazol-2-yl)-2-hydroxybenzonitrile (**4-CN**)



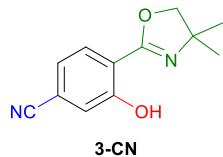
Prepared according to **GP 2** from **2-Oxa** (100 mg, 500 μ mol, 1.00 eq) in THF (1.25 mL, 0.4 M) and TMPMgCl-LiCl (1.25 mL, 1.50 mmol, 3.00 eq, 1.20 M in THF). Stirring for one hour was followed by flushing with oxygen and stirring for another 24 hours. Saturated NH₄Cl solution (10 mL), water (10 mL) and CH₂Cl₂ (20 mL) were added and the phases were separated. The aqueous phase was extracted with CH₂Cl₂ (4 \times 20 mL). Purification by flash column chromatography (SiO₂, CH:EE 20:1 v:v) afforded **2-CN** (83.0 mg, 384 μ mol, 77 %) as a colorless solid. Polar fractions were further purified by flash column chromatography (SiO₂, CH₂Cl₂:MeOH 100:1 v:v) to obtain **4-CN** (10.4 mg, 48.1 μ mol, 10 %) as a colorless solid. Single crystals suitable for X-ray analysis were grown from CH₂Cl₂ solution by rapid solvent evaporation.

2-CN: $R_f = 0.08$ (SiO₂, CH:EE 20:1 v:v). **Mp.:** 133 – 135 °C. **¹H-NMR (601 MHz, CDCl₃):** $\delta = 12.93$ (s, 1H), 7.96 (d, $^4J_{HH} = 2.0$ Hz, 1H), 7.60 (dd, $^3J_{HH} = 8.7$ Hz, $^4J_{HH} = 2.2$ Hz, 1H), 7.05 (d, $^3J_{HH} = 8.7$ Hz, 1H), 4.15 (s, 2H), 1.41 (s, 6H) ppm. **¹H-NMR (600 MHz, C₆D₆):** $\delta = 12.96$ (s, 1H), 7.74 (d, $^4J_{HH} = 2.1$ Hz, 1H), 6.89 (dd, $^3J_{HH} = 8.6$ Hz, $^4J_{HH} = 2.1$ Hz, 1H), 6.66 (d, $^3J_{HH} = 8.6$ Hz, 1H), 3.33 (s, 2H), 0.84 (s, 6H) ppm. **¹³C{¹H}-NMR (151 MHz, CDCl₃):** $\delta = 163.4, 162.4, 136.4, 132.9, 118.9, 118.2, 111.9, 102.2, 78.9, 67.6, 28.5$ (2x) ppm. **¹³C{¹H}-NMR (151 MHz, C₆D₆):** $\delta = 163.4, 162.6, 136.5, 132.8, 118.6, 118.1, 111.8, 102.9, 78.2, 67.1, 27.8$ (2x) ppm. **IR (ATR, neat):** $\tilde{\nu} = 2978$ (w), 2931 (w), 2222 (m), 1636 (s), 1589 (m), 1488 (s), 1463 (m), 1420 (w), 1383 (m), 1370 (s), 1332 (m), 1301 (s), 1274 (s), 1249 (s), 1211 (m), 1190 (s), 1141 (m), 1063 (s), 985 (w), 964 (s), 943 (s), 910 (m), 829 (m), 815 (s), 798 (m), 742 (s), 676 (m) cm⁻¹. **MS (APCI):** m/z = 217.1 [C₁₂H₁₂N₂O₂+H]⁺. **HR-MS (ESI):** calculated for C₁₂H₁₃N₂O₂⁺ [M+H]⁺: m/z = 217.09715, found: 217.09734 (Dev.: 0.19 mu; 0.87 ppm); calculated for C₁₂H₁₂N₂NaO₂⁺ [M+Na]⁺: m/z = 239.07910, found: 239.07909 (Dev.: -0.01 mu; -0.06 ppm). The analytical data are in accordance with the literature.¹⁸

4-CN: $R_f = 0.03$ (SiO₂, CH:EE 20:1 v:v). $R_f = 0.14$ (SiO₂, CH₂Cl₂:MeOH 100:1 v:v). **Mp.:** 122 – 124 °C. **¹H-NMR (601 MHz, CDCl₃):** $\delta = 13.38$ (br. s, 1H), 7.82 (dd, $^3J_{HH} = 7.8$ Hz, $^4J_{HH} = 1.7$ Hz, 1H), 7.62 (dd, $^3J_{HH} = 7.7$ Hz, $^4J_{HH} = 1.7$ Hz, 1H), 6.92 (t, $^3J_{HH} = 7.8$ Hz, 1H), 4.15 (s, 2H), 1.41 (s, 6H) ppm. **¹H-NMR (600 MHz, C₆D₆):** $\delta = 13.34$ (s, 1H), 7.50 (dd, $^3J_{HH} = 7.8$ Hz, $^4J_{HH} = 1.6$ Hz, 1H), 6.99 (dd, $^3J_{HH} = 7.7$ Hz, $^4J_{HH} = 1.6$ Hz, 1H), 6.20 (t, $^3J_{HH} = 7.8$ Hz, 1H), 3.34 (s, 2H), 0.81 (s, 6H) ppm. **¹³C{¹H}-NMR (151 MHz, CDCl₃):** $\delta = 162.8, 162.2, 136.7, 132.5, 118.7, 116.1, 112.1, 101.2, 79.0, 67.4, 28.5$ (2x) ppm. **¹³C{¹H}-NMR (151 MHz, C₆D₆):** $\delta = 162.8, 162.4, 136.9, 131.8, 118.5, 115.8, 112.1, 102.3,$

78.4, 67.0, 27.7 (2x) ppm. **IR (ATR, neat):** $\tilde{\nu} = 2968$ (w), 2934 (w), 2872 (w), 2230 (w), 1641 (m), 1617 (m), 1583 (w), 1485 (w), 1465 (w), 1456 (m), 1431 (m), 1385 (m), 1370 (m), 1360 (m), 1336 (w), 1291 (m), 1252 (w), 1221 (w), 1181 (m), 1174 (m), 1129 (s), 1091 (m), 1074 (m), 1013 (w), 975 (s), 943 (s), 900 (m), 847 (m), 815 (s), 797 (s), 753 (s) cm^{-1} . **MS (APCI):** m/z = 217.1 [C₁₂H₁₂N₂O₂+H]⁺. **HR-MS (ESI):** calculated for C₁₂H₁₃N₂O₂⁺ [M+H]⁺: m/z = 217.09715, found: 217.09713 (Dev.: -0.03 mu; -0.12 ppm); calculated for C₁₂H₁₂N₂NaO₂⁺ [M+Na]⁺: m/z = 239.07910, found: 239.07904 (Dev.: -0.06 mu; -0.25 ppm). The analytical data are in accordance with the literature.¹⁸

2.3.4 4-(4,4-Dimethyl-4,5-dihydrooxazol-2-yl)-3-hydroxybenzonitrile (3-CN)

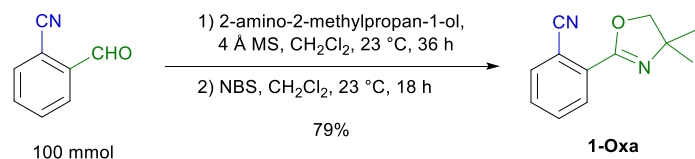


Prepared according to **GP 2** from **3-Oxa** (100 mg, 500 μmol , 1.00 eq) in THF (1.25 mL, 0.4 M) and TMPMgCl·LiCl (1.23 mL, 1.50 mmol, 3.00 eq, 1.22 M in THF). Stirring for one hour was followed by flushing with oxygen and stirring for another 24 hours. Saturated NH₄Cl solution (10 mL), water (10 mL) and CH₂Cl₂ (20 mL) were added and the phases were separated. The aqueous phase was extracted with CH₂Cl₂ (4 \times 20 mL). Purification by flash column chromatography (SiO₂, CH:EE 20:1 v:v) afforded **3-CN** (105 mg, 486 μmol , 97 %) as a colorless solid. Single crystals suitable for X-ray analysis were grown from CH₂Cl₂ solution by rapid solvent evaporation.

R_f = 0.10 (SiO₂, CH:EE 20:1 v:v). **Mp.:** 121 – 123 °C. **¹H-NMR (601 MHz, CDCl₃):** δ = 12.50 (s, 1H), 7.71 (d, ³J_{HH} = 8.0 Hz, 1H), 7.27 (d, ⁴J_{HH} = 1.5 Hz, 1H), 7.13 (dd, ³J_{HH} = 8.0 Hz, ⁴J_{HH} = 1.5 Hz, 1H), 4.14 (s, 2H), 1.41 (s, 6H) ppm. **¹H-NMR (600 MHz, C₆D₆):** δ = 12.54 (s, 1H), 7.36 (d, ³J_{HH} = 8.0 Hz, 1H), 7.01 (d, ⁴J_{HH} = 1.4 Hz, 1H), 6.54 (dd, ³J_{HH} = 8.0 Hz, ⁴J_{HH} = 1.5 Hz, 1H), 3.35 (s, 2H), 0.83 (s, 6H) ppm. **¹³C{¹H}-NMR (151 MHz, CDCl₃):** δ = 162.6, 159.9, 128.9, 121.8, 120.6, 118.3, 116.1, 114.9, 78.8, 67.7, 28.5 (2x) ppm. **¹³C{¹H}-NMR (151 MHz, C₆D₆):** δ = 162.8, 160.4, 128.7, 121.7, 120.7, 118.2, 116.9, 114.6, 78.2, 67.2, 27.8 (2x) ppm. **IR (ATR, neat):** $\tilde{\nu} = 2970$ (w), 2932 (w), 2872 (w), 2227 (w), 1640 (m), 1613 (m), 1563 (m), 1505 (m), 1489 (m), 1481 (m), 1461 (m), 1398 (m), 1361 (s), 1328 (w), 1313 (m), 1303 (m), 1270 (s), 1238 (m), 1209 (s), 1188 (s), 1146 (m), 1135 (m), 1109 (w), 1064 (s), 962 (s), 939 (s), 864 (m), 829 (s), 795 (s), 745 (m), 722 (m), 682 (s) cm^{-1} . **MS (APCI):** m/z = 217.1 [C₁₂H₁₂N₂O₂+H]⁺. **HR-MS (ESI):** calculated for C₁₂H₁₃N₂O₂⁺ [M+H]⁺: m/z = 217.09715, found: 217.09715 (Dev.: 0.00 mu; 0.00 ppm); calculated for C₁₂H₁₂N₂NaO₂⁺ [M+Na]⁺: m/z = 239.07910, found: 239.07907 (Dev.: -0.03 mu; -0.11 ppm).

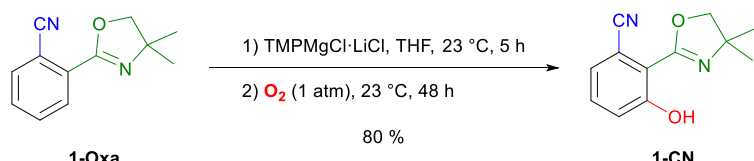
2.4 Detailed Large-Scale Procedures

2.4.1 Decagram Preparation of **1-Oxa**



A 500 mL round bottom flask equipped with a large, elliptical magnetic stirring bar and a rubber septum on top was charged with 2-formylbenzonitrile (13.1 g, 100 mmol, 1.00 eq) and non-anhydrous CH₂Cl₂ (250 mL) was added. Upon dissolution of the starting material, 2-amino-2-methylpropan-1-ol (17.8 g, 200 mmol, 2.00 eq) and 4 Å molecular sieve (100 g) were added successively. The flask was purged for five minutes with nitrogen and finally a nitrogen-filled balloon was placed on top. After 36 hours of slowly stirring (300 rpm) a 23 °C tempered water bath was placed under the reaction flask and *N*-bromosuccinimide (35.6 g, 200 mmol, 2.00 eq) was added in small portions (5 g every 10 minutes), while the stirring rate was increased to 800 rpm. Eight hours after the last addition all intermediately formed *N,O*-acetale was converted to the oxazoline. All solids were filtered over compressed cotton and washed thoroughly with CH₂Cl₂ (200 mL in sum). The organic phase was washed with saturated NaHCO₃ solution (3 × 200 mL) and the combined aqueous phases were extracted with CH₂Cl₂ (2 × 100 mL). All organic phases were washed with saturated Na₂S₂O₃ solution (200 mL) and the aqueous phase was extracted with CH₂Cl₂ (50 mL). The combined organic phases were dried over anhydrous Na₂SO₄ and the solvent was removed under reduced pressure on a rotary evaporator. Adsorption of the crude (25 g) on silica gel (40 g) and purification by flash column chromatography (CH:EE 4:1 v:v) afforded **1-Oxa** (15.8 g, 78.9 mmol, 79 %) as a brown oil which solidified upon standing at 5 °C to form a pale brown solid.

2.4.2 Decagram Preparation of **1-CN**



A heat gun-dried and nitrogen-flushed three-necked round bottom flask equipped with a large, elliptical magnetic stirring bar and a rubber septum on top was charged with **1-Oxa** (12.0 g, 60.0 mmol, 1.00 eq) and anhydrous tetrahydrofuran (150 mL) was added. Due to the large amount of TMPMgCl·LiCl (144 mL, 180 mmol, 3.00 eq, 1.25 M in THF), addition was accomplished using two parallel running syringe pumps (1.2 mL/min) at 23 °C (see figure 1). After complete addition the dark brown/red solution

was stirred in total for five hours under the same conditions, while no warming was observed. Then a 10 °C tempered water bath was placed under the reaction flask and a thermometer was immersed into the reaction mixture to monitor the exothermic oxidation. The nitrogen atmosphere was replaced by an oxygen atmosphere using several oxygen-filled balloons and the mixture was stirred for an additional 48 hours at 23 °C (see Figure 2). During the first half an hour the reaction temperature raised up to 38 °C and sank back to ambient temperature after another one hour. While stirring the solution turned from dark brown/red to brown/red and no solids precipitation was observed. Upon complete oxidation a 10 °C tempered water bath was placed under the reaction flask and saturated NH₄Cl solution (100 mL) and water (100 mL) were added successively, permanently observing the mixture temperature. Afterwards the mixture was transferred to a separation funnel (2 L) using ethyl acetate (100 mL) for washing all contaminated components. The phases were separated and the aqueous layer was extracted with ethyl acetate (4 × 100 mL). The combined organic layers were dried over anhydrous Na₂SO₄ and concentrated under reduced pressure on a rotary evaporator. Prior to purification by flash column chromatography the semi-solid residue was subjected to distillation to remove TMP-H (60 °C oil bath temperature at 18 mbar) as a colorless liquid and TMP-OH (70 °C oil bath temperature at 10 mbar) as colorless crystals (trapping flasks were cooled to 0 °C) from the crude product. Afterwards, adsorption of the crude (15 g) on silica gel (30 g) and purification by flash column chromatography (CH:EE 10:1 v:v) afforded **1-CN** (10.4 g, 48.1 mmol, 80 %) as a colorless solid (see Figure 3). Yellow/brown impurities can be removed from the solid by washing with small amounts of methanol.



Figure S1: Addition of TMPMgCl·LiCl *via* syringe pumps at 23 °C to a 60 mmol (12.0 g) scale of **1-Oxa**.

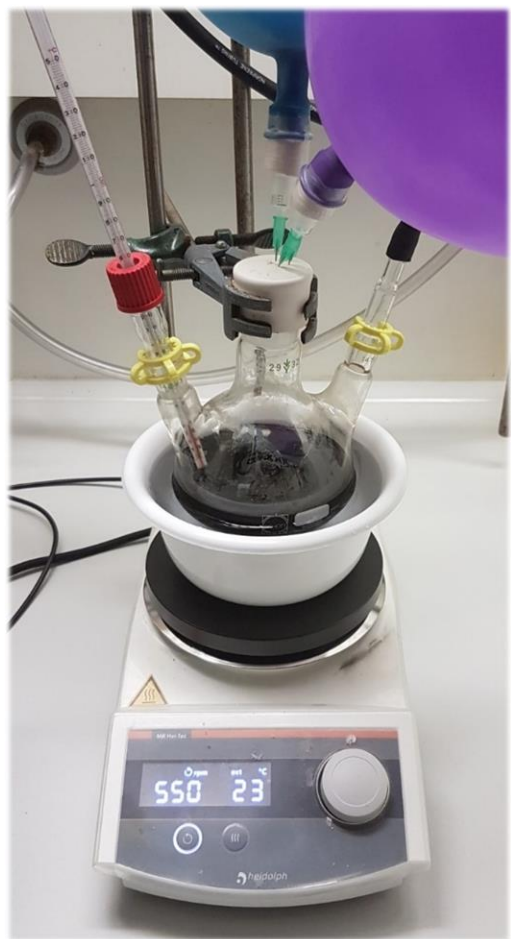


Figure S2: Oxidation of magnesiated **1-Oxa** with molecular oxygen at 23 °C on a 60 mmol (12.0 g) scale.



Figure S3: Large amount of **1-CN** (10.4 g, 48.1 mmol) under ambient light (left) and under 366 nm irradiation (right) in a 50 mL round bottom flask.

3 Optical Properties

3.1 2-(4,4-Dimethyl-4,5-dihydrooxazol-2-yl)-3-hydroxybenzonitrile (1-CN)

3.1.1 Absorption and Emission Properties in Solution and Solid-State

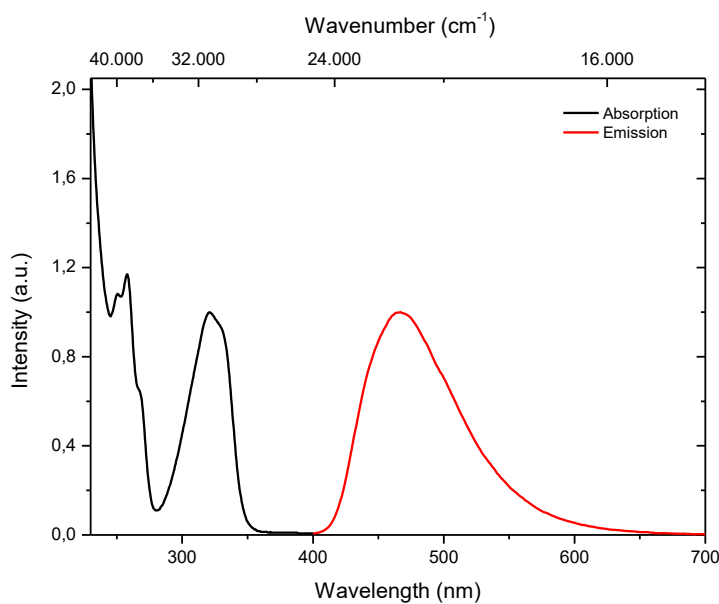


Figure S4: Normalized absorption (black line) and emission (red line) spectra of **1-CN** in methanol solution ($c = 10^{-5}$ mol L $^{-1}$). Emission was monitored by excitation at the absorption maximum wavelength of 321 nm.

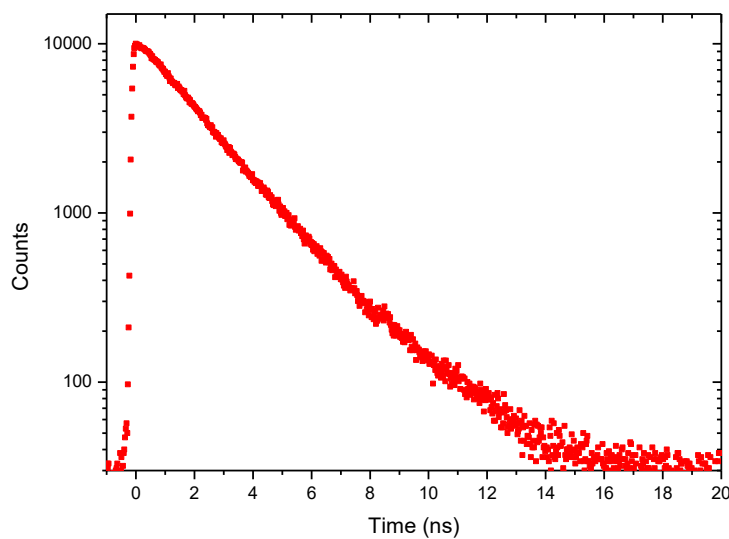


Figure S5: Fluorescence decay profile of **1-CN** in methanol solution ($c = 10^{-5}$ mol L $^{-1}$) with excitation at 376 nm: $\tau_1 = 1.872 \pm 0.046$ (71.6%) ns; $\tau_2 = 2.87 \pm 0.16$ (28.4%) ns; $\chi^2 = 1.133$.

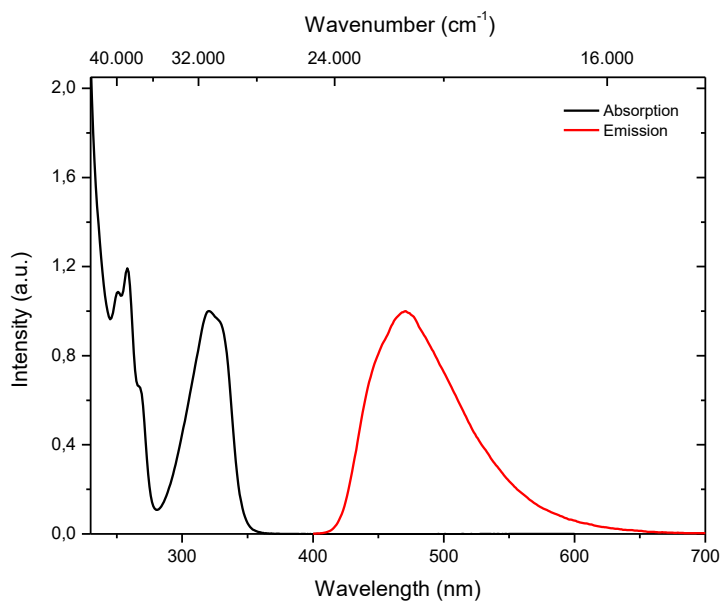


Figure S6: Normalized absorption (black line) and emission (red line) spectra of **1-CN** in acetonitrile solution ($c = 10^{-5}$ mol L $^{-1}$). Emission was monitored by excitation at the absorption maximum wavelength of 320 nm.

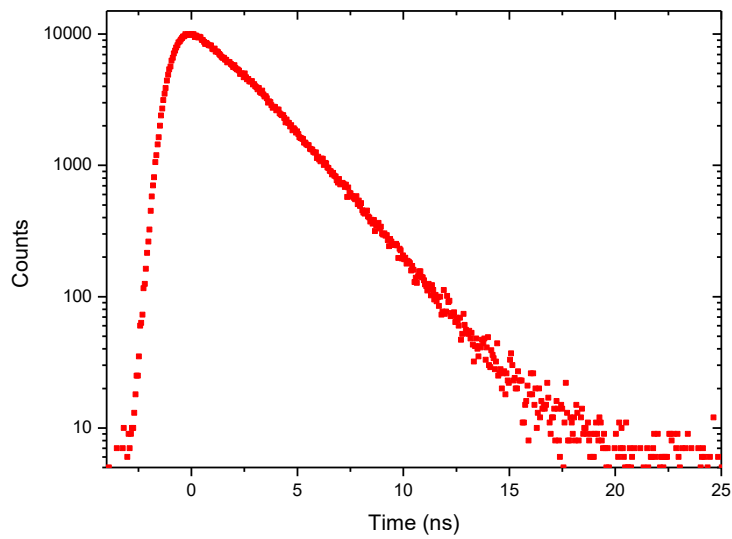


Figure S7: Fluorescence decay profile of **1-CN** in acetonitrile solution ($c = 10^{-5}$ mol L $^{-1}$) with excitation at 254 nm: $\tau = 2.084 \pm 0.004$ ns; $\chi^2 = 1.149$.

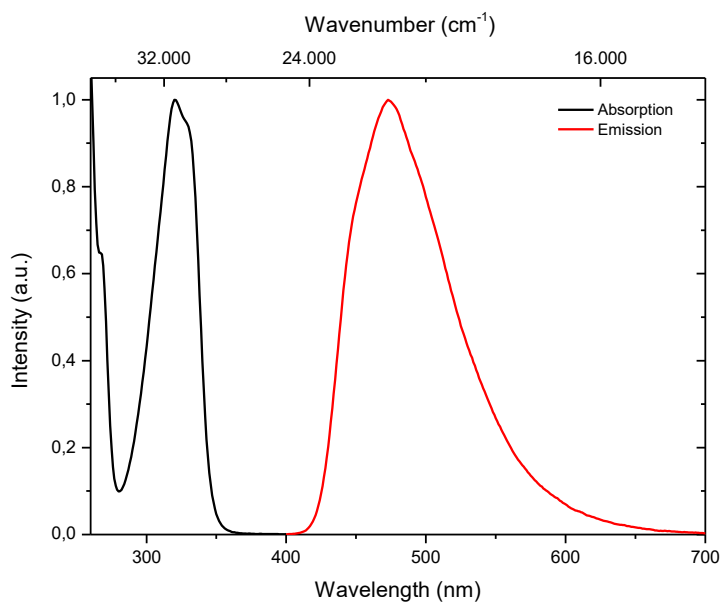


Figure S8: Normalized absorption (black line) and emission (red line) spectra of **1-CN** in ethyl acetate solution ($c = 10^{-5}$ mol L⁻¹). Emission was monitored by excitation at the absorption maximum wavelength of 320 nm.

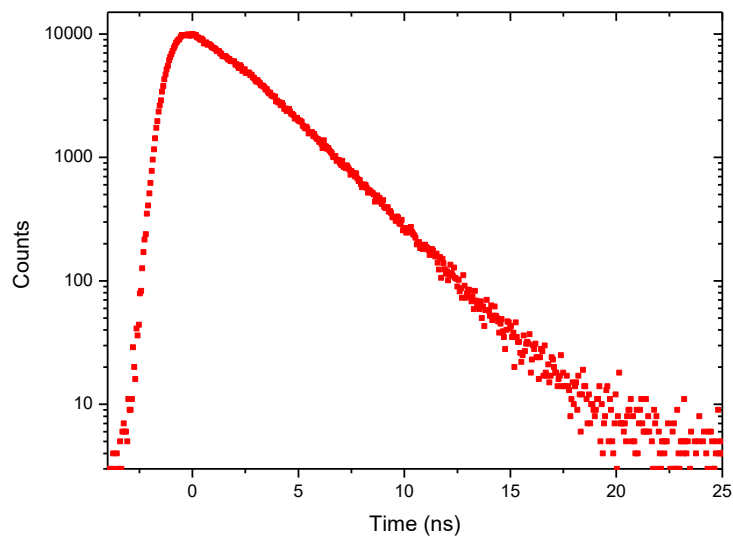


Figure S9: Fluorescence decay profile of **1-CN** in ethyl acetate solution ($c = 10^{-5}$ mol L⁻¹) with excitation at 254 nm: $\tau = 2.337 \pm 0.005$ ns; $\chi^2 = 1.628$.

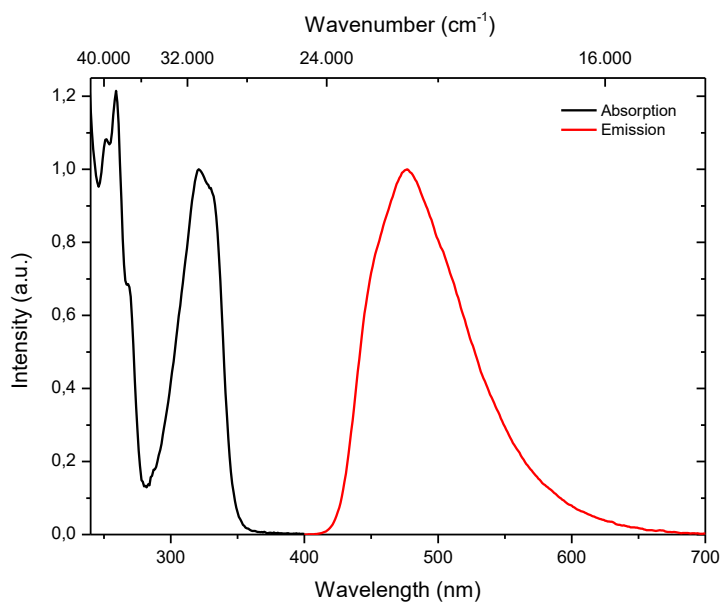


Figure S10: Normalized absorption (black line) and emission (red line) spectra of **1-CN** in tetrahydrofuran solution ($c = 10^{-5}$ mol L⁻¹). Emission was monitored by excitation at the absorption maximum wavelength of 321 nm.

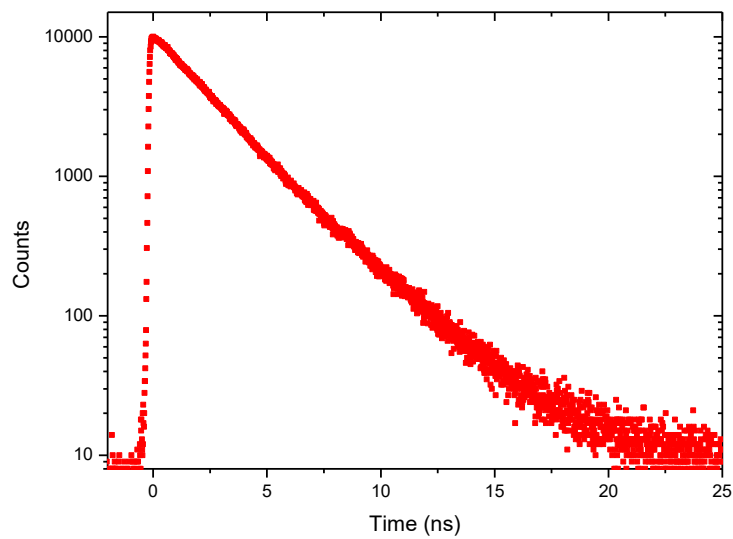


Figure S11: Fluorescence decay profile of **1-CN** in tetrahydrofuran solution ($c = 10^{-5}$ mol L⁻¹) with excitation at 376 nm: $\tau_1 = 2.378 \pm 0.008$ (92.5%) ns; $\tau_2 = 5.10 \pm 0.15$ (7.5%) ns; $\chi^2 = 1.302$.

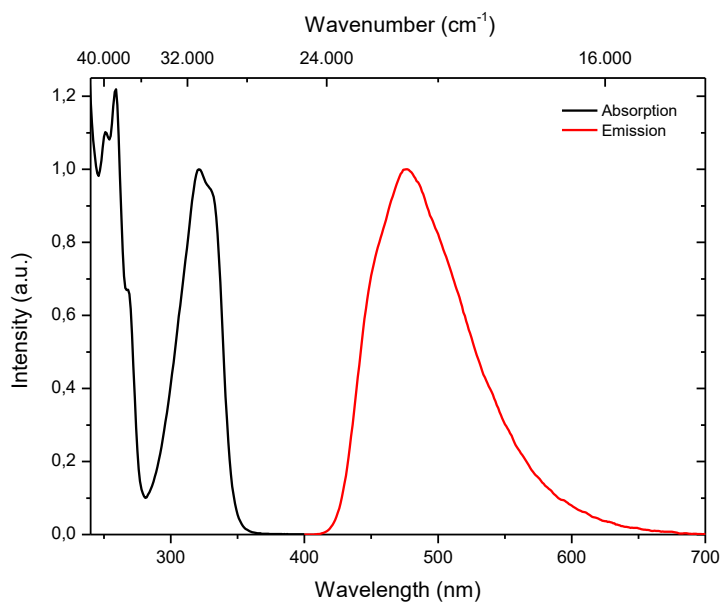


Figure S12: Normalized absorption (black line) and emission (red line) spectra of **1-CN** in 2-methyltetrahydrofuran solution ($c = 10^{-5}$ mol L⁻¹). Emission was monitored by excitation at the absorption maximum wavelength of 321 nm.

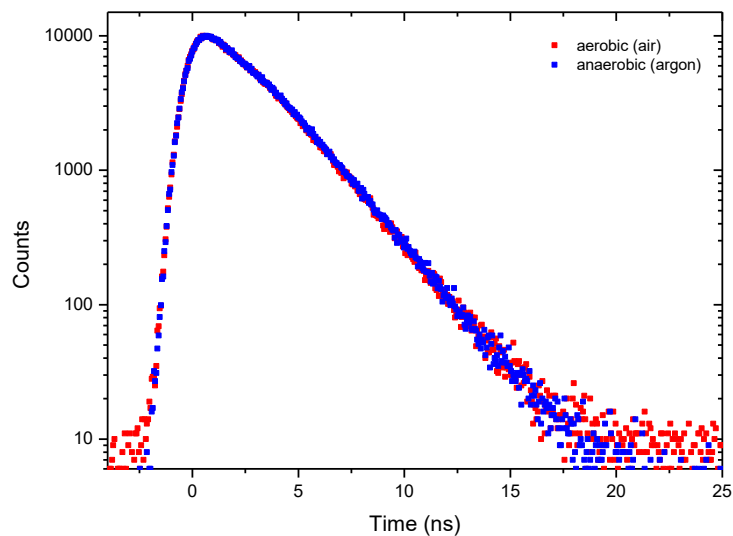


Figure S13: Fluorescence decay profile of **1-CN** in 2-methyltetrahydrofuran solution ($c = 10^{-5}$ mol L⁻¹) under aerobic (red dots) and anaerobic (blue dots; after argon bubbling for 30 minutes) conditions with excitation at 254 nm: Air: $\tau = 2.067 \pm 0.004$ ns; $\chi^2 = 1.569$. Argon: $\tau = 2.108 \pm 0.004$ ns; $\chi^2 = 1.292$.

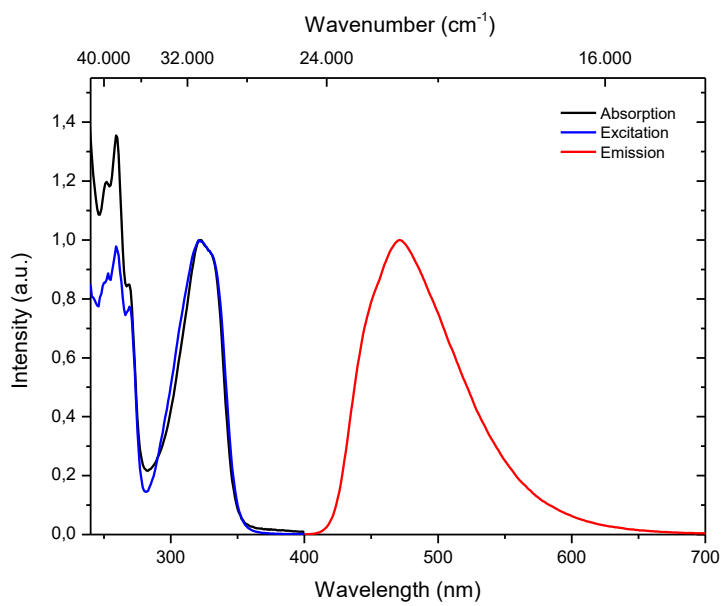


Figure S14: Normalized absorption (black line), excitation (blue line) and emission (red line) spectra of **1-CN** in dichloromethane solution ($c = 10^{-5} \text{ mol L}^{-1}$). Emission was monitored by excitation at the absorption maximum wavelength of 322 nm and excitation was monitored at fluorescence maximum wavelength of 471 nm.

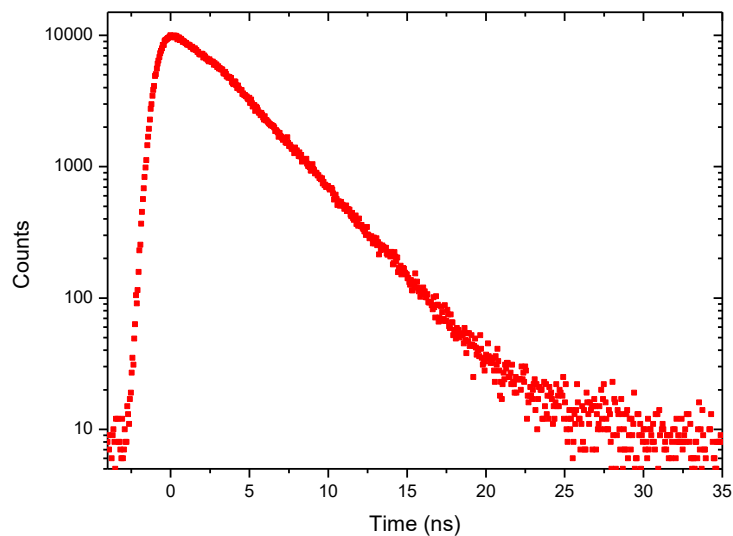


Figure S15: Fluorescence decay profile of **1-CN** in dichloromethane solution ($c = 10^{-5} \text{ mol L}^{-1}$) with excitation at 254 nm: $\tau = 3.085 \pm 0.005 \text{ ns}$; $\chi^2 = 1.376$.

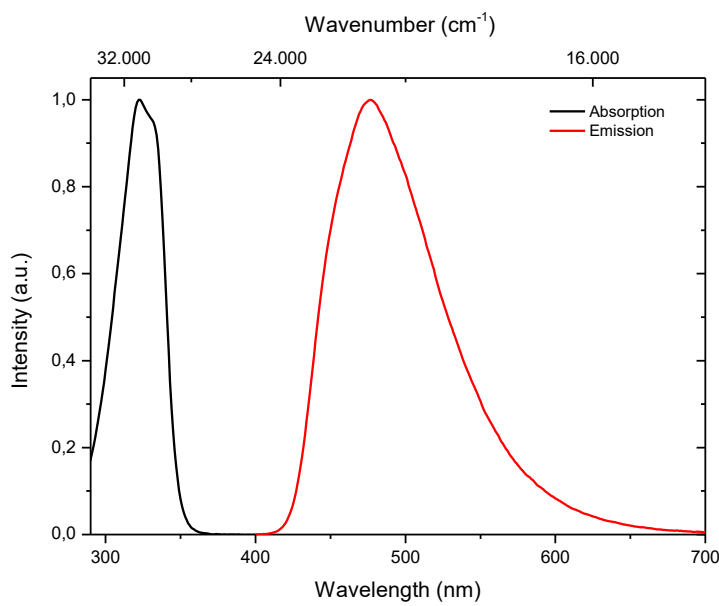


Figure S16: Normalized absorption (black line) and emission (red line) spectra of **1-CN** in toluene solution ($c = 10^{-5}$ mol L⁻¹). Emission was monitored by excitation at the absorption maximum wavelength of 322 nm.

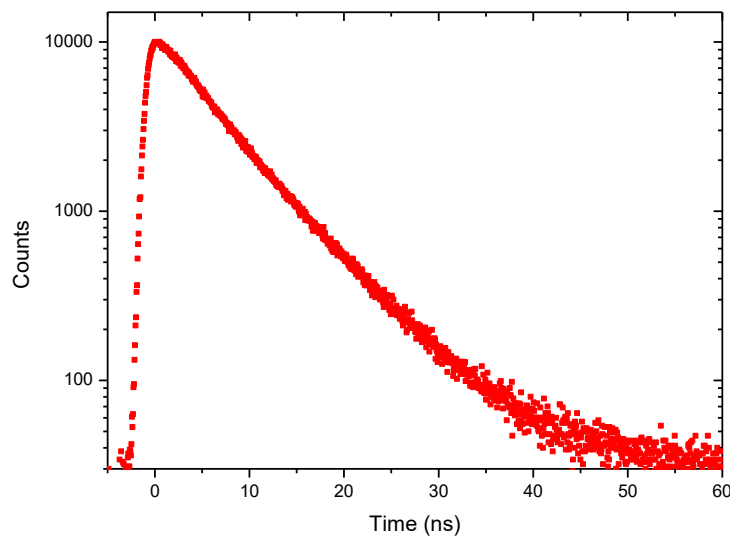


Figure S17: Fluorescence decay profile of **1-CN** in toluene solution ($c = 10^{-5}$ mol L⁻¹) with excitation at 254 nm: $\tau_1 = 2.31 \pm 0.05$ (21.5%) ns; $\tau_2 = 7.090 \pm 0.015$ (78.5%) ns; $\chi^2 = 1.283$.

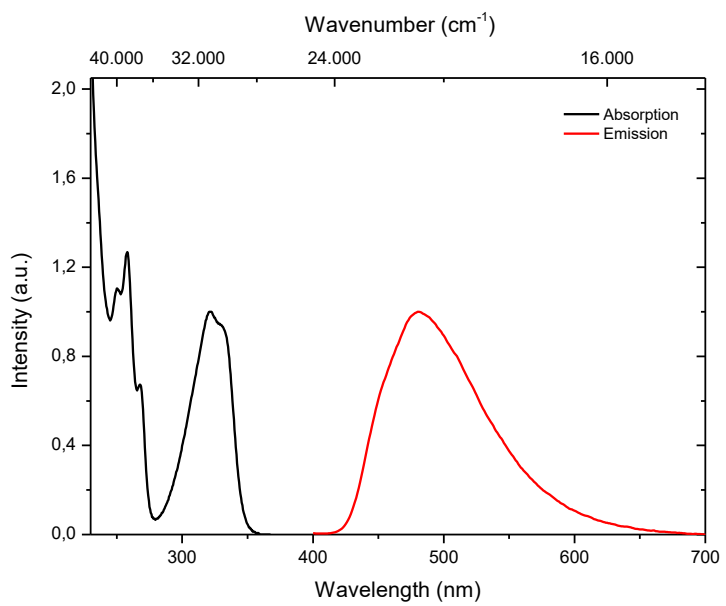


Figure S18: Normalized absorption (black line) and emission (red line) spectra of **1-CN** in cyclohexane solution ($c = 10^{-5} \text{ mol L}^{-1}$). Emission was monitored by excitation at the absorption maximum wavelength of 322 nm.

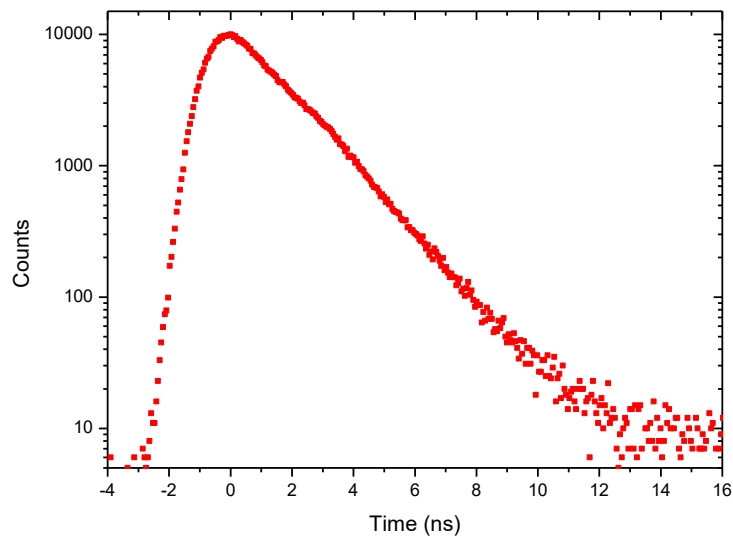


Figure S19: Fluorescence decay profile of **1-CN** in cyclohexane solution ($c = 10^{-5} \text{ mol L}^{-1}$) with excitation at 254 nm: $\tau = 1.125 \pm 0.004 \text{ ns}$; $\chi^2 = 1.254$.

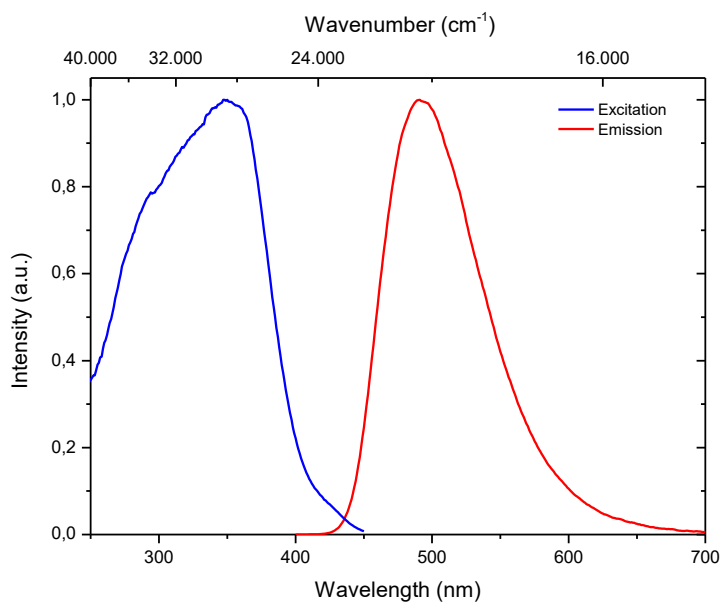


Figure S20: Normalized excitation (blue line) and emission (red line) spectra of **1-CN** in the solid-state. Emission was monitored by excitation at the absorption wavelength of 330 nm and excitation was monitored at fluorescence maximum wavelength of 491 nm.

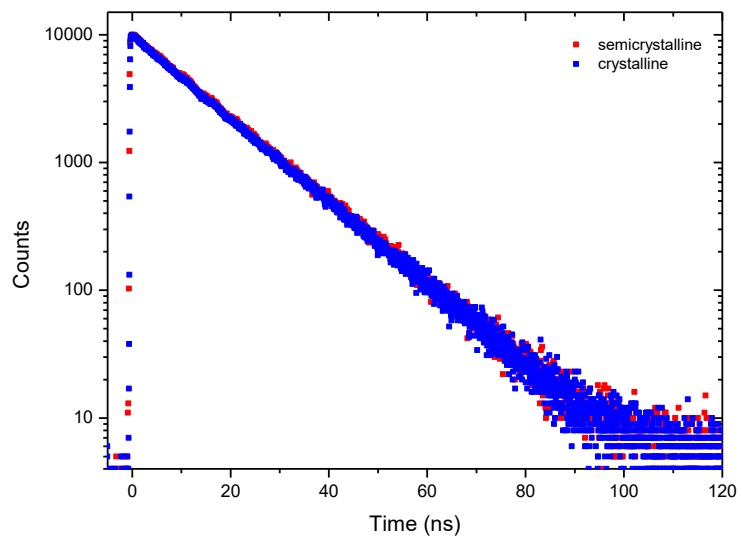


Figure S21: Fluorescence decay profile of **1-CN** in the semicrystalline state (red dots) and the crystalline state (blue dots) with excitation at 376 nm: Semicrystalline: $\tau = 13.430 \pm 0.012$ ns; $\chi^2 = 1.303$. Crystallin: $\tau = 13.310 \pm 0.008$ ns; $\chi^2 = 1.167$.

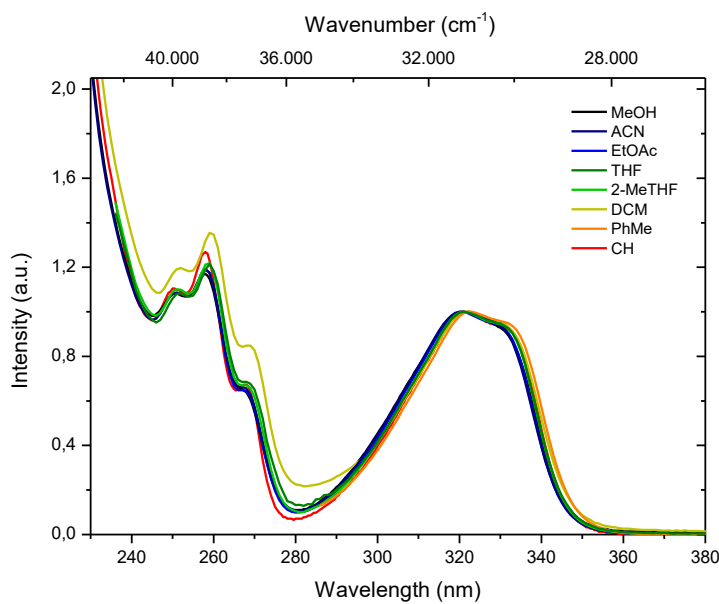


Figure S22: Normalized absorption spectra of **1-CN** in various solvents ($c = 10^{-5} \text{ mol L}^{-1}$) exhibiting differing polarities: methanol (MeOH, black line), acetonitrile (ACN, navy line), ethyl acetate (EtOAc, blue line), tetrahydrofuran (THF, olive line), 2-methyltetrahydrofuran (2-MeTHF, green line), dichloromethane (DCM, yellow line), toluene (PhMe, orange line) and cyclohexane (CH, red line).

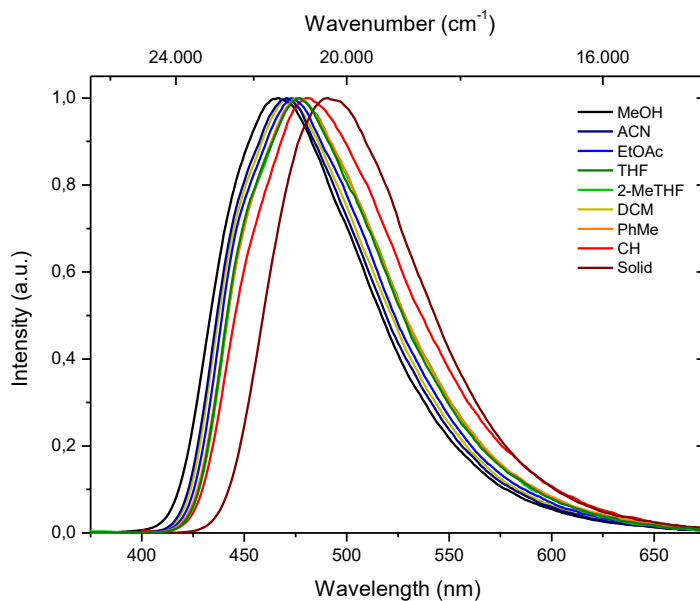


Figure S23: Normalized emission spectra of **1-CN** in various solvents ($c = 10^{-5} \text{ mol L}^{-1}$) exhibiting differing polarities as well as the solid-state: methanol (MeOH, black line), acetonitrile (ACN, navy line), ethyl acetate (EtOAc, blue line), tetrahydrofuran (THF, olive line), 2-methyltetrahydrofuran (2-MeTHF, green line), dichloromethane (DCM, yellow line), toluene (PhMe, orange line), cyclohexane (CH, red line) and solid-state (wine line).

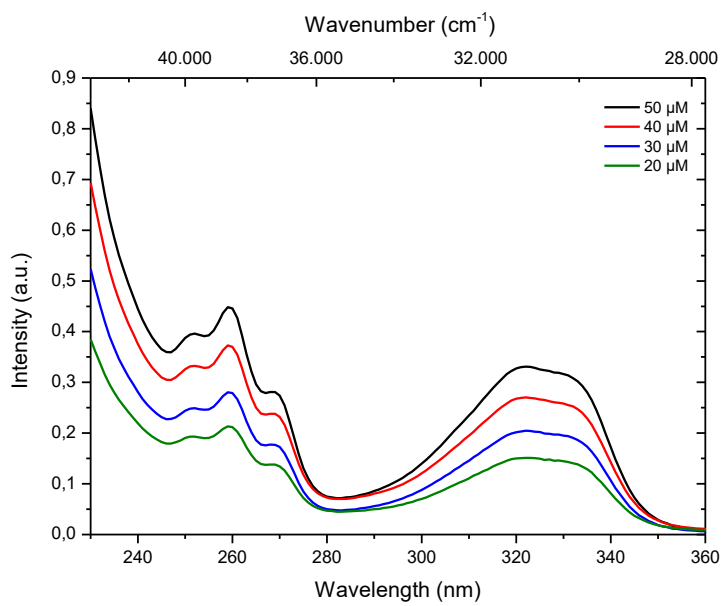


Figure S24: Absorption spectra of **1-CN** at various concentration in dichloromethane solution.

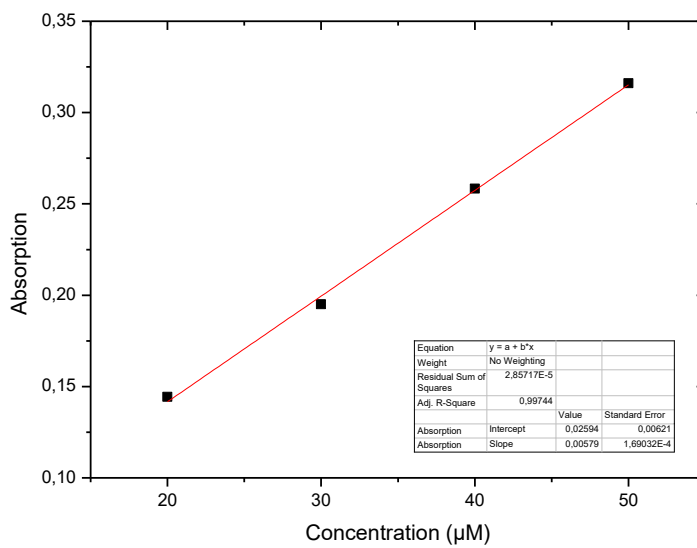


Figure S25: Linear regression for extinction coefficient determination (with respect to Figure S24): $\varepsilon_{322} = 5790 \text{ L mol}^{-1} \text{ cm}^{-1}$.

3.1.2 Temperature-Dependent Emission

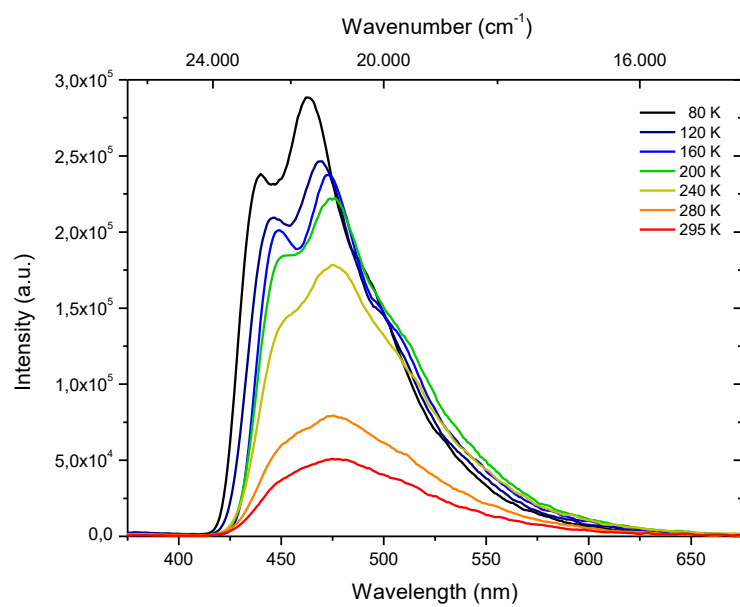


Figure S26: Temperature dependent emission spectra of **1-CN** in deaerated 2-methyltetrahydrofuran solution ($c = 10^{-5} \text{ mol L}^{-1}$) during heating from 80 K to 295 K with excitation at 321 nm.

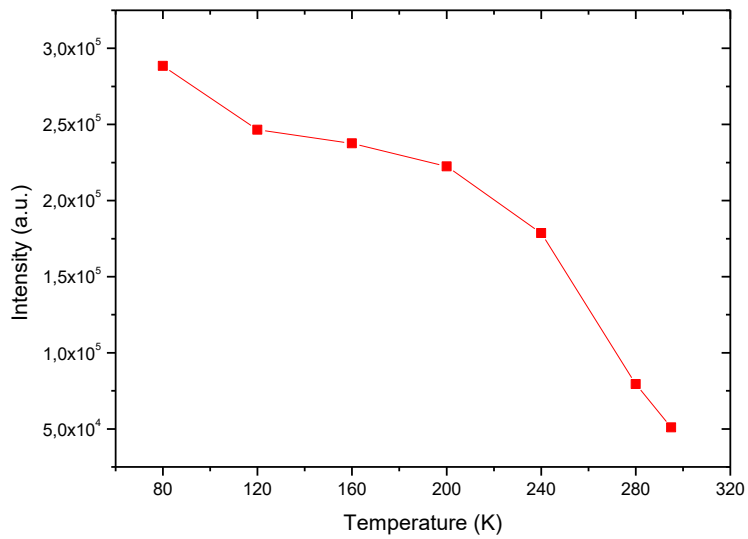


Figure S27: Temperature dependent intensity trend of **1-CN** using the maximum intensity at the given temperature (with respect to Figure S26). Compared to 295 K the emission intensity has multiplied by the factor of 5.65 at 80 K.

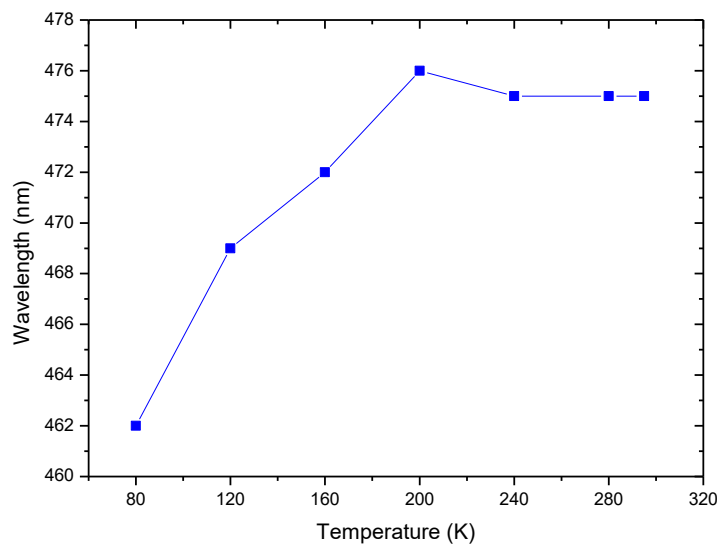


Figure S28: Temperature dependent wavelength trend of **1-CN** using the maximum intensity wavelength at the given temperature (with respect to Figure S26). Starting from 475 nm at 295 K the wavelength drops continuously to 462 nm at 80 K.

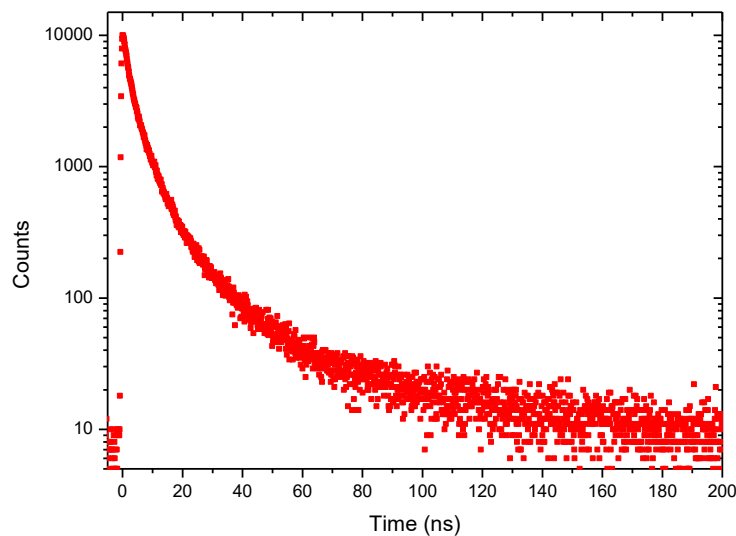


Figure S29: Fluorescence decay profile of **1-CN** in deaerated 2-methyltetrahydrofuran solution ($c = 10^{-5}$ mol L $^{-1}$) with excitation at 376 nm: $\tau_1 = 2.22 \pm 0.03$ (36.4%) ns; $\tau_2 = 8.17 \pm 0.09$ (51.7%) ns; $\tau_3 = 44.0 \pm 0.8$ (11.9%) ns; $\chi^2 = 1.265$.

3.1.3 Emission Properties in Doped PMMA Films

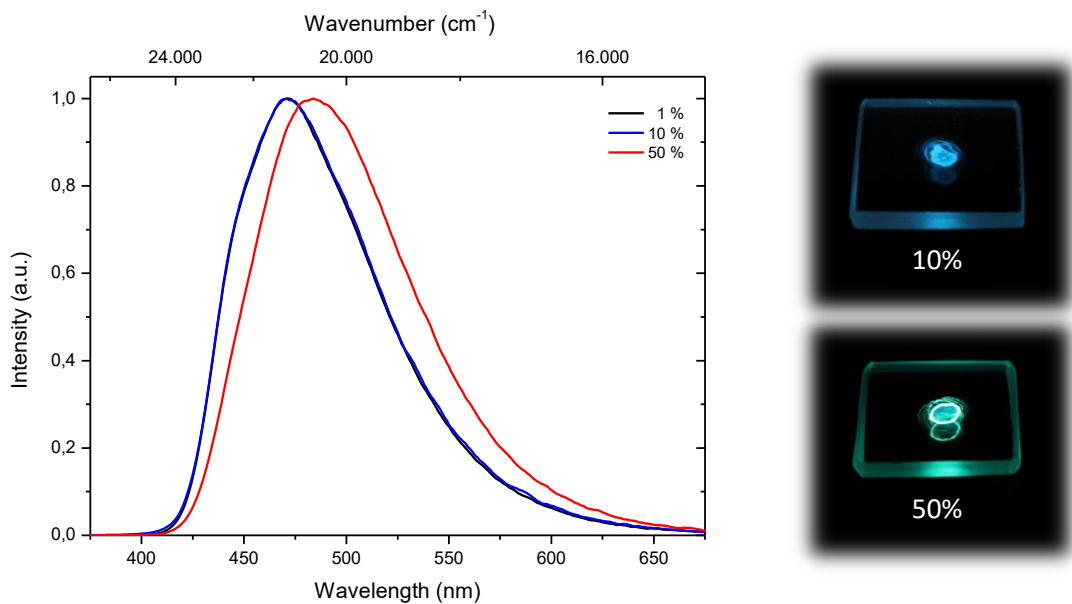


Figure S30: Left: Normalized emission spectra of PMMA films doped with different weight concentration of **1-CN** (1% – black line; 10% – blue line; 50% – red line). Films were prepared *via* drop-cast method of a dichloromethane solution ($c = 10^{-3}$ mol L $^{-1}$) on a glass slide. Right: Representative images of PMMA films containing 10wt% (top) and 50wt% (bottom) of **1-CN**, respectively.

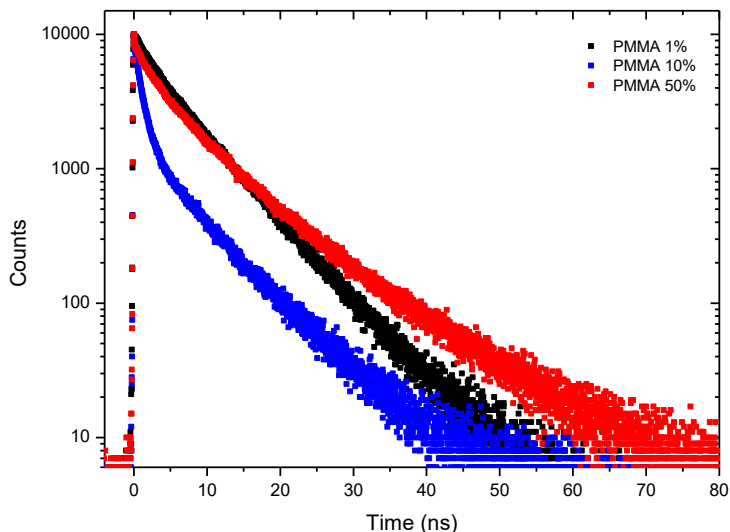


Figure S31: Fluorescence decay profile of PMMA films doped with different weight concentration of **1-CN** (1% – black dots; 10% – blue dots; 50% – red dots) with excitation at 376 nm.
 1%-Film: $\tau_1 = 2.61 \pm 0.04$ (14.5%) ns; $\tau_2 = 7.174 \pm 0.014$ (85.5%) ns; $\chi^2 = 1.135$.
 10%-Film: $\tau_1 = 1.027 \pm 0.004$ (40.0%) ns; $\tau_2 = 7.543 \pm 0.018$ (60.0%) ns; $\chi^2 = 1.283$.
 50%-Film: $\tau_1 = 3.89 \pm 0.03$ (35.5%) ns; $\tau_2 = 10.80 \pm 0.04$ (64.5%) ns; $\chi^2 = 1.419$.

3.2 3-(4,4-Dimethyl-4,5-dihydrooxazol-2-yl)-4-hydroxybenzonitrile (2-CN)

3.2.1 Absorption and Emission Properties in Solution and Solid-State

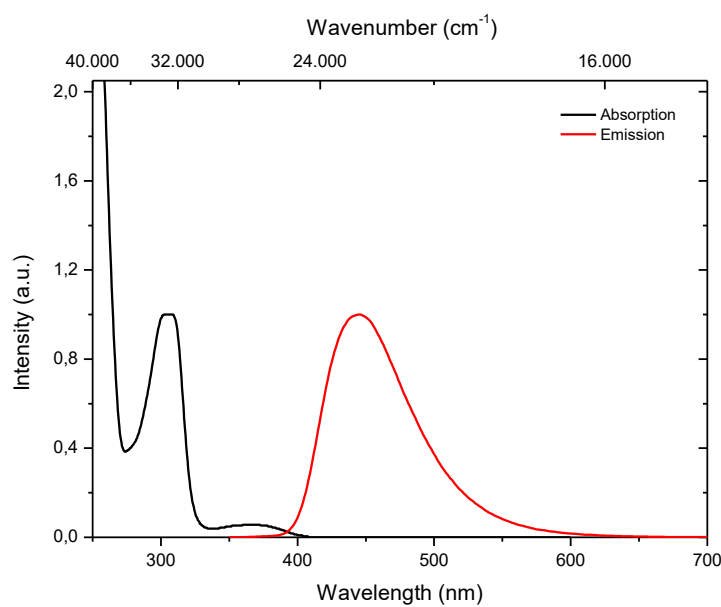


Figure S32: Normalized absorption (black line) and emission (red line) spectra of **2-CN** in methanol solution ($c = 10^{-5} \text{ mol L}^{-1}$). Emission was monitored by excitation at the absorption maximum wavelength of 303 nm.

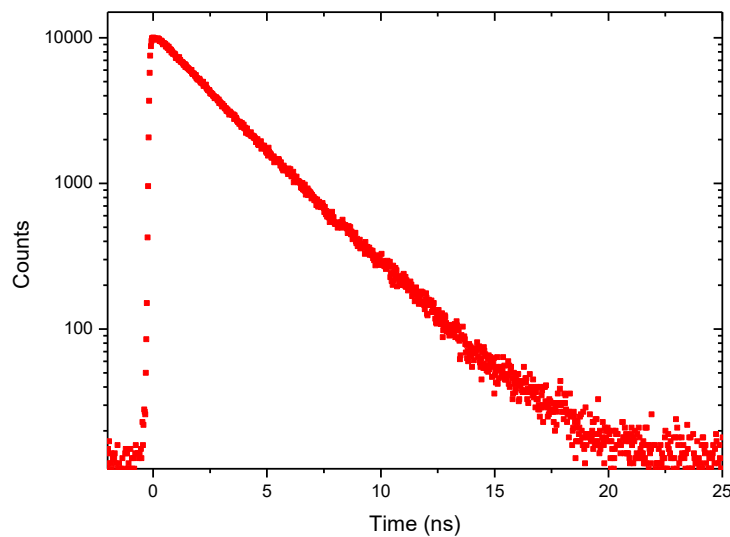


Figure S33: Fluorescence decay profile of **2-CN** in methanol solution ($c = 10^{-5} \text{ mol L}^{-1}$) with excitation at 376 nm: $\tau = 2.706 \pm 0.003 \text{ ns}$; $\chi^2 = 1.217$.

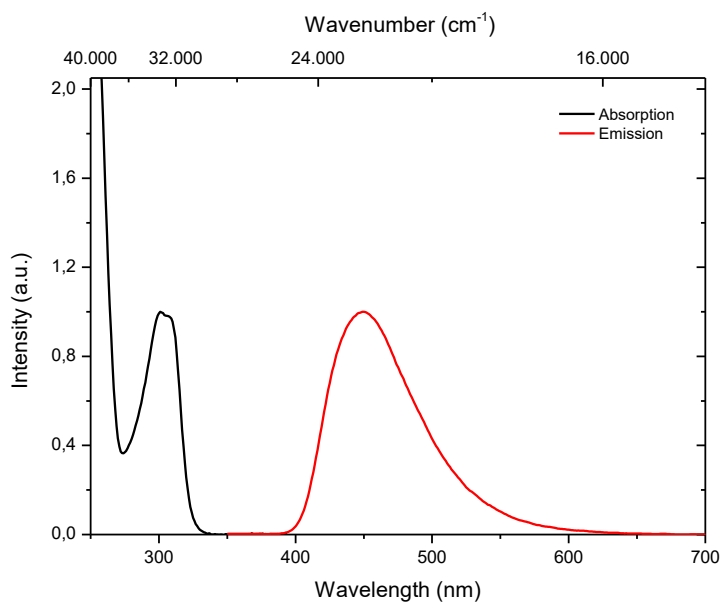


Figure S34: Normalized absorption (black line) and emission (red line) spectra of **2-CN** in acetonitrile solution ($c = 10^{-5} \text{ mol L}^{-1}$). Emission was monitored by excitation at the absorption maximum wavelength of 301 nm.

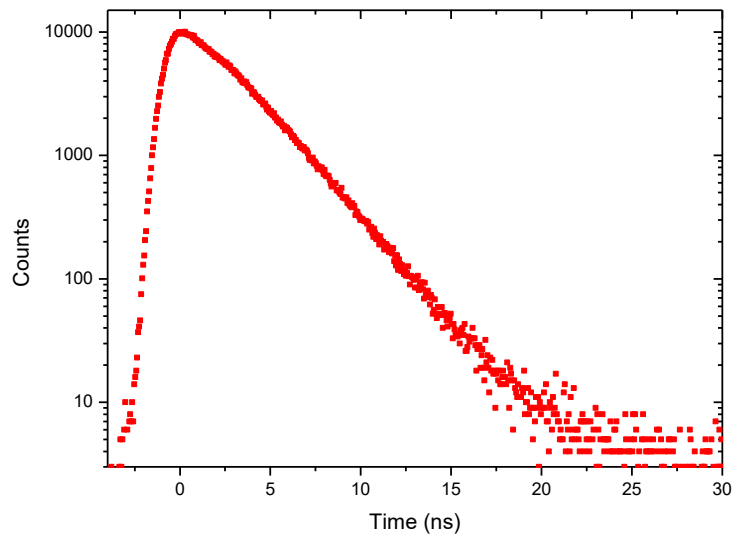


Figure S35: Fluorescence decay profile of **2-CN** in acetonitrile solution ($c = 10^{-5} \text{ mol L}^{-1}$) with excitation at 254 nm: $\tau = 2.351 \pm 0.004 \text{ ns}$; $\chi^2 = 1.379$.

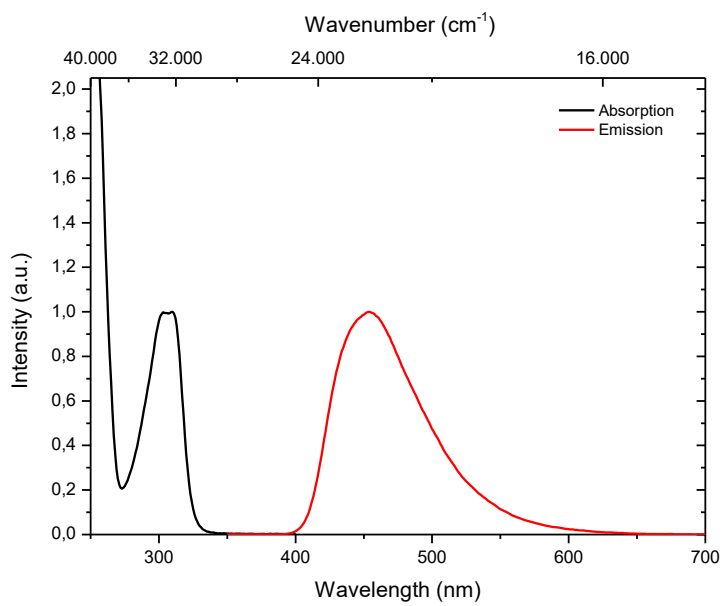


Figure S36: Normalized absorption (black line) and emission (red line) spectra of **2-CN** in ethyl acetate solution ($c = 10^{-5}$ mol L⁻¹). Emission was monitored by excitation at the absorption maximum wavelength of 303 nm.

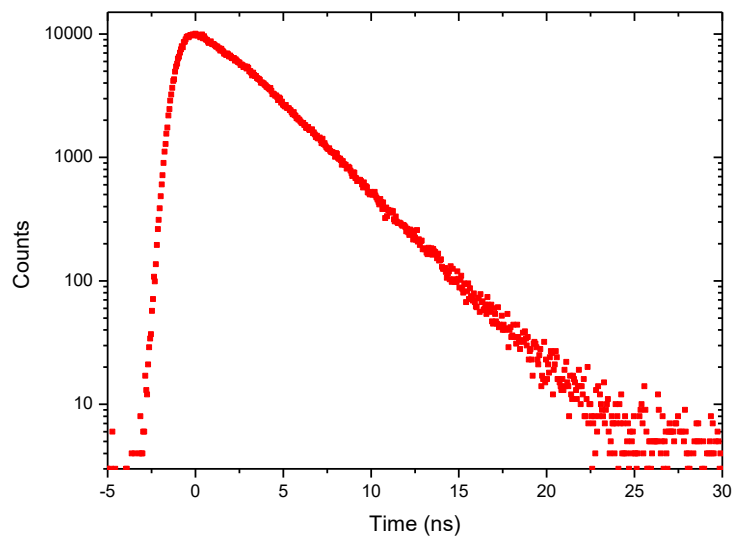


Figure S37: Fluorescence decay profile of **2-CN** in ethyl acetate solution ($c = 10^{-5}$ mol L⁻¹) with excitation at 254 nm: $\tau = 2.857 \pm 0.004$ ns; $\chi^2 = 1.264$.

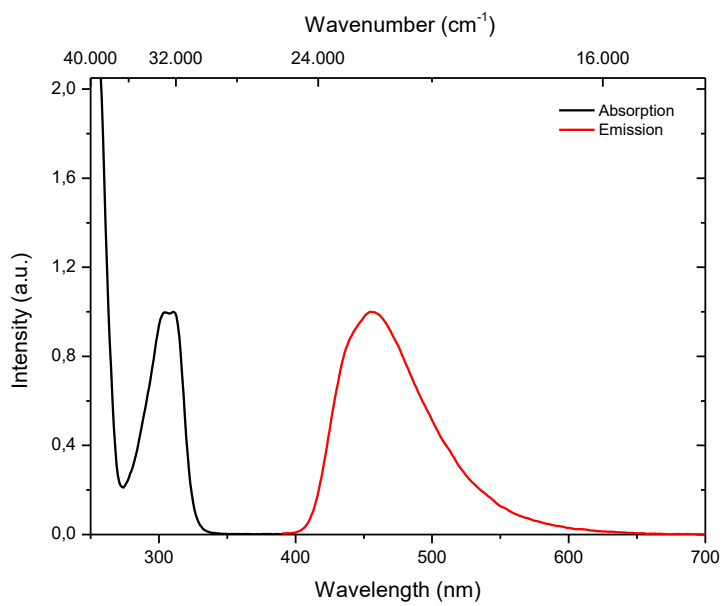


Figure S38: Normalized absorption (black line) and emission (red line) spectra of **2-CN** in 2-methyltetrahydrofuran solution ($c = 10^{-5} \text{ mol L}^{-1}$). Emission was monitored by excitation at the absorption maximum wavelength of 304 nm.

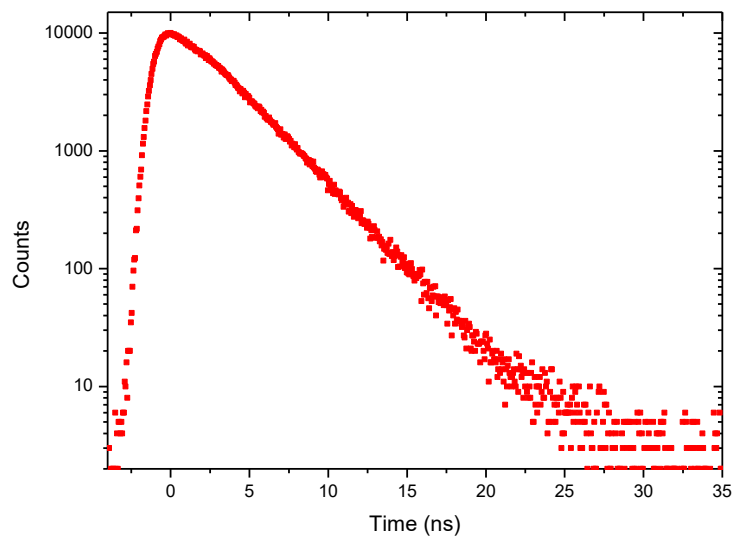


Figure S39: Fluorescence decay profile of **2-CN** in 2-methyltetrahydrofuran solution ($c = 10^{-5} \text{ mol L}^{-1}$) with excitation at 254 nm: $\tau = 2.880 \pm 0.005 \text{ ns}$; $\chi^2 = 1.394$.

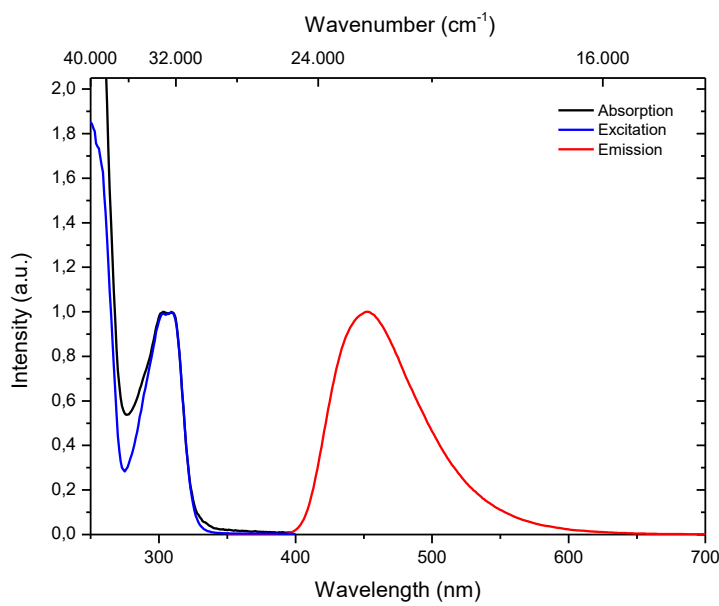


Figure S40: Normalized absorption (black line), excitation (blue line) and emission (red line) spectra of **2-CN** in dichloromethane solution ($c = 10^{-5} \text{ mol L}^{-1}$). Emission was monitored by excitation at the absorption maximum wavelength of 303 nm and excitation was monitored at fluorescence maximum wavelength of 452 nm.

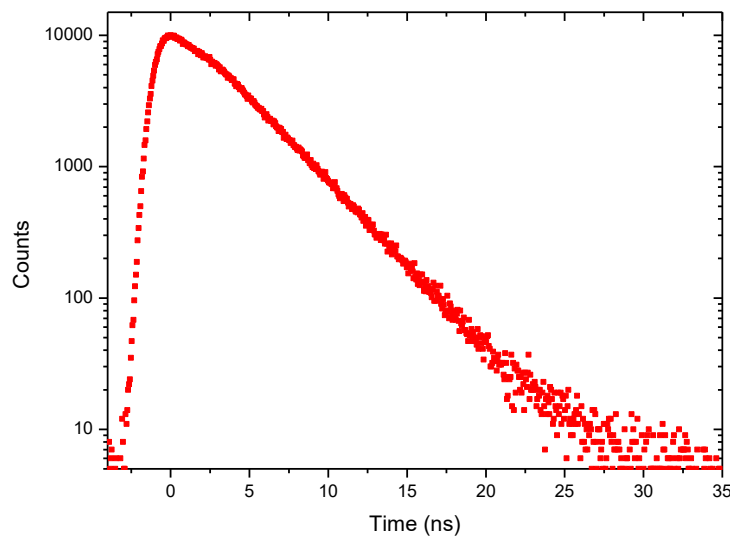


Figure S41: Fluorescence decay profile of **2-CN** in dichloromethane solution ($c = 10^{-5} \text{ mol L}^{-1}$) with excitation at 254 nm: $\tau = 3.296 \pm 0.004 \text{ ns}$; $\chi^2 = 1.193$.

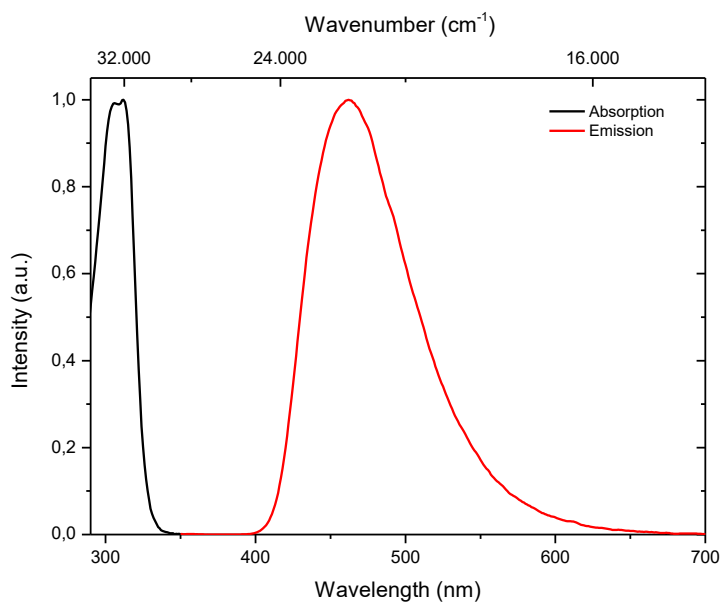


Figure S42: Normalized absorption (black line) and emission (red line) spectra of **2-CN** in toluene solution ($c = 10^{-5}$ mol L⁻¹). Emission was monitored by excitation at the absorption maximum wavelength of 306 nm.

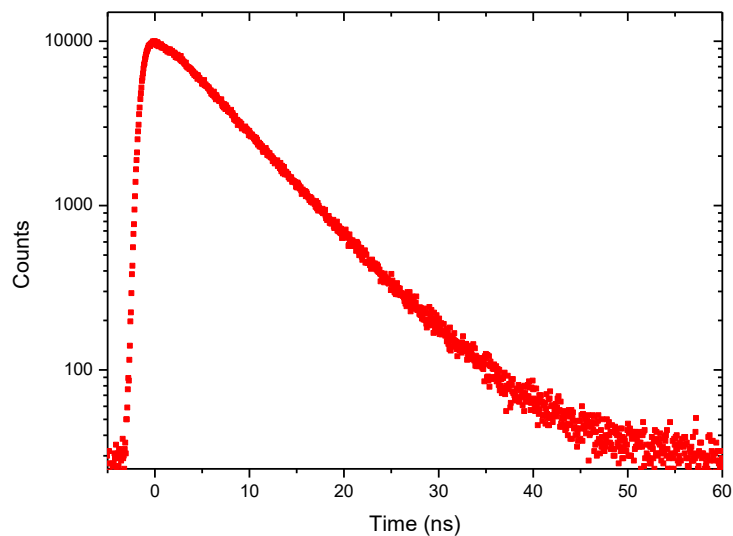


Figure S43: Fluorescence decay profile of **2-CN** in toluene solution ($c = 10^{-5}$ mol L⁻¹) with excitation at 254 nm: $\tau = 6.738 \pm 0.008$ ns; $\chi^2 = 1.660$.

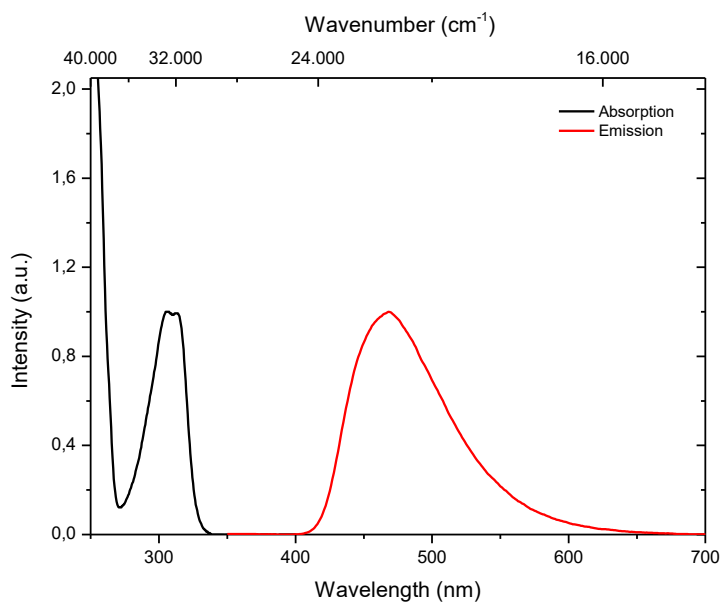


Figure S44: Normalized absorption (black line) and emission (red line) spectra of **2-CN** in cyclohexane solution ($c = 10^{-5} \text{ mol L}^{-1}$). Emission was monitored by excitation at the absorption maximum wavelength of 306 nm.

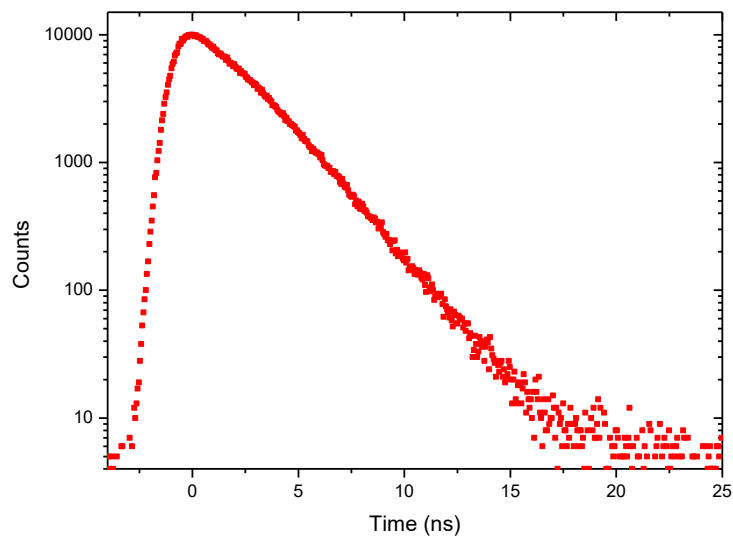


Figure S45: Fluorescence decay profile of **2-CN** in cyclohexane solution ($c = 10^{-5} \text{ mol L}^{-1}$) with excitation at 254 nm: $\tau = 2.035 \pm 0.004 \text{ ns}$; $\chi^2 = 1.198$.

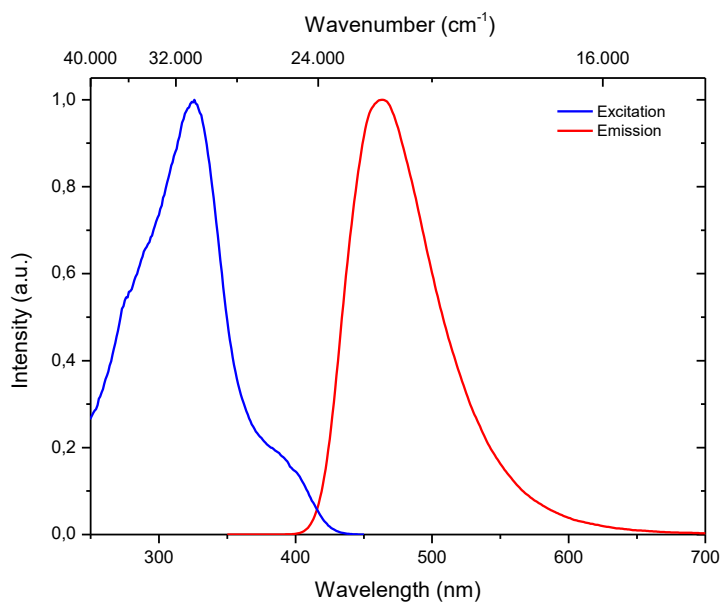


Figure S46: Normalized excitation (blue line) and emission (red line) spectra of **2-CN** in the solid-state. Emission was monitored by excitation at the absorption wavelength of 309 nm and excitation was monitored at fluorescence maximum wavelength of 463 nm.

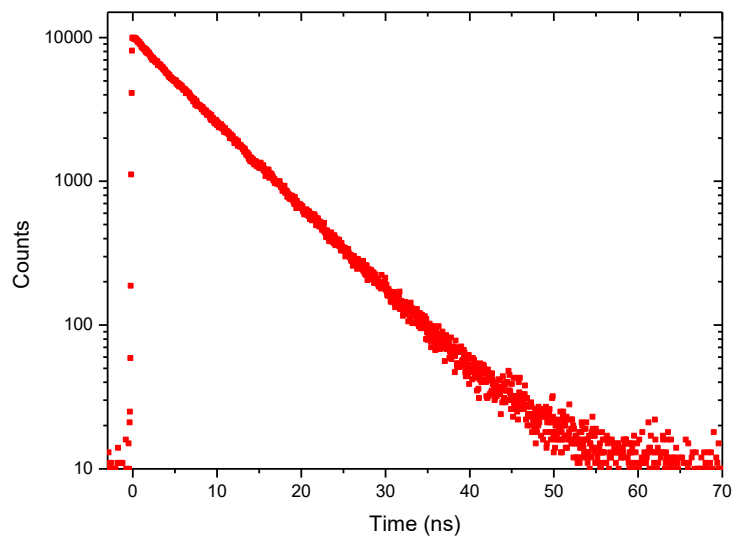


Figure S47: Fluorescence decay profile of **2-CN** in the crystalline state with excitation at 376 nm: $\tau = 7.354 \pm 0.006$ ns; $\chi^2 = 1.131$.

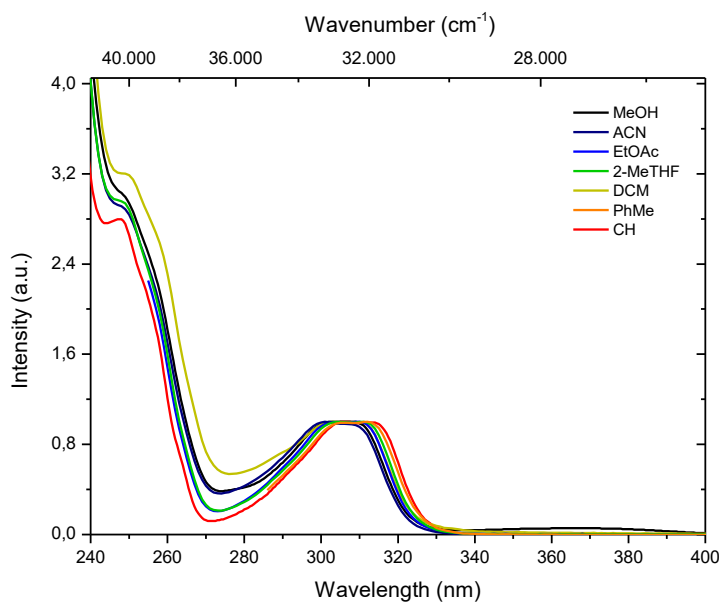


Figure S48: Normalized absorption spectra of **2-CN** in various solvents ($c = 10^{-5}$ mol L⁻¹) exhibiting differing polarities: methanol (MeOH, black line), acetonitrile (ACN, navy line), ethyl acetate (EtOAc, blue line), 2-methyltetrahydrofuran (2-MeTHF, green line), dichloromethane (DCM, yellow line), toluene (PhMe, orange line) and cyclohexane (CH, red line).

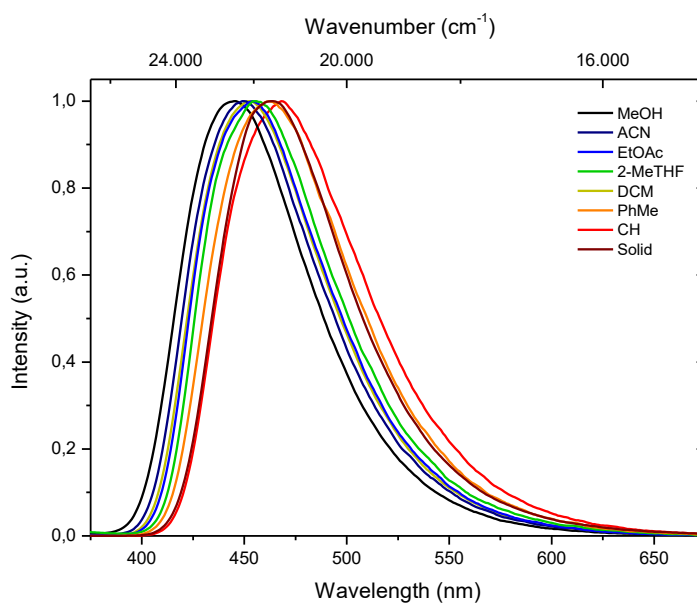


Figure S49: Normalized emission spectra of **2-CN** in various solvents ($c = 10^{-5}$ mol L⁻¹) exhibiting differing polarities as well as the solid-state: methanol (MeOH, black line), acetonitrile (ACN, navy line), ethyl acetate (EtOAc, blue line), 2-methyltetrahydrofuran (2-MeTHF, green line), dichloromethane (DCM, yellow line), toluene (PhMe, orange line), cyclohexane (CH, red line) and solid-state (wine line).

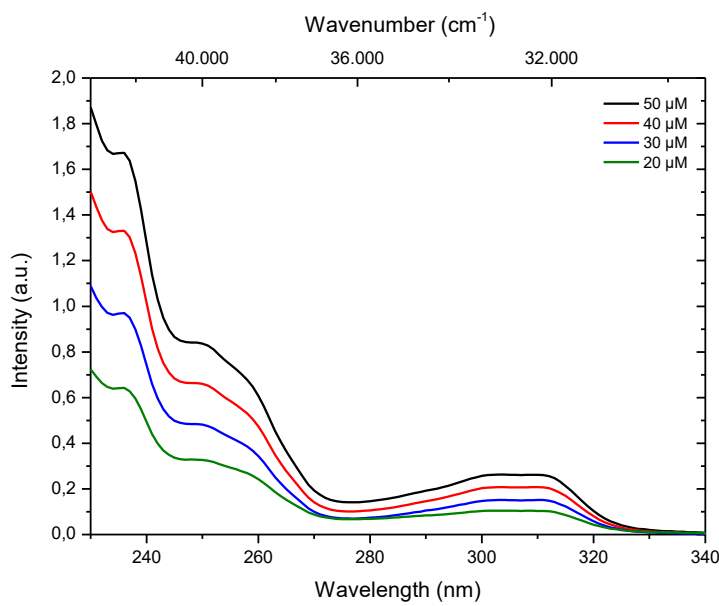


Figure S50: Absorption spectra of **2-CN** at various concentration in dichloromethane solution.

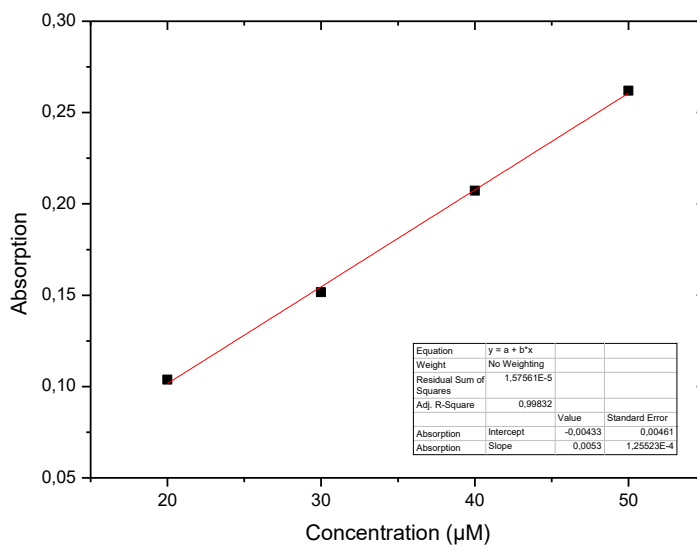


Figure S51: Linear regression for extinction coefficient determination (with respect to Figure S50): $\varepsilon_{303} = 5300 \text{ L mol}^{-1} \text{ cm}^{-1}$.

3.2.2 Temperature-Dependent Emission

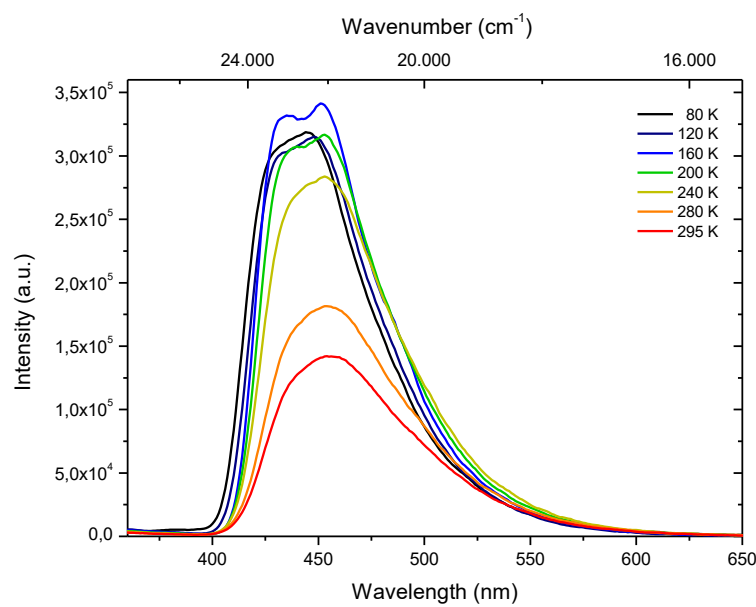


Figure S52: Temperature dependent emission spectra of **2-CN** in deaerated 2-methyltetrahydrofuran solution ($c = 10^{-5} \text{ mol L}^{-1}$) during heating from 80 K to 295 K with excitation at 304 nm.

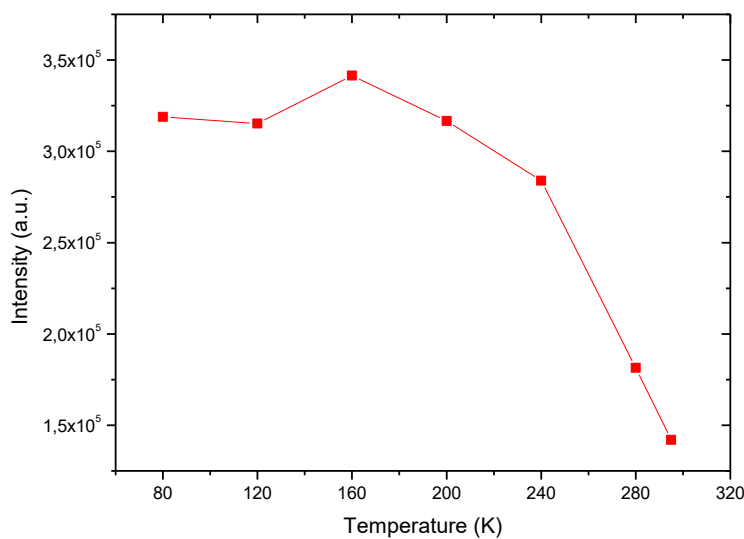


Figure S53: Temperature dependent intensity trend of **2-CN** using the maximum intensity at the given temperature (with respect to Figure S52). Compared to 295 K the emission intensity has multiplied by the factor of 2.40 at 160 K and 2.24 at 80 K, respectively.

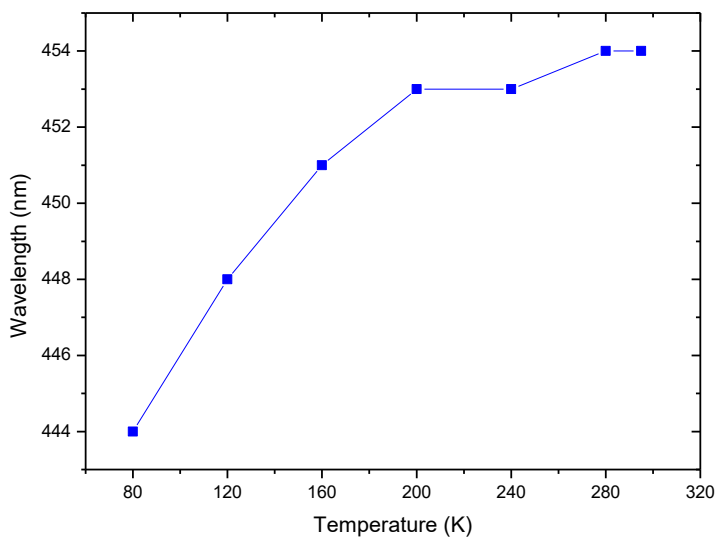


Figure S54: Temperature dependent wavelength trend of **2-CN** using the maximum intensity wavelength at the given temperature (with respect to Figure S52). Starting from 454 nm at 295 K the wavelength drops continuously to 444 nm at 80 K.

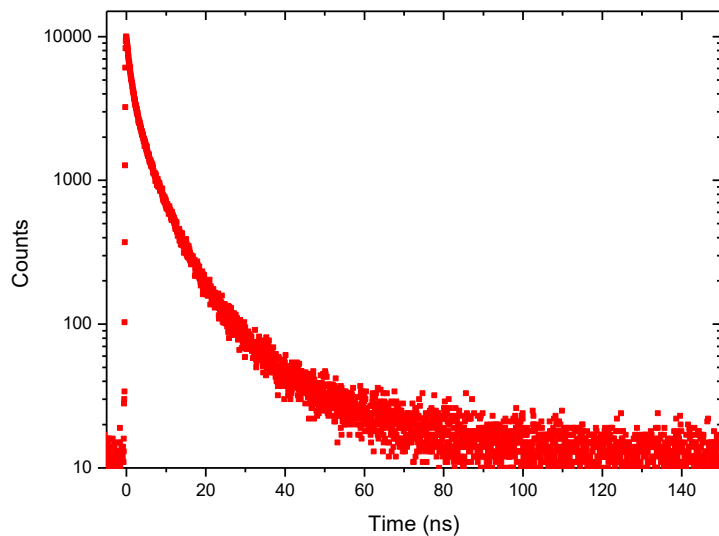


Figure S55: Fluorescence decay profile of **2-CN** in deaerated 2-methyltetrahydrofuran solution ($c = 10^{-5}$ mol L⁻¹) with excitation at 376 nm: $\tau_1 = 1.221 \pm 0.014$ (24.2%) ns; $\tau_2 = 5.58 \pm 0.05$ (61.6%) ns; $\tau_3 = 23.0 \pm 0.4$ (14.2%) ns; $\chi^2 = 1.123$.

3.3 4-(4,4-Dimethyl-4,5-dihydrooxazol-2-yl)-3-hydroxybenzonitrile (3-CN)

3.3.1 Absorption and Emission Properties in Solution and Solid-State

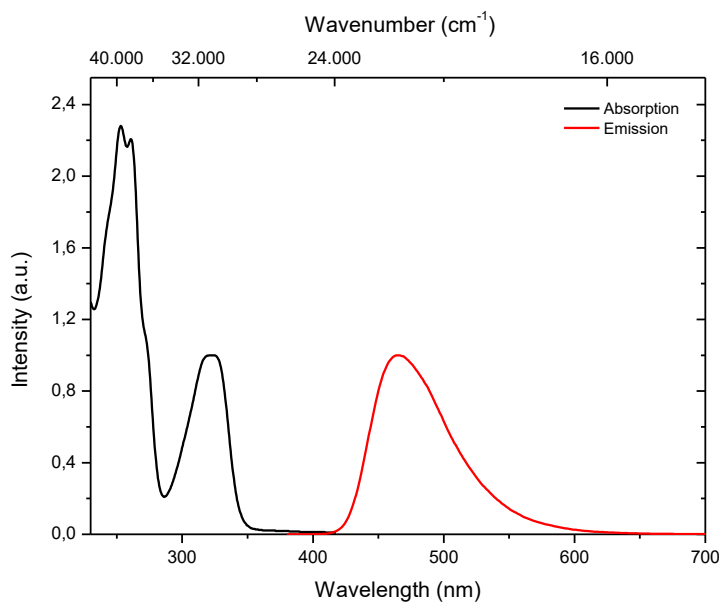


Figure S56: Normalized absorption (black line) and emission (red line) spectra of **3-CN** in methanol solution ($c = 10^{-5}$ mol L $^{-1}$). Emission was monitored by excitation at the absorption maximum wavelength of 323 nm.

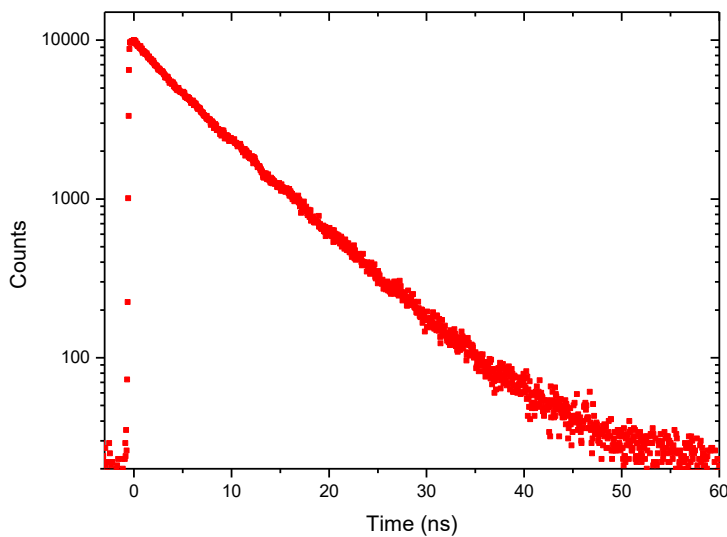


Figure S57: Fluorescence decay profile of **3-CN** in methanol solution ($c = 10^{-5}$ mol L $^{-1}$) with excitation at 376 nm: $\tau_1 = 2.53 \pm 0.12$ (5.5%) ns; $\tau_2 = 7.596 \pm 0.019$ (94.5%) ns; $\chi^2 = 1.225$.

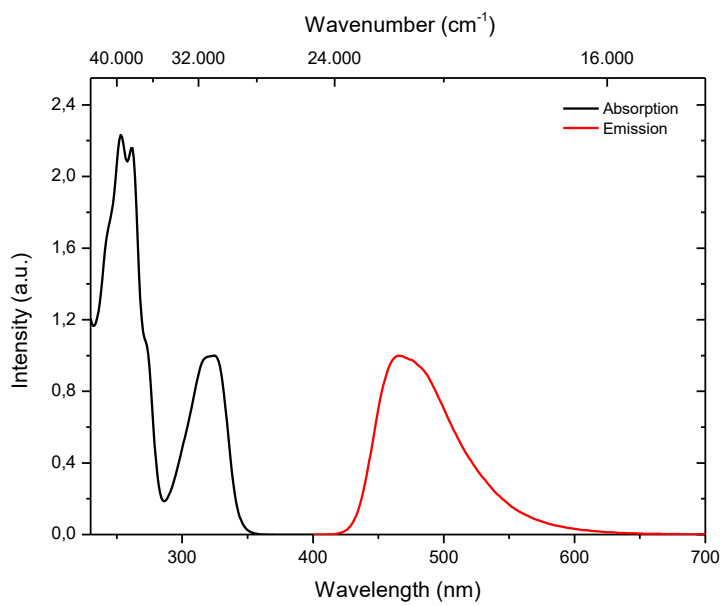


Figure S58: Normalized absorption (black line) and emission (red line) spectra of **3-CN** in acetonitrile solution ($c = 10^{-5} \text{ mol L}^{-1}$). Emission was monitored by excitation at the absorption maximum wavelength of 324 nm.

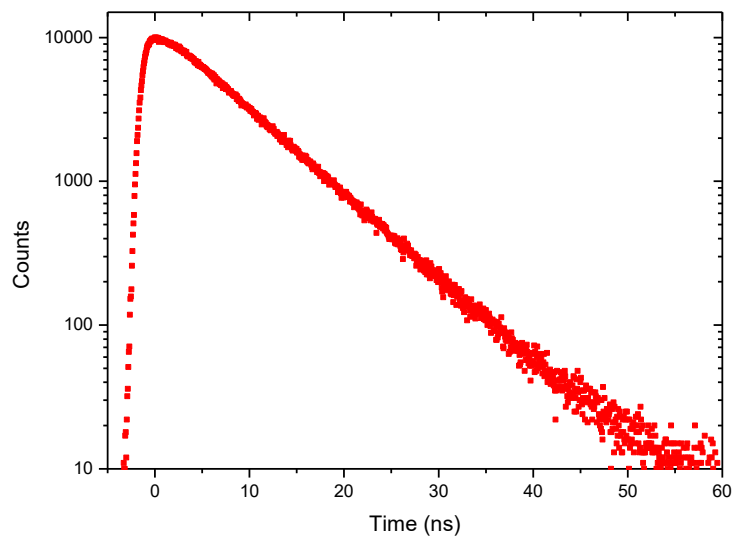


Figure S59: Fluorescence decay profile of **3-CN** in acetonitrile solution ($c = 10^{-5} \text{ mol L}^{-1}$) with excitation at 254 nm: $\tau = 7.290 \pm 0.007 \text{ ns}$; $\chi^2 = 1.329$.

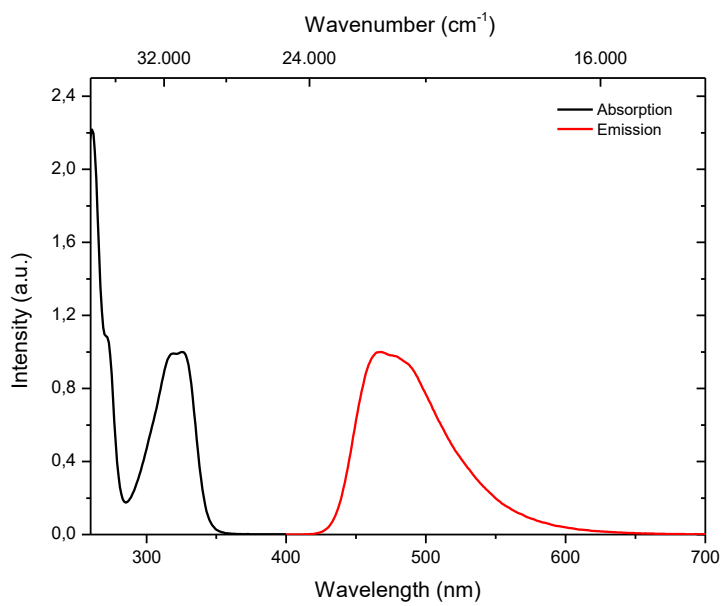


Figure S60: Normalized absorption (black line) and emission (red line) spectra of **3-CN** in ethyl acetate solution ($c = 10^{-5} \text{ mol L}^{-1}$). Emission was monitored by excitation at the absorption maximum wavelength of 326 nm.

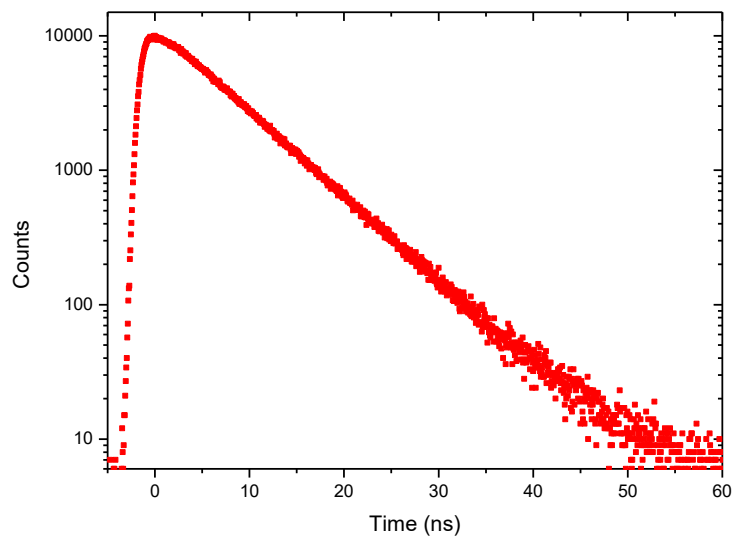


Figure S61: Fluorescence decay profile of **3-CN** in ethyl acetate solution ($c = 10^{-5} \text{ mol L}^{-1}$) with excitation at 254 nm: $\tau = 6.751 \pm 0.006 \text{ ns}$; $\chi^2 = 1.250$.

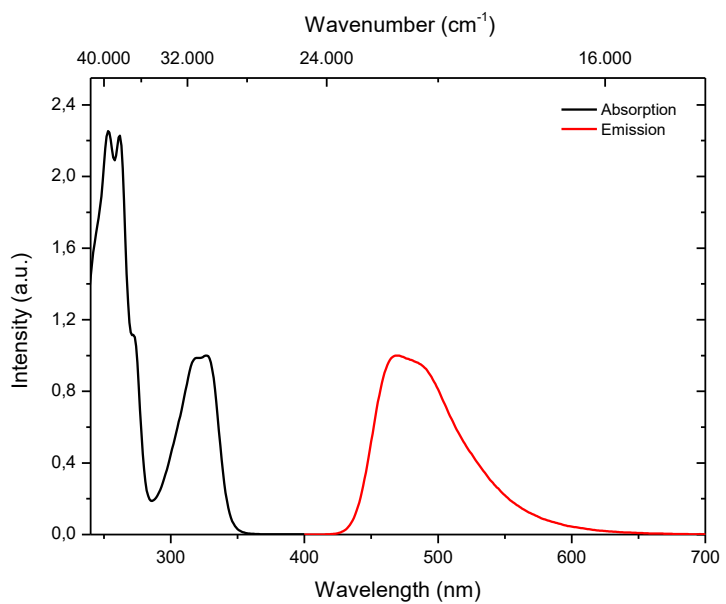


Figure S62: Normalized absorption (black line) and emission (red line) spectra of **3-CN** in 2-methyltetrahydrofuran solution ($c = 10^{-5} \text{ mol L}^{-1}$). Emission was monitored by excitation at the absorption maximum wavelength of 327 nm.

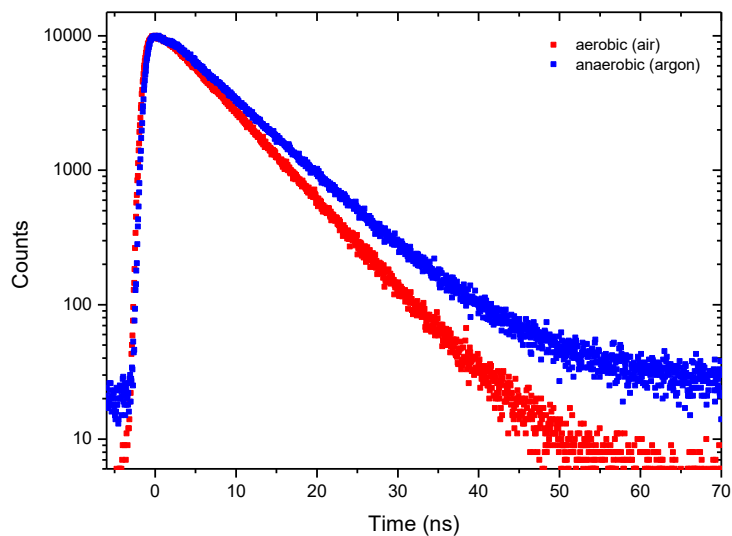


Figure S63: Fluorescence decay profile of **3-CN** in 2-methyltetrahydrofuran solution ($c = 10^{-5} \text{ mol L}^{-1}$) under aerobic (red dots) and anaerobic (blue dots; after argon bubbling for 30 minutes) conditions with excitation at 254 nm: Air: $\tau = 6.528 \pm 0.006 \text{ ns}; \chi^2 = 1.304$. Argon: $\tau = 7.667 \pm 0.008 \text{ ns}; \chi^2 = 1.742$.

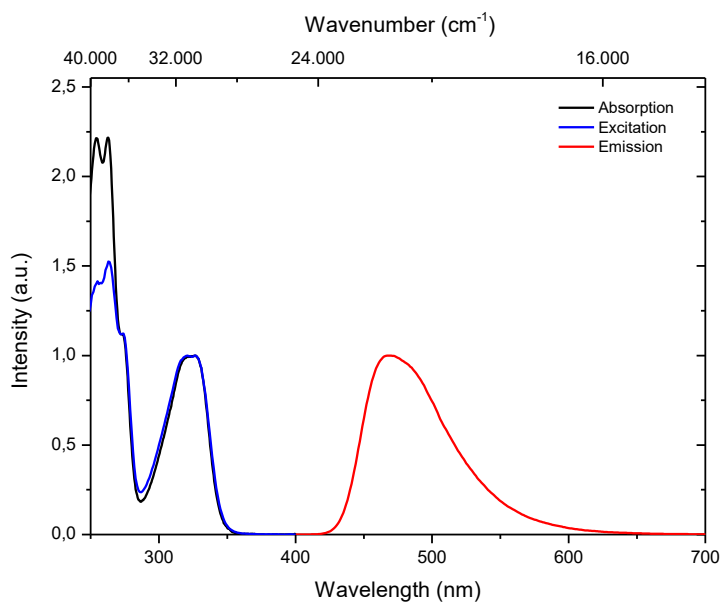


Figure S64: Normalized absorption (black line), excitation (blue line) and emission (red line) spectra of **3-CN** in dichloromethane solution ($c = 10^{-5} \text{ mol L}^{-1}$). Emission was monitored by excitation at the absorption maximum wavelength of 326 nm and excitation was monitored at fluorescence maximum wavelength of 468 nm.

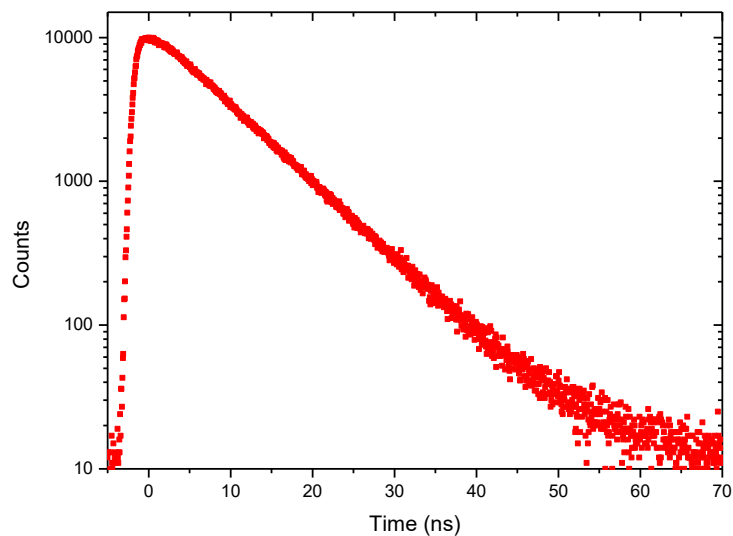


Figure S65: Fluorescence decay profile of **3-CN** in dichloromethane solution ($c = 10^{-5} \text{ mol L}^{-1}$) with excitation at 254 nm: $\tau = 8.103 \pm 0.011 \text{ ns}$; $\chi^2 = 1.335$.

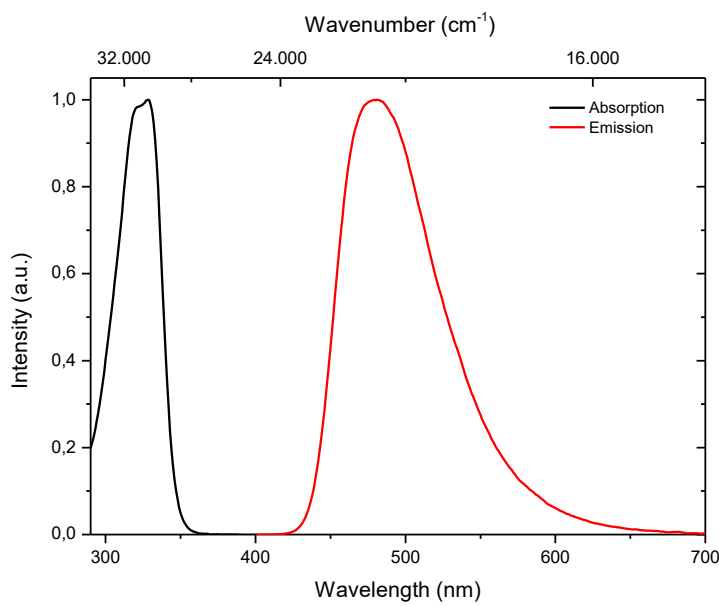


Figure S66: Normalized absorption (black line) and emission (red line) spectra of **3-CN** in toluene solution ($c = 10^{-5}$ mol L⁻¹). Emission was monitored by excitation at the absorption maximum wavelength of 328 nm.

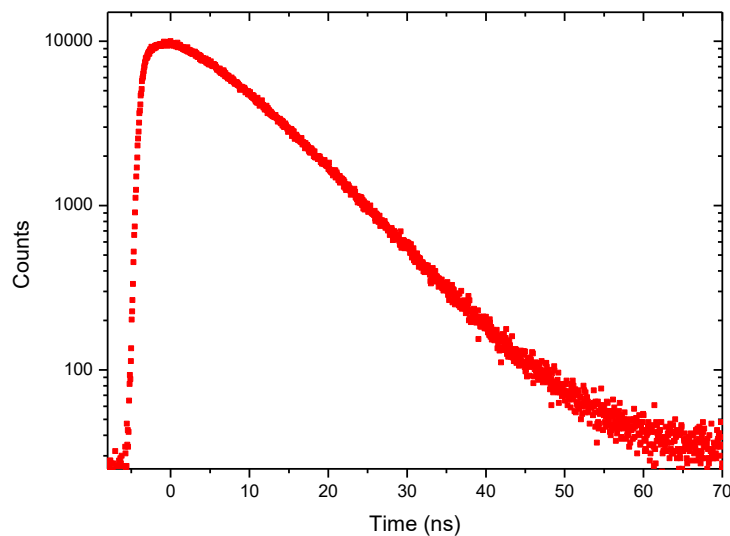


Figure S67: Fluorescence decay profile of **3-CN** in toluene solution ($c = 10^{-5}$ mol L⁻¹) with excitation at 254 nm: $\tau = 8.946 \pm 0.019$ ns; $\chi^2 = 1.714$.

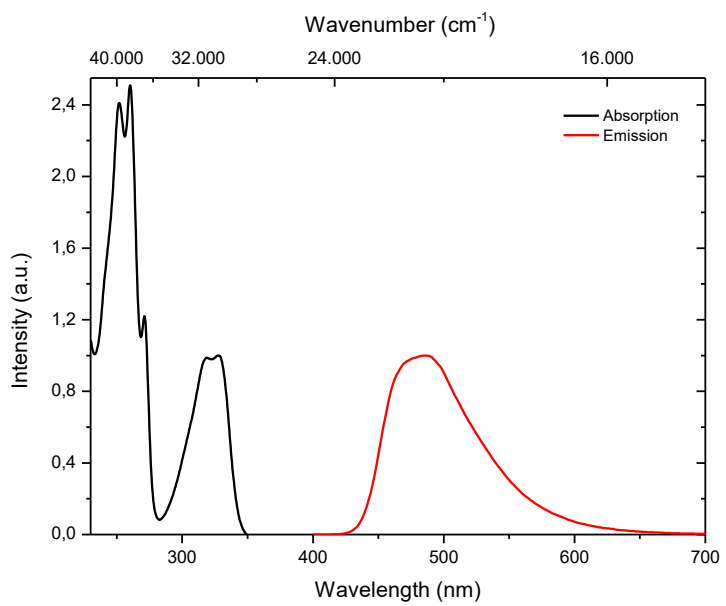


Figure S68: Normalized absorption (black line) and emission (red line) spectra of **3-CN** in cyclohexane solution ($c = 10^{-5}$ mol L⁻¹). Emission was monitored by excitation at the absorption maximum wavelength of 327 nm.

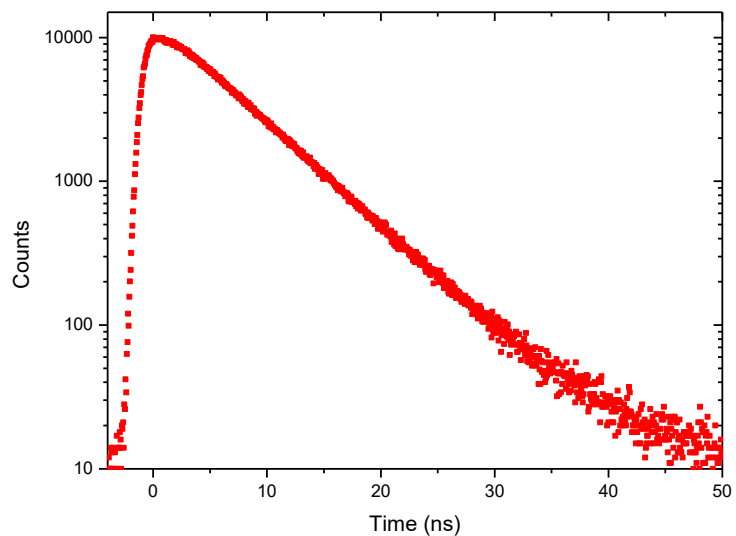


Figure S69: Fluorescence decay profile of **3-CN** in cyclohexane solution ($c = 10^{-5}$ mol L⁻¹) with excitation at 254 nm: $\tau = 6.017 \pm 0.007$ ns; $\chi^2 = 1.175$.

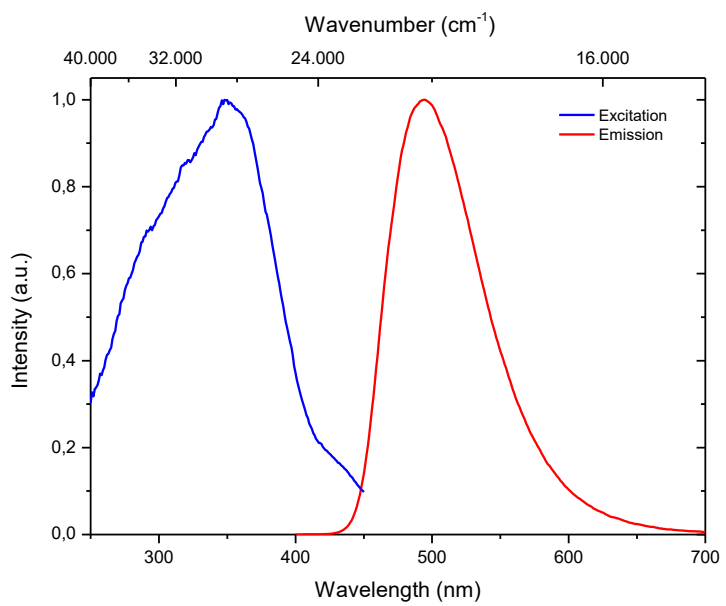


Figure S70: Normalized excitation (blue line) and emission (red line) spectra of **3-CN** in the solid-state. Emission was monitored by excitation at the absorption wavelength of 330 nm and excitation was monitored at fluorescence maximum wavelength of 494 nm.

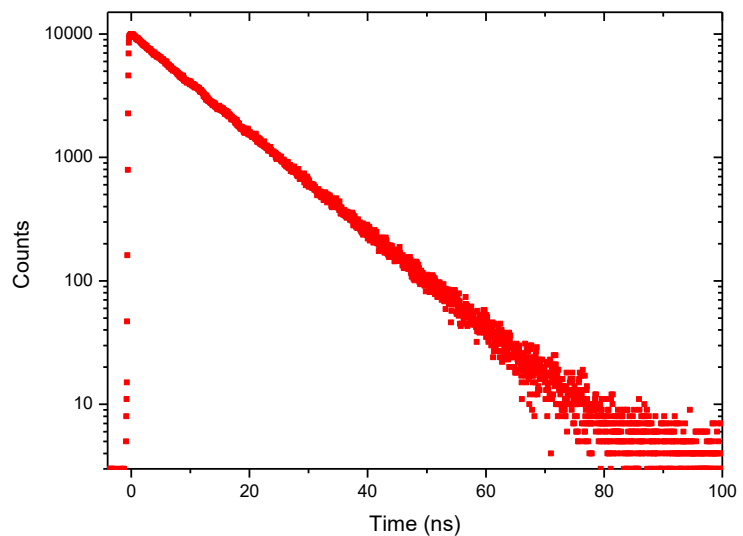


Figure S71: Fluorescence decay profile of **3-CN** in the crystalline state with excitation at 376 nm: $\tau = 10.800 \pm 0.007$ ns; $\chi^2 = 1.156$.

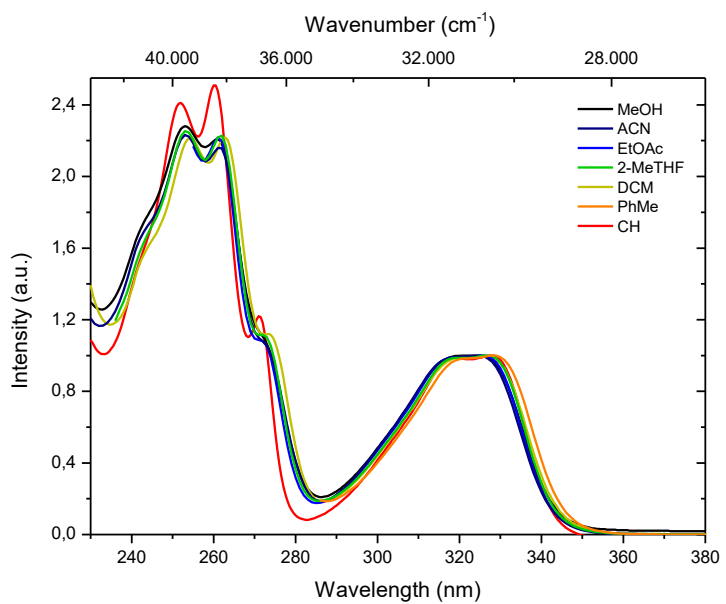


Figure S72: Normalized absorption spectra of **3-CN** in various solvents ($c = 10^{-5} \text{ mol L}^{-1}$) exhibiting differing polarities: methanol (MeOH, black line), acetonitrile (ACN, navy line), ethyl acetate (EtOAc, blue line), 2-methyltetrahydrofuran (2-MeTHF, green line), dichloromethane (DCM, yellow line), toluene (PhMe, orange line) and cyclohexane (CH, red line).

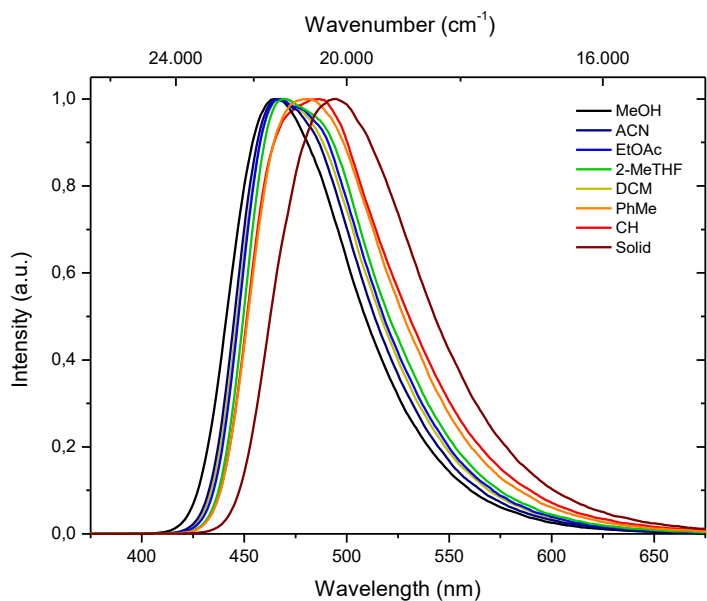


Figure S73: Normalized emission spectra of **3-CN** in various solvents ($c = 10^{-5} \text{ mol L}^{-1}$) exhibiting differing polarities as well as the solid-state: methanol (MeOH, black line), acetonitrile (ACN, navy line), ethyl acetate (EtOAc, blue line), 2-methyltetrahydrofuran (2-MeTHF, green line), dichloromethane (DCM, yellow line), toluene (PhMe, orange line), cyclohexane (CH, red line) and solid-state (wine line).

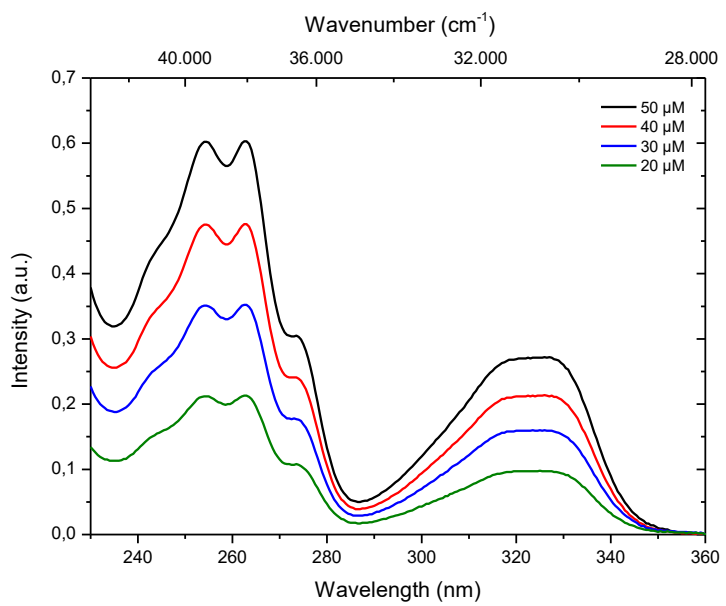


Figure S74: Absorption spectra of **3-CN** at various concentration in dichloromethane solution.

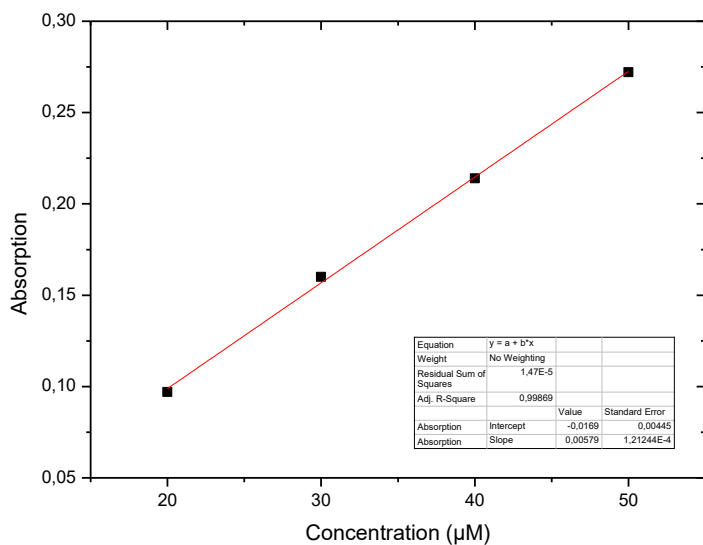


Figure S75: Linear regression for extinction coefficient determination (with respect to Figure S74): $\epsilon_{326} = 5790 \text{ L mol}^{-1} \text{ cm}^{-1}$.

3.3.2 Temperature-Dependent Emission

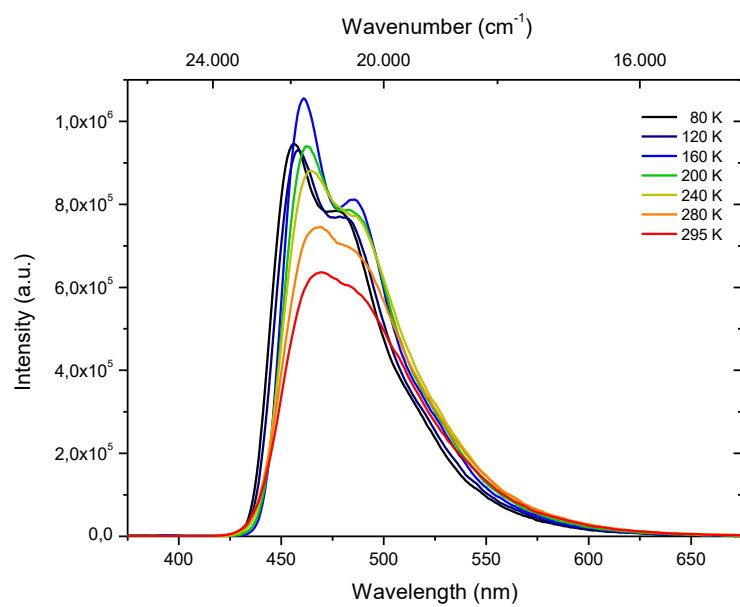


Figure S76: Temperature dependent emission spectra of **3-CN** in deaerated 2-methyltetrahydrofuran solution ($c = 10^{-5} \text{ mol L}^{-1}$) during heating from 80 K to 295 K with excitation at 327 nm.

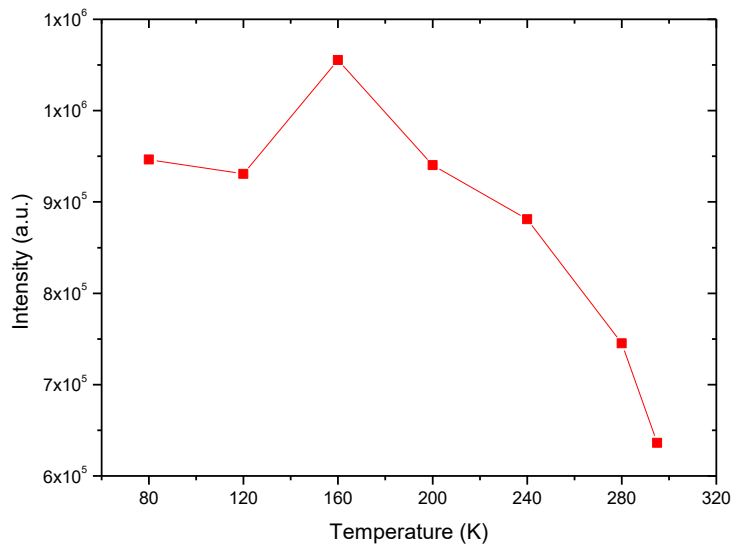


Figure S77: Temperature dependent intensity trend of **3-CN** using the maximum intensity at the given temperature (with respect to Figure S76). Compared to 295 K the emission intensity has multiplied by the factor of 1.66 at 160 K and 1.49 at 80 K, respectively.

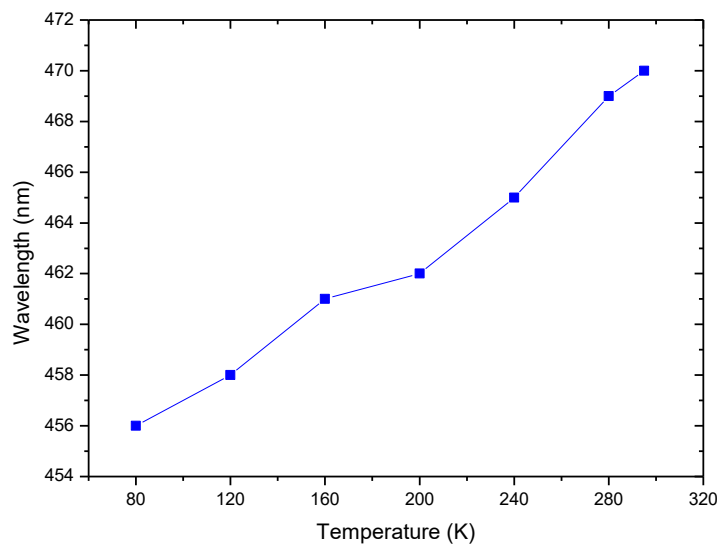


Figure S78: Temperature dependent wavelength trend of **3-CN** using the maximum intensity wavelength at the given temperature (with respect to Figure S76). Starting from 470 nm at 295 K the wavelength drops continuously to 456 nm at 80 K.

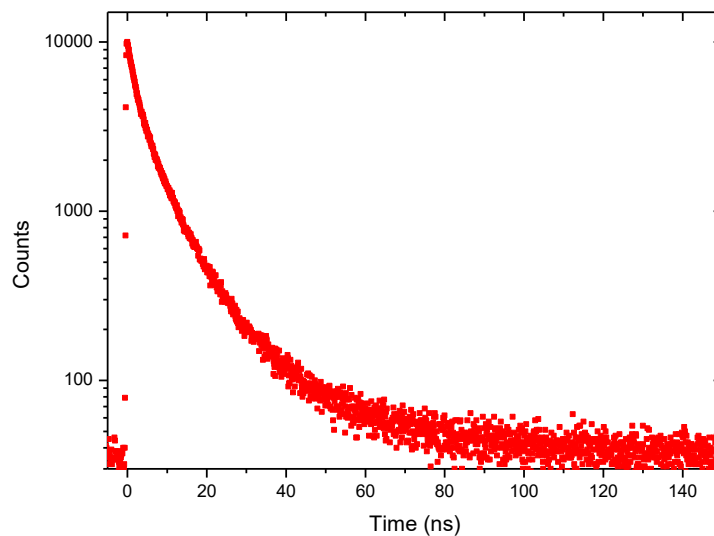


Figure S79: Fluorescence decay profile of **3-CN** in deaerated 2-methyltetrahydrofuran solution ($c = 10^{-5}$ mol L $^{-1}$) with excitation at 376 nm: $\tau_1 = 1.95 \pm 0.04$ (20.2%) ns; $\tau_2 = 7.29 \pm 0.11$ (63.8%) ns; $\tau_3 = 24.1 \pm 0.8$ (16.0%) ns; $\chi^2 = 1.061$.

3.4 3-(4,4-Dimethyl-4,5-dihydrooxazol-2-yl)-2-hydroxybenzonitrile (4-CN)

3.4.1 Absorption and Emission Properties in Solution and Solid-State

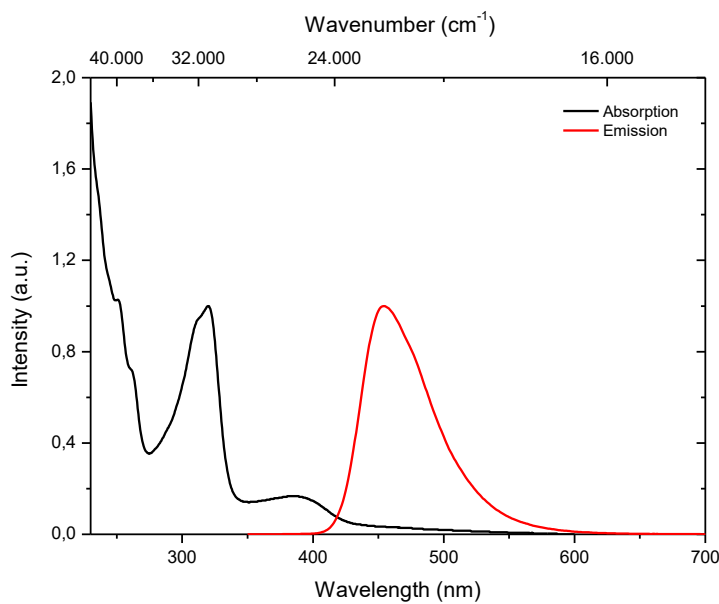


Figure S80: Normalized absorption (black line) and emission (red line) spectra of **4-CN** in methanol solution ($c = 10^{-5} \text{ mol L}^{-1}$). Emission was monitored by excitation at the absorption maximum wavelength of 320 nm.

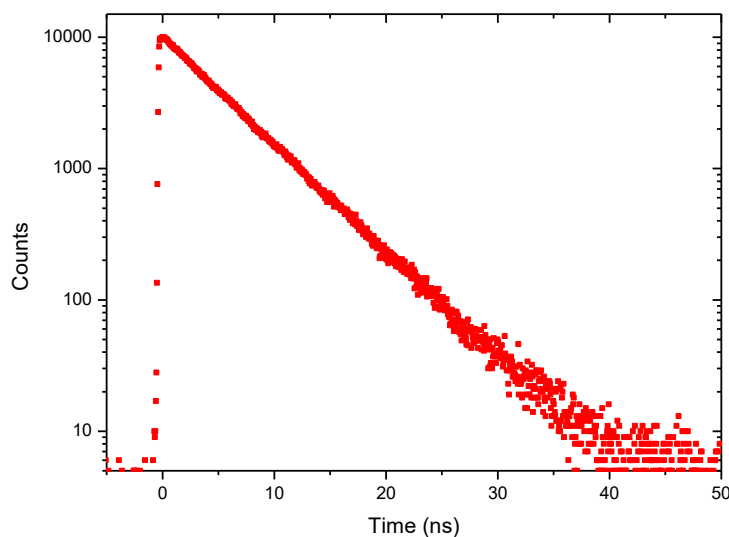


Figure S81: Fluorescence decay profile of **4-CN** in methanol solution ($c = 10^{-5} \text{ mol L}^{-1}$) with excitation at 376 nm: $\tau = 5.267 \pm 0.005 \text{ ns}$; $\chi^2 = 1.155$.

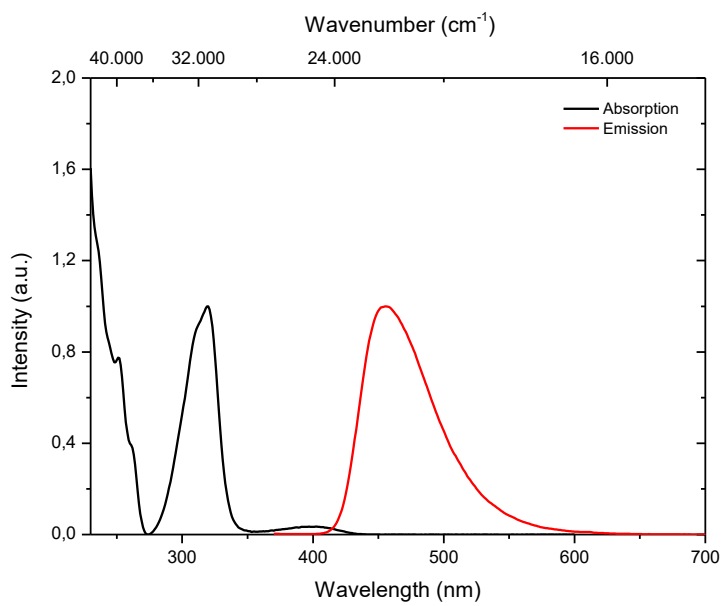


Figure S82: Normalized absorption (black line) and emission (red line) spectra of **4-CN** in acetonitrile solution ($c = 10^{-5} \text{ mol L}^{-1}$). Emission was monitored by excitation at the absorption maximum wavelength of 319 nm.

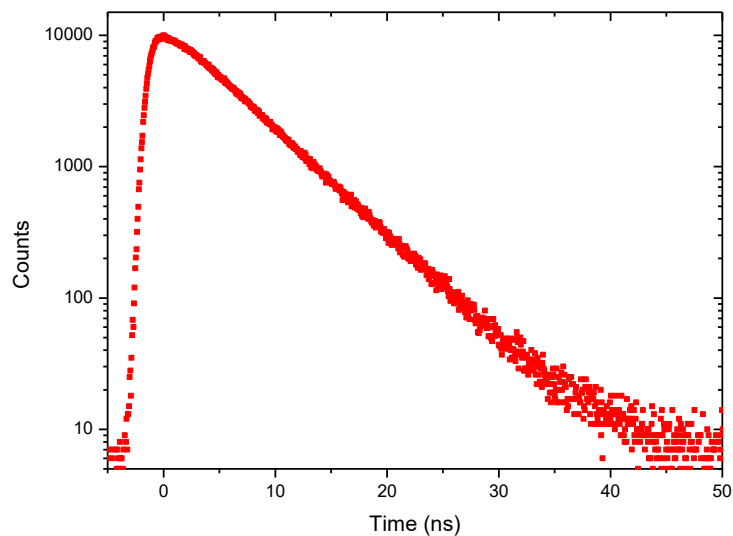


Figure S83: Fluorescence decay profile of **4-CN** in acetonitrile solution ($c = 10^{-5} \text{ mol L}^{-1}$) with excitation at 254 nm: $\tau = 5.267 \pm 0.006 \text{ ns}$; $\chi^2 = 1.246$.

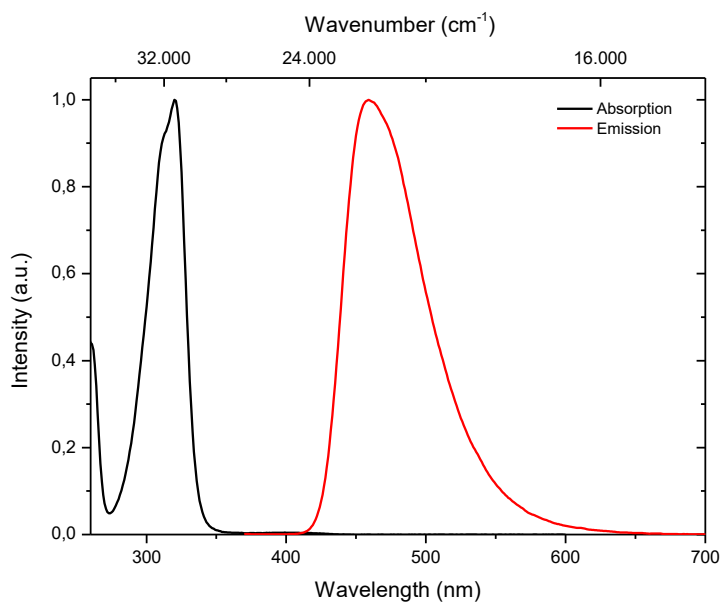


Figure S84: Normalized absorption (black line) and emission (red line) spectra of **4-CN** in ethyl acetate solution ($c = 10^{-5}$ mol L⁻¹). Emission was monitored by excitation at the absorption maximum wavelength of 320 nm.

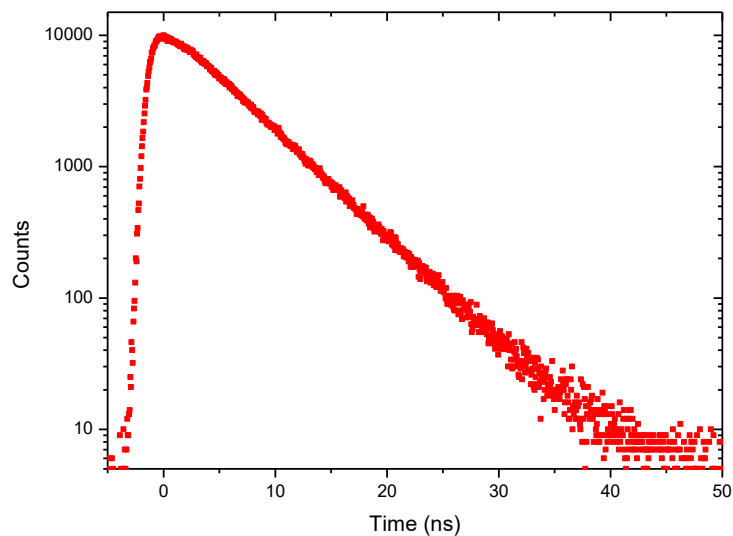


Figure S85: Fluorescence decay profile of **4-CN** in ethyl acetate solution ($c = 10^{-5}$ mol L⁻¹) with excitation at 254 nm: $\tau = 5.221 \pm 0.006$ ns; $\chi^2 = 1.234$.

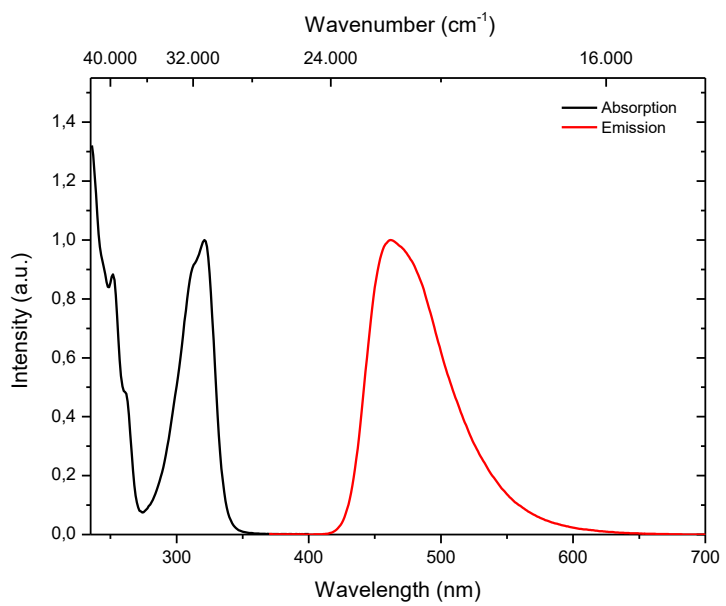


Figure S86: Normalized absorption (black line) and emission (red line) spectra of **4-CN** in 2-methyltetrahydrofuran solution ($c = 10^{-5}$ mol L $^{-1}$). Emission was monitored by excitation at the absorption maximum wavelength of 321 nm.

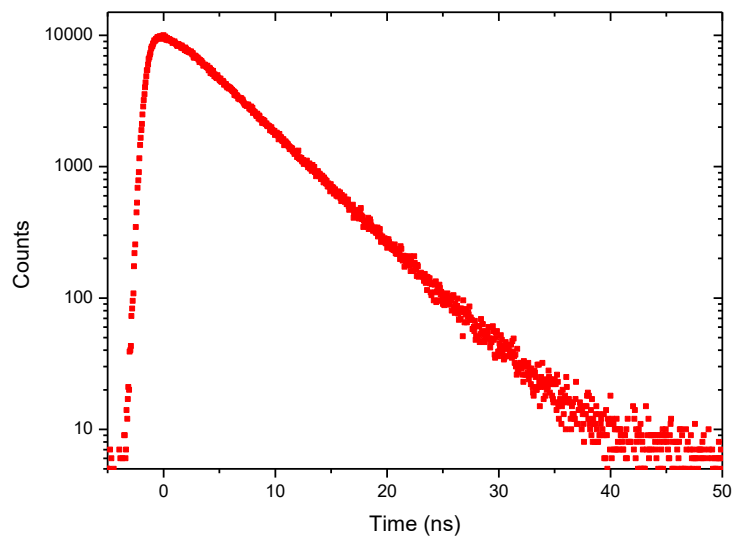


Figure S87: Fluorescence decay profile of **4-CN** in 2-methyltetrahydrofuran solution ($c = 10^{-5}$ mol L $^{-1}$) with excitation at 254 nm: $\tau = 5.144 \pm 0.005$ ns; $\chi^2 = 1.206$.

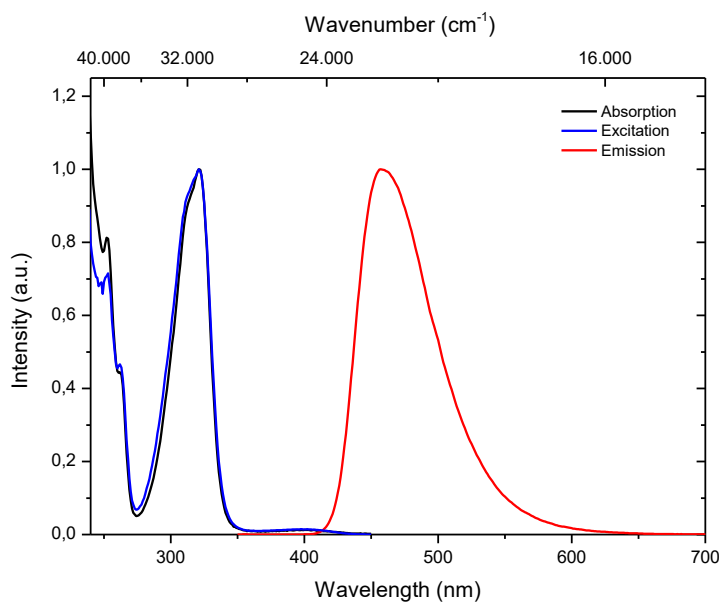


Figure S88: Normalized absorption (black line), excitation (blue line) and emission (red line) spectra of **4-CN** in dichloromethane solution ($c = 10^{-5} \text{ mol L}^{-1}$). Emission was monitored by excitation at the absorption maximum wavelength of 321 nm and excitation was monitored at fluorescence maximum wavelength of 457 nm.

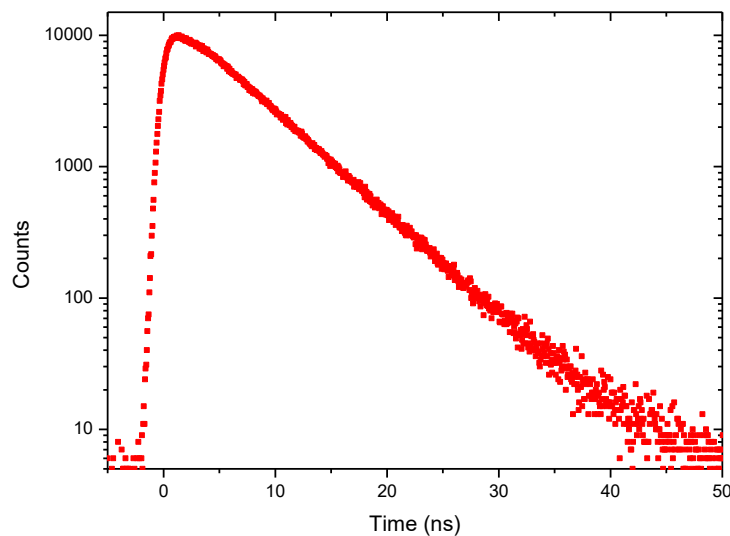


Figure S89: Fluorescence decay profile of **4-CN** in dichloromethane solution ($c = 10^{-5} \text{ mol L}^{-1}$) with excitation at 254 nm: $\tau = 5.516 \pm 0.006 \text{ ns}$; $\chi^2 = 1.277$.

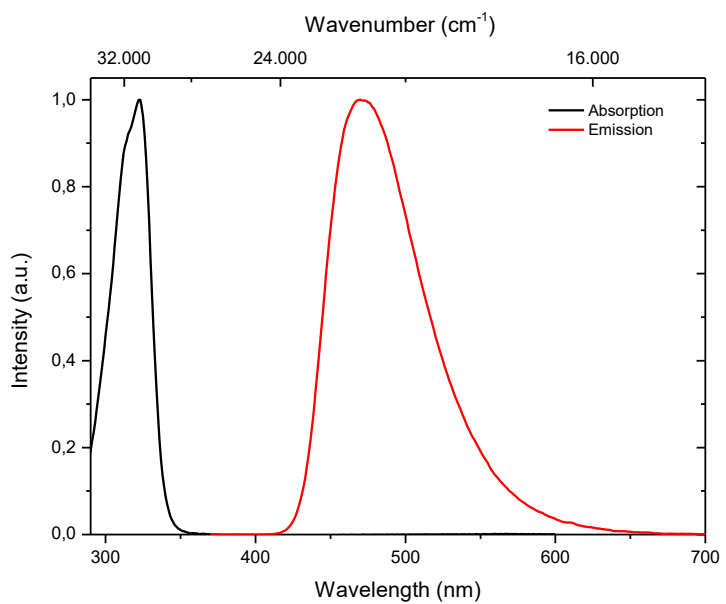


Figure S90: Normalized absorption (black line) and emission (red line) spectra of **4-CN** in toluene solution ($c = 10^{-5}$ mol L⁻¹). Emission was monitored by excitation at the absorption maximum wavelength of 322 nm.

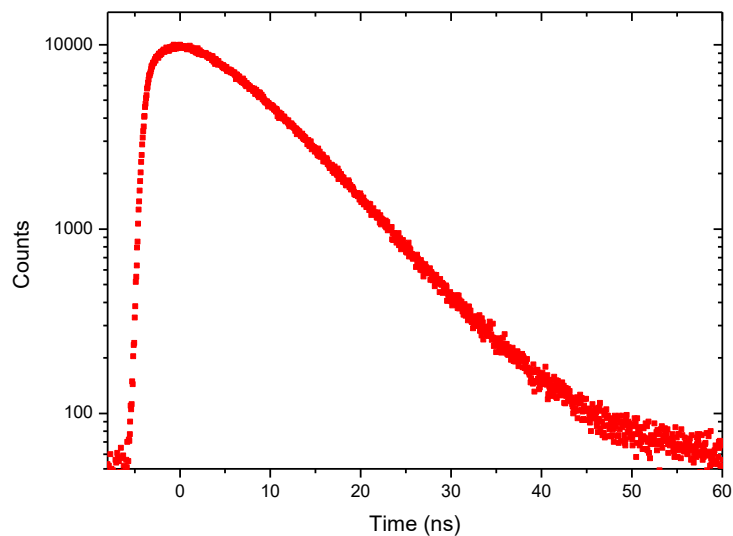


Figure S91: Fluorescence decay profile of **4-CN** in toluene solution ($c = 10^{-5}$ mol L⁻¹) with excitation at 254 nm: $\tau = 7.923 \pm 0.017$ ns; $\chi^2 = 1.464$.

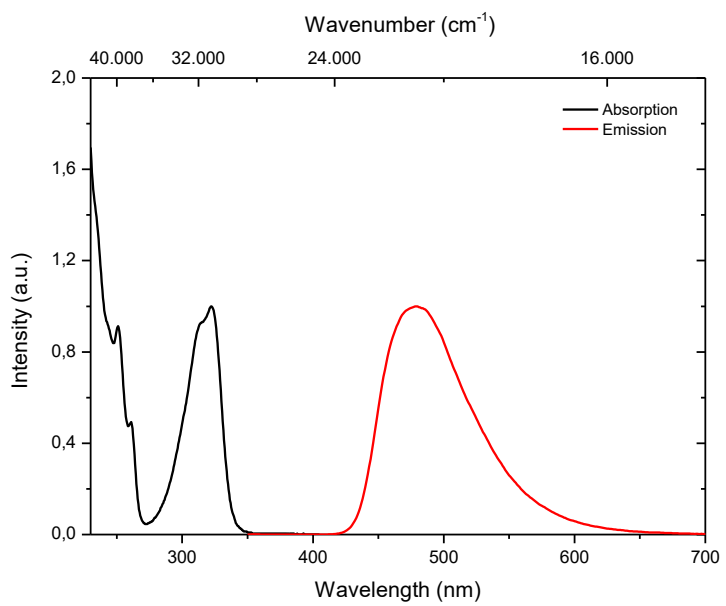


Figure S92: Normalized absorption (black line) and emission (red line) spectra of **4-CN** in cyclohexane solution ($c = 10^{-5}$ mol L⁻¹). Emission was monitored by excitation at the absorption maximum wavelength of 322 nm.

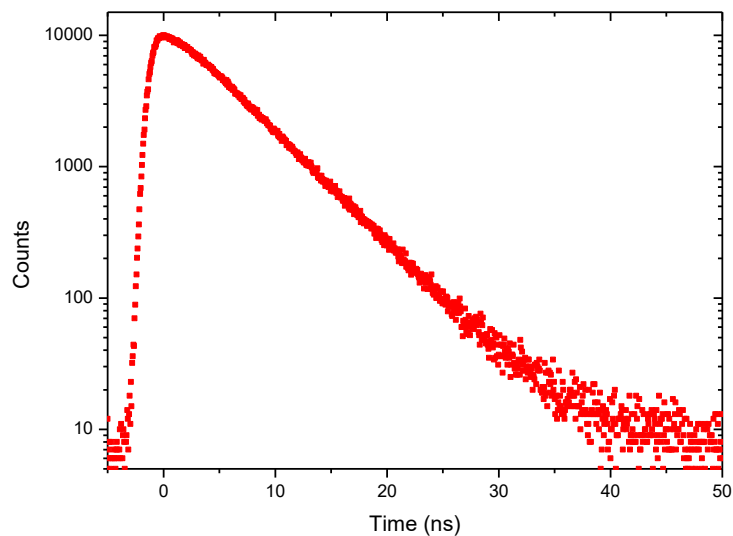


Figure S93: Fluorescence decay profile of **4-CN** in cyclohexane solution ($c = 10^{-5}$ mol L⁻¹) with excitation at 254 nm: $\tau = 5.096 \pm 0.008$ ns; $\chi^2 = 1.224$.

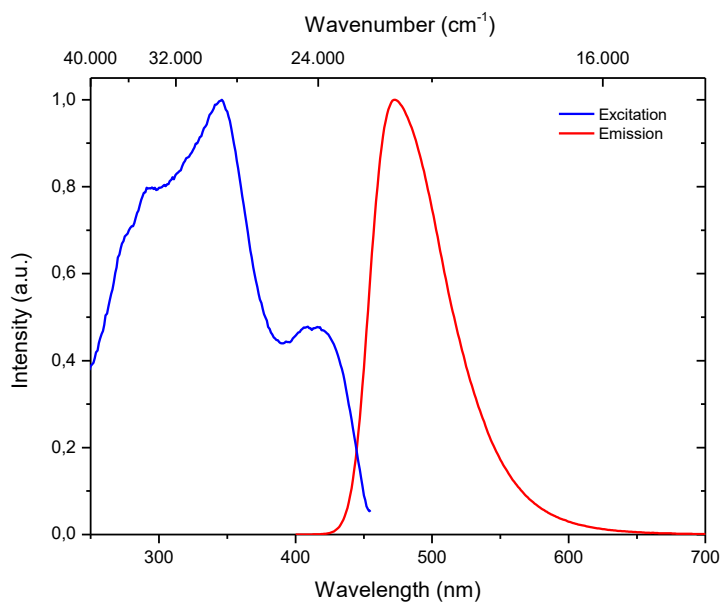


Figure S94: Normalized excitation (blue line) and emission (red line) spectra of **4-CN** in the solid-state. Emission was monitored by excitation at the absorption wavelength of 321 nm and excitation was monitored at fluorescence maximum wavelength of 473 nm.

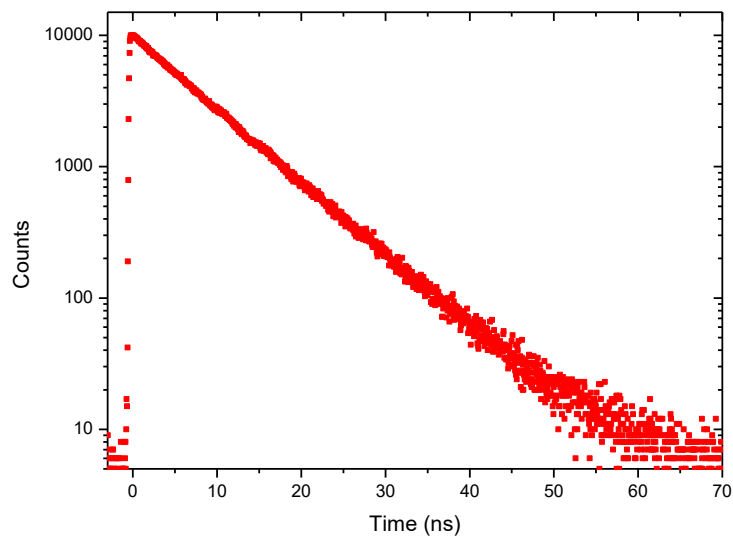


Figure S95: Fluorescence decay profile of **4-CN** in the crystalline state with excitation at 376 nm: $\tau = 7.757 \pm 0.006$ ns; $\chi^2 = 1.311$.

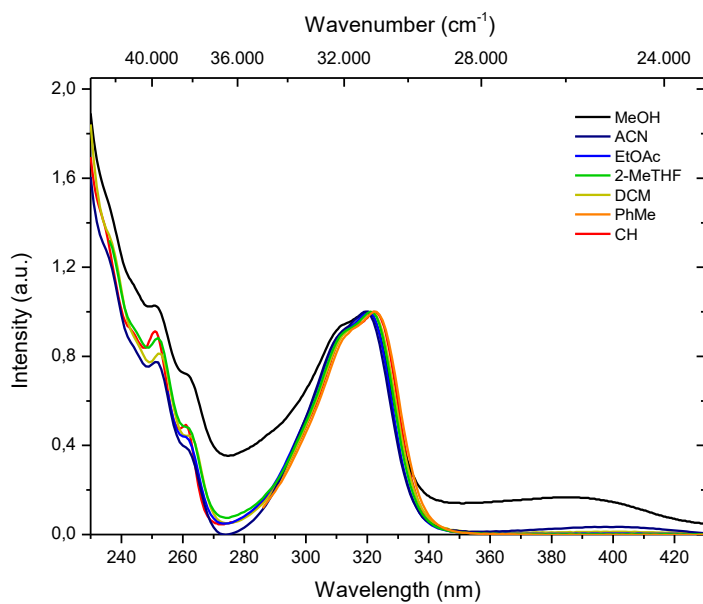


Figure S96: Normalized absorption spectra of **4-CN** in various solvents ($c = 10^{-5}$ mol L⁻¹) exhibiting differing polarities: methanol (MeOH, black line), acetonitrile (ACN, navy line), ethyl acetate (EtOAc, blue line), 2-methyltetrahydrofuran (2-MeTHF, green line), dichloromethane (DCM, yellow line), toluene (PhMe, orange line) and cyclohexane (CH, red line).

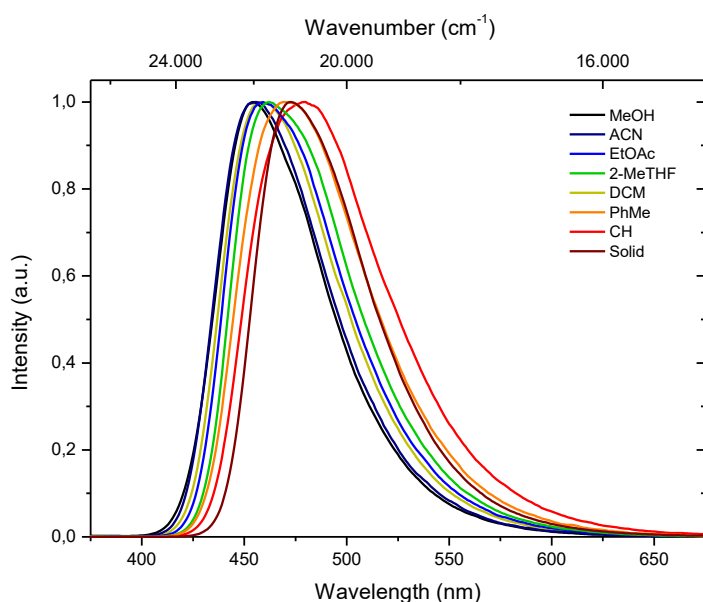


Figure S97: Normalized emission spectra of **4-CN** in various solvents ($c = 10^{-5}$ mol L⁻¹) exhibiting differing polarities as well as the solid-state: methanol (MeOH, black line), acetonitrile (ACN, navy line), ethyl acetate (EtOAc, blue line), 2-methyltetrahydrofuran (2-MeTHF, green line), dichloromethane (DCM, yellow line), toluene (PhMe, orange line), cyclohexane (CH, red line) and solid-state (wine line).

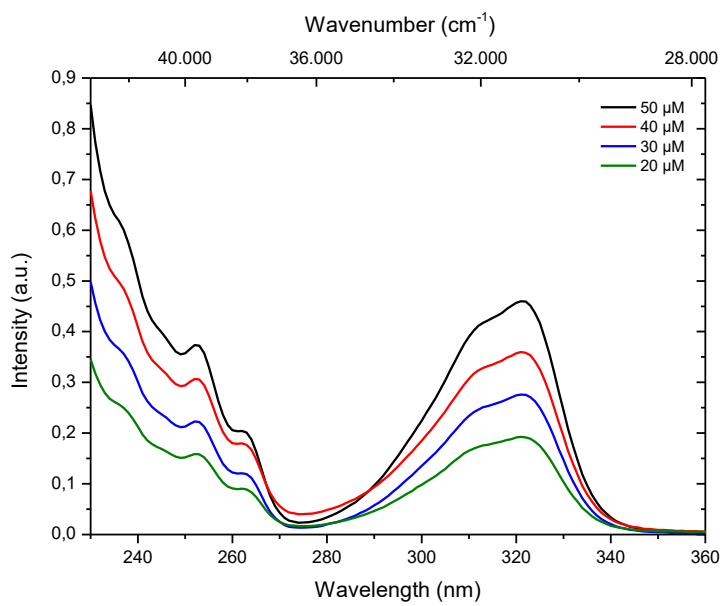


Figure S98: Absorption spectra of **4-CN** at various concentration in dichloromethane solution.

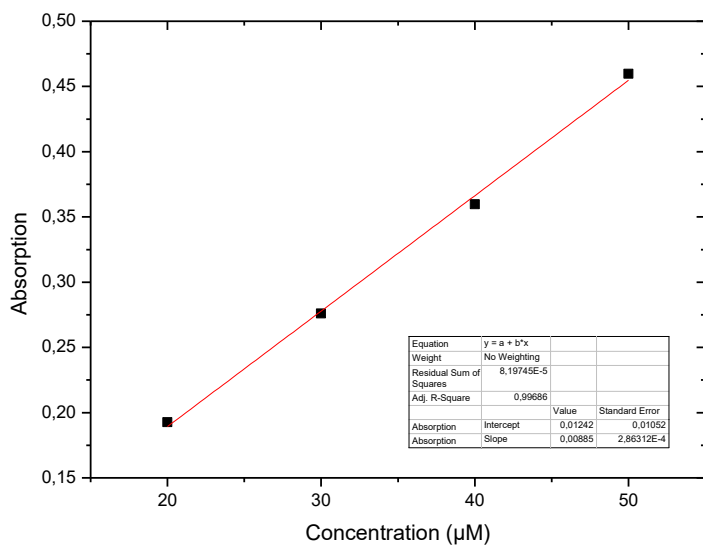


Figure S99: Linear regression for extinction coefficient determination (with respect to Figure S98): $\varepsilon_{321} = 8850 \text{ L mol}^{-1} \text{ cm}^{-1}$.

3.4.2 Temperature-Dependent Emission

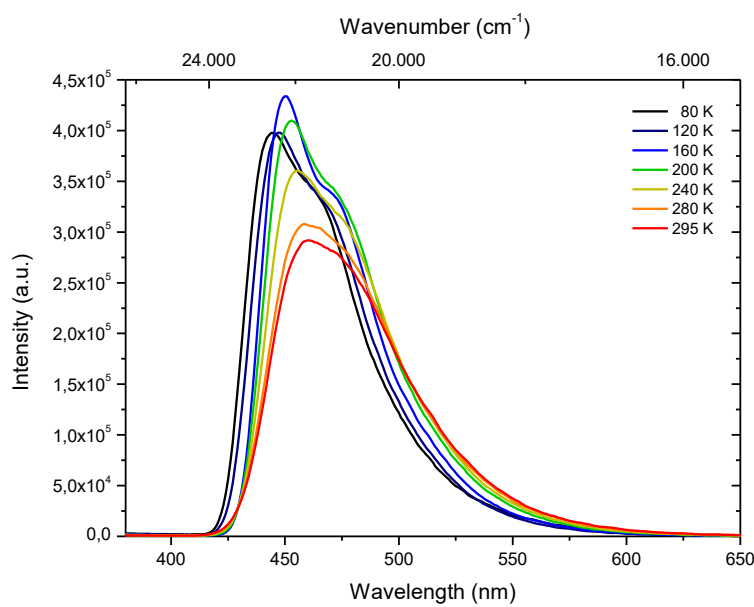


Figure S100: Temperature dependent emission spectra of **4-CN** in deaerated 2-methyltetrahydrofuran solution ($c = 10^{-5}$ mol L $^{-1}$) during heating from 80 K to 295 K with excitation at 321 nm.

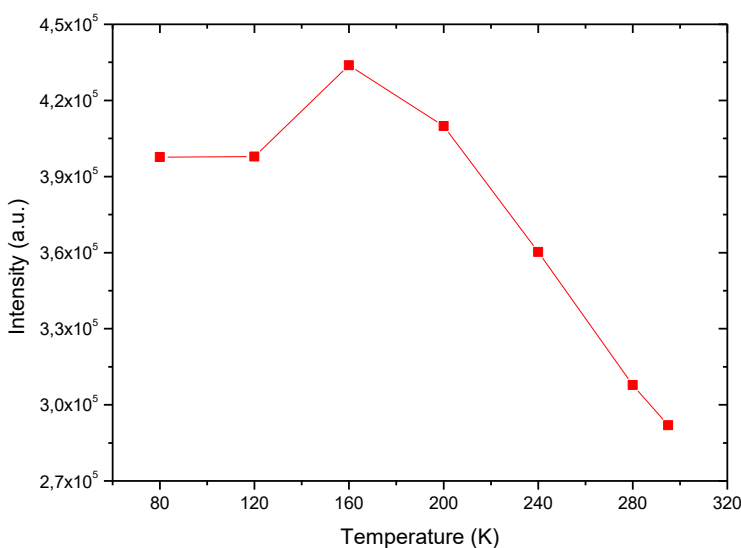


Figure S101: Temperature dependent **intensity** trend of **4-CN** using the maximum intensity at the given temperature (with respect to Figure S100). Compared to 295 K the emission intensity has multiplied by the factor of 1.49 at 160 K and 1.36 at 80 K, respectively.

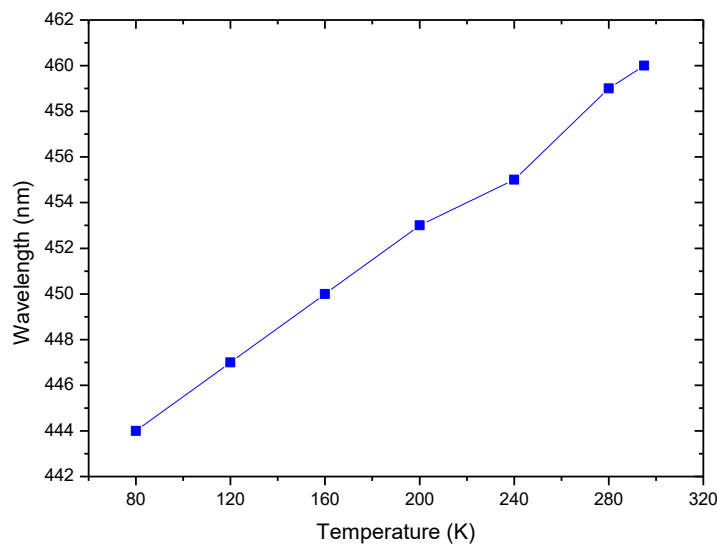


Figure S102: Temperature dependent wavelength trend of **4-CN** using the maximum intensity wavelength at the given temperature (with respect to Figure S100). Starting from 460 nm at 295 K the wavelength drops continuously to 444 nm at 80 K.

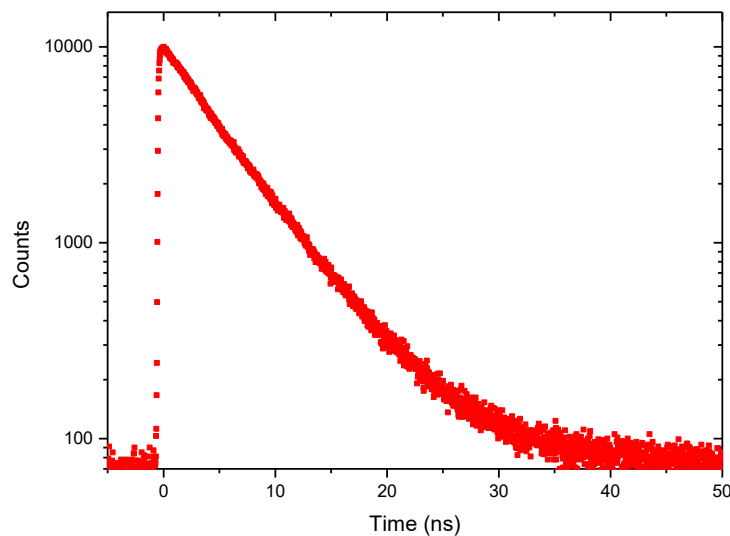


Figure S103: Fluorescence decay profile of **4-CN** in deaerated 2-methyltetrahydrofuran solution ($c = 10^{-5}$ mol L $^{-1}$) with excitation at 376 nm: $\tau = 5.431 \pm 0.004$ ns; $\chi^2 = 1.329$.

3.5 Photophysical Data of 1-CN, 2-CN, 3-CN and 4-CN

Table S1: Photophysical data of 1-CN, 2-CN, 3-CN and 4-CN measured in aerated solution and the solid-state at 295 K.

Compd	Solvent	λ_{abs} [nm] (ϵ [mol L ⁻¹ cm ⁻¹])	λ_{em} [nm]	$A\tilde{\nu}$ [cm ⁻¹]	Φ_F [%] ^a	τ [ns] (Rel %) ^b	k_r [10 ⁸ s ⁻¹] ^c	k_{nr} [10 ⁸ s ⁻¹] ^c
1-CN	MeOH	321	467	9,740	13.7	1.87 (71.6)	0.64	4.00
						2.87 (28.4)		
	ACN	320	471	10,020	15.2	2.08	0.73	4.07
	EtOAc	320	473	10,110	15.6	2.34	0.67	3.61
	2-MeTHF	321	476	10,140	14.0	2.07	0.68	4.16
						2.11 ^d		
	THF	321	477	10,190	17.2	2.38 (92.5)	0.67	3.21
						5.10 (7.5)		
	DCM	322 (5790)	471	9,820	24.9	3.09	0.81	2.43
2-CN	PhMe	322	477	10,090	18.1	2.31 (21.5)	0.30	1.35
						7.09 (78.5)		
	CH	322	481	10,270	8.2	1.13	0.73	8.16
	Solid	347 ^e	491	8,450	87.3	13.3	0.66	0.10
3-CN	MeOH	323	465	9,450	51.0	2.53 (5.5)	0.70	0.67
						7.60 (94.5)		
	ACN	324	465	9,360	49.4	7.29	0.68	0.69
	EtOAc	326	468	9,310	47.4	6.75	0.70	0.78
	2-MeTHF	327	469	9,260	47.0	6.53	0.72	0.81
						7.67 ^d		
	DCM	326 (5790)	468	9,310	55.6	8.10	0.69	0.55
	PhMe	328	479	9,610	55.0	8.95	0.61	0.50
	CH	327	487	10,050	39.7	6.02	0.66	1.00
4-CN	Solid	348 ^e	494	8,490	74.1	10.8	0.69	0.24
	MeOH	320	454	9,220	49.8	5.27	0.95	0.95
	ACN	319	456	9,420	40.5	5.30	0.76	1.12
	EtOAc	320	459	9,460	63.0	5.22	1.21	0.71
	2-MeTHF	321	462	9,510	48.7	5.14	0.95	1.00
	DCM	321 (8850)	457	9,270	52.9	5.52	0.96	0.85
	PhMe	322	469	9,730	52.4	7.92	0.66	0.60
	CH	322	479	10,180	44.8	5.10	0.88	1.08

^a Absolute quantum yields were determined by using an integration sphere. ^b Relative ratio of the species of a double exponential function are given in parentheses. ^c k_r (10⁸ s⁻¹) and k_{nr} (10⁸ s⁻¹) were calculated using the equations $k_r = \Phi_F/\tau$ and $k_{\text{nr}} = (1 - \Phi_F)/\tau$.

^d Half lifetimes were measured after bubbling with argon for 30 minutes. ^e Excitation maximum.

3.6 Photographs of Luminophores

3.6.1 Images of 1-CN

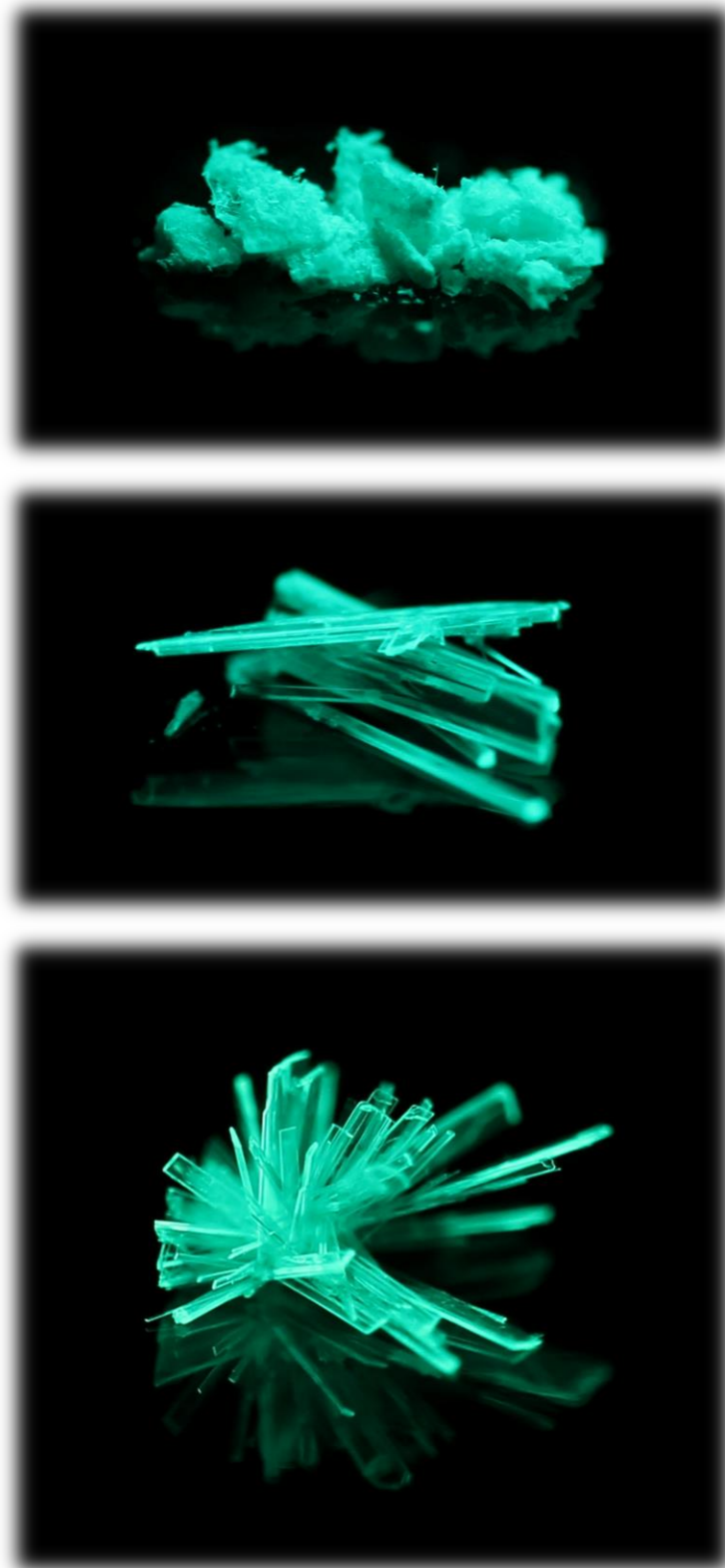


Figure S104: Representative Images of **1-CN** in the amorphous state (top) and the crystalline state (middle and bottom) under 366 nm irradiation.

3.6.2 Images of 2-CN

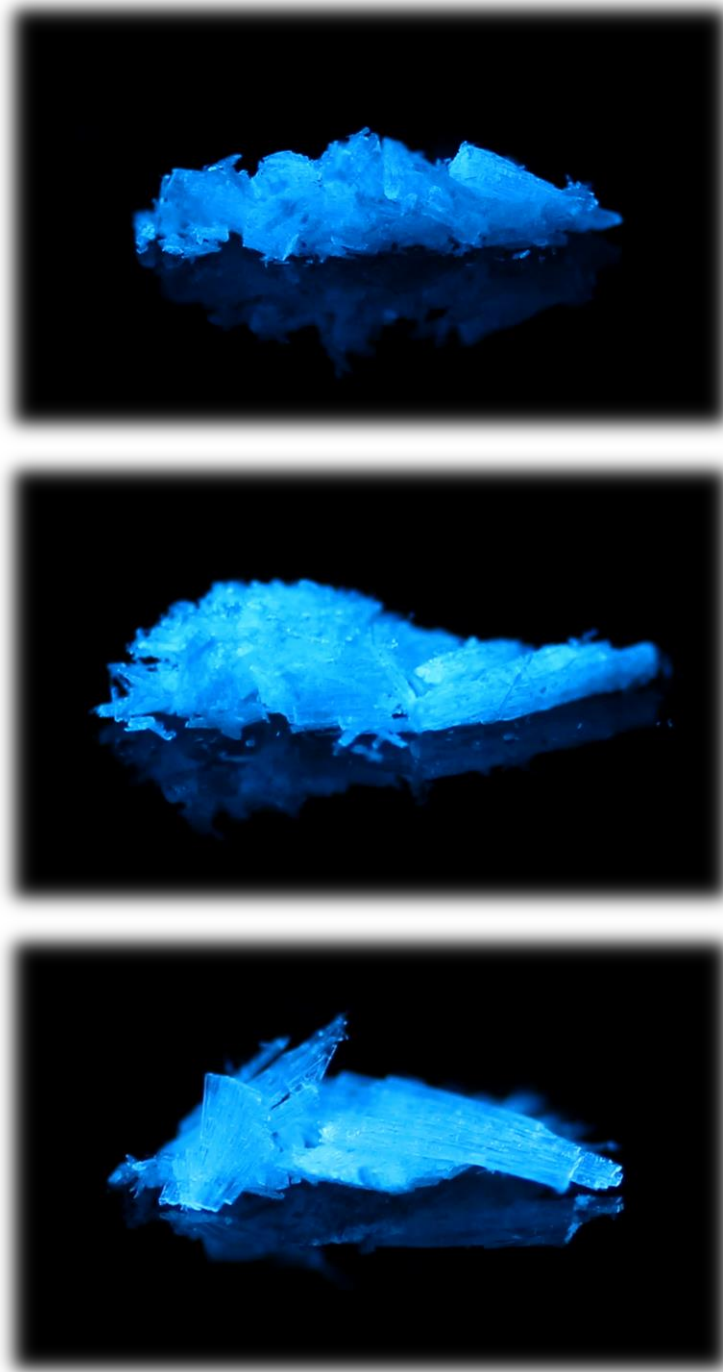


Figure S105: Representative Images of **2-CN** in the semi-crystalline state (top) and the crystalline state (middle and bottom) under 366 nm irradiation.

3.6.3 Images of 3-CN

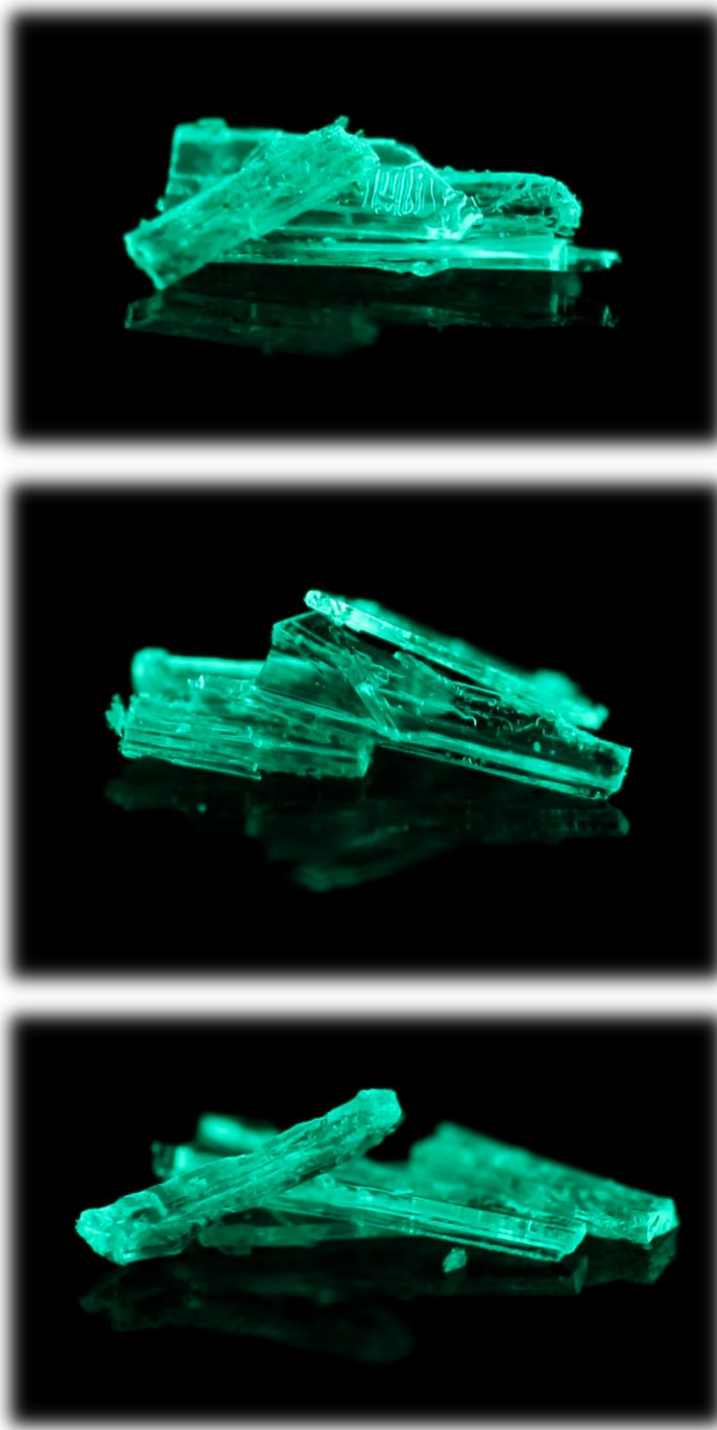


Figure S106: Representative Images of **3-CN** in the crystalline state (top, middle and bottom) under 366 nm irradiation.

3.6.4 Images of 4-CN

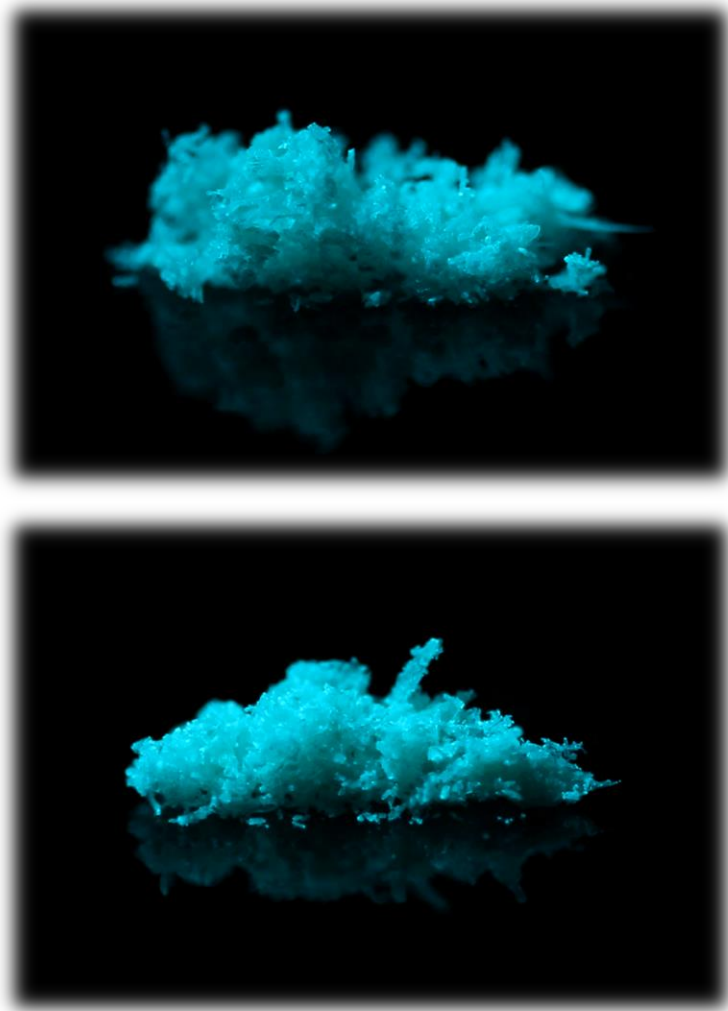


Figure S107: Representative Images of **4-CN** in the microcrystalline state (top and bottom) under 366 nm irradiation.

4 Crystal Structures

4.1 2-(4,4-Dimethyl-4,5-dihydrooxazol-2-yl)-3-hydroxybenzonitrile (1-CN)

4.1.1 Crystal Data for 1-CN

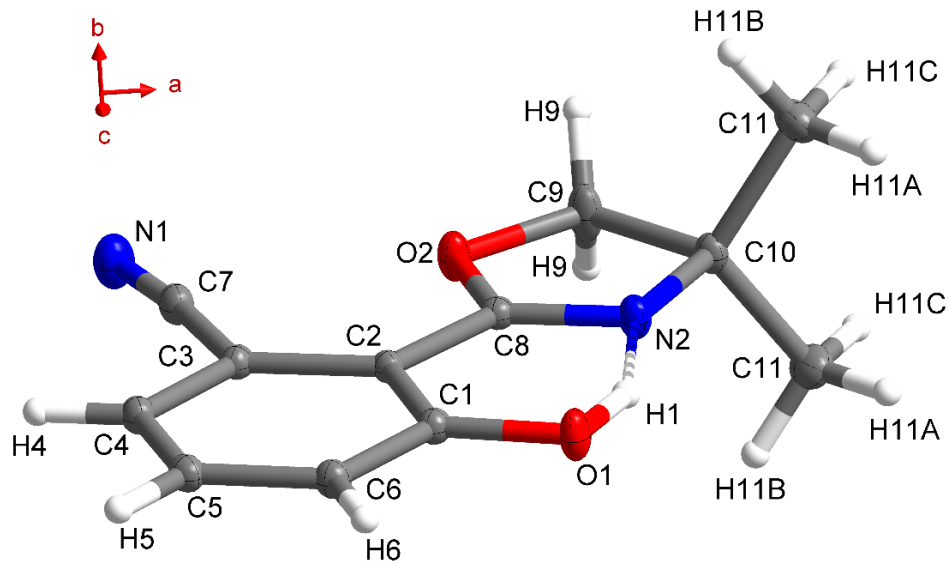


Figure S108: Asymmetric unit of 1-CN with atom labels.

Table S2: Crystal data and structure refinement for 1-CN.

Empirical formula	C ₁₂ H ₁₂ N ₂ O ₂
Formula weight, g mol ⁻¹	216.24
Crystal system	Orthorhombic
Crystal size, mm ³	0.3 × 0.3 × 0.25
Space group	Pnma
a/Å	19.3821(5)
b/Å	6.6585(2)
c/Å	8.0463(2)
α/°	90
β/°	90
γ/°	90
Volume/Å ³	1038.42(5)
Z	4
ρ _{calc} , g/cm ³	1.383
μ/mm ⁻¹	0.096

F(000)	456.0
2 θ range for data collection/ $^{\circ}$	6.582 to 66.368
	-29 \leq h \leq 24
Index ranges	-10 \leq k \leq 9
	-12 \leq l \leq 12
No. of reflections collected	16938
No of independent reflections	2131 [R _{int} = 0.0429, R _{sigma} = 0.0232]
Data/restraints/parameters	2131/0/101
Goodness-of-fit on F ²	1.065
Final R indexes [I \geq 2 σ (I)]	R ₁ = 0.0410, wR ₂ = 0.1077
Final R indexes [all data]	R ₁ = 0.0526, wR ₂ = 0.1155
Largest diff. peak/hole / e Å ⁻³	0.50/-0.31
CCDC number	1908035

Table S3: Fractional Atomic Coordinates ($\times 10^4$) and Equivalent Isotropic Displacement Parameters (Å² $\times 10^3$) for **1-CN**. U_{eq} is defined as 1/3 of the trace of the orthogonalized U_{II} tensor.

Atom	x	y	z	U(eq)
O1	6205.4(4)	2500	6636.8(11)	16.75(19)
O2	5713.8(4)	2500	1598.7(10)	15.58(19)
N1	4097.1(6)	2500	1131.5(14)	21.0(2)
N2	6542.2(5)	2500	3562.3(12)	14.0(2)
C1	5542.1(6)	2500	6154.5(14)	11.7(2)
C2	5348.6(5)	2500	4466.1(13)	10.07(19)
C3	4637.4(6)	2500	4075.8(14)	11.4(2)
C4	4140.9(6)	2500	5327.8(14)	12.6(2)
C5	4345.1(6)	2500	6983.3(15)	13.3(2)
C6	5036.2(6)	2500	7401.9(14)	13.3(2)
C7	4373.8(6)	2500	2399.2(15)	14.1(2)
C8	5895.0(6)	2500	3211.7(13)	10.9(2)
C9	6355.6(6)	2500	660.6(16)	19.6(3)
C10	6933.9(6)	2500	1980.2(14)	13.0(2)
C11	7379.0(5)	4381.4(14)	1890.8(12)	20.07(19)

Table S4: Bond Lengths for **1-CN**.

Atom	Atom	Length/Å	Atom	Atom	Length/Å
O1	C1	1.3429(13)	C2	C8	1.4629(14)
O2	C8	1.3445(13)	C3	C4	1.3932(15)
O2	C9	1.4551(14)	C3	C7	1.4426(16)
N1	C7	1.1525(16)	C4	C5	1.3896(16)
N2	C8	1.2858(14)	C5	C6	1.3811(16)
N2	C10	1.4822(15)	C9	C10	1.5438(17)
C1	C2	1.4094(16)	C10	C11	1.5227(11)
C1	C6	1.4032(15)	C10	C11 ¹	1.5227(11)
C2	C3	1.4137(15)			

¹+X,1/2-Y,+Z**Table S5:** Bond Angles for **1-CN**.

Atom	Atom	Atom	Angle/°	Atom	Atom	Atom	Angle/°
C8	O2	C9	106.10(9)	C5	C6	C1	120.21(11)
C8	N2	C10	108.14(9)	N1	C7	C3	173.01(12)
O1	C1	C2	122.23(10)	O2	C8	C2	118.48(9)
O1	C1	C6	117.54(10)	N2	C8	O2	117.82(10)
C6	C1	C2	120.24(10)	N2	C8	C2	123.70(10)
C1	C2	C3	118.26(10)	O2	C9	C10	105.30(9)
C1	C2	C8	118.19(9)	N2	C10	C9	102.64(9)
C3	C2	C8	123.54(10)	N2	C10	C11 ¹	109.31(6)
C2	C3	C7	123.58(10)	N2	C10	C11	109.31(6)
C4	C3	C2	120.86(10)	C11	C10	C9	112.26(6)
C4	C3	C7	115.56(10)	C11 ¹	C10	C9	112.26(6)
C5	C4	C3	119.76(10)	C11	C10	C11 ¹	110.71(10)
C6	C5	C4	120.67(11)				

¹+X,1/2-Y,+Z

Table S6: Torsion Angles for **1-CN**.

A	B	C	D	Angle/°	A	B	C	D	Angle/°
O1	C1	C2	C3	180.000(0)	C4	C5	C6	C1	0.000(0)
O1	C1	C2	C8	0.000(0)	C6	C1	C2	C3	0.000(0)
O1	C1	C6	C5	180.000(0)	C6	C1	C2	C8	180.000(0)
O2	C9	C10	N2	0.0	C7	C3	C4	C5	180.000(0)
O2	C9	C10	C11	-117.26(7)	C8	O2	C9	C10	0.0
O2	C9	C10	C11 ¹	117.26(7)	C8	N2	C10	C9	0.0
C1	C2	C3	C4	0.000(0)	C8	N2	C10	C11 ¹	-119.34(7)
C1	C2	C3	C7	180.000(0)	C8	N2	C10	C11	119.34(7)
C1	C2	C8	O2	180.000(0)	C8	C2	C3	C4	180.000(0)
C1	C2	C8	N2	0.000(0)	C8	C2	C3	C7	0.000(0)
C2	C1	C6	C5	0.000(0)	C9	O2	C8	N2	0.0
C2	C3	C4	C5	0.000(0)	C9	O2	C8	C2	180.0
C3	C2	C8	O2	0.000(0)	C10	N2	C8	O2	0.0
C3	C2	C8	N2	180.0	C10	N2	C8	C2	180.0
C3	C4	C5	C6	0.000(0)					

¹+X,1/2-Y,+Z**Table S7:** Hydrogen Atom Coordinates ($\text{\AA} \times 10^4$) and Isotropic Displacement Parameters ($\text{\AA}^2 \times 10^3$) for **1-CN**.

Atom	x	y	z	U(eq)
H1	6465(12)	2500	5630(30)	45(6)
H4	3664.45	2500	5050.74	15
H5	4005.95	2500	7835.62	16
H6	5169.42	2500	8538.15	16
H9	6350(6)	1300(20)	-13(15)	23
H11A	7727.19	4340.9	2773.25	30
H11B	7087.64	5571.66	2034.93	30
H11C	7608.5	4442.41	806.8	30

4.1.2 Crystal Packing Views of 1-CN

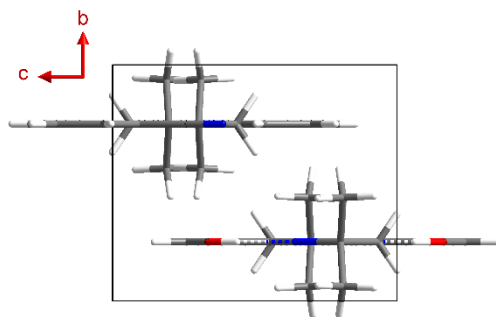


Figure S109: Unit cell packing view of a **1-CN** crystal along the *a*-axis.

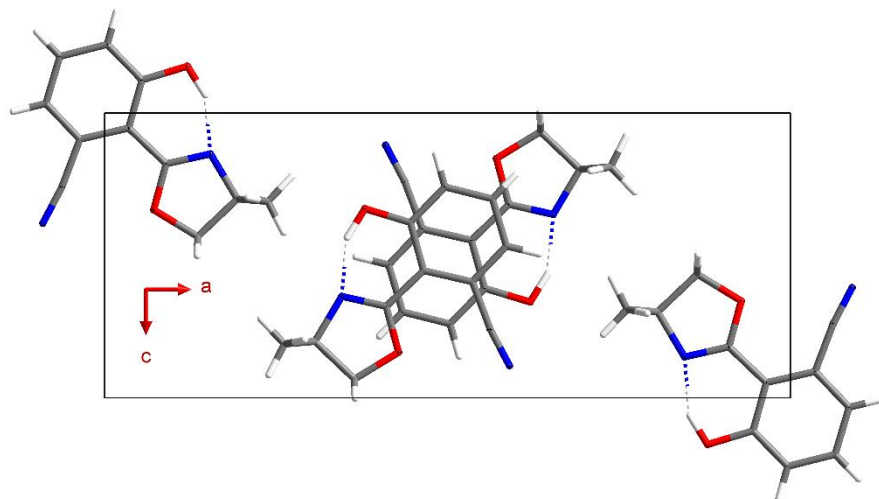


Figure S110: Unit cell packing view of a **1-CN** crystal along the *b*-axis.

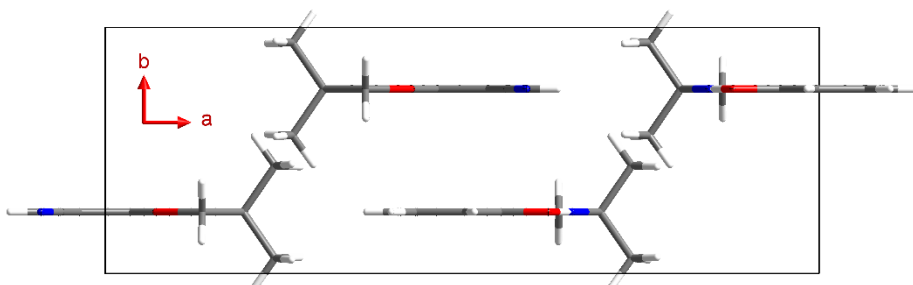


Figure S111: Unit cell packing view of a **1-CN** crystal along the *c*-axis.

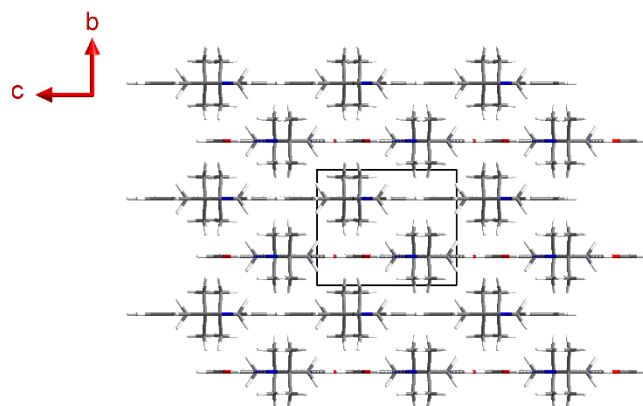


Figure S112: Unit cell (3x3x3) packing view of a **1-CN** crystal along the *a*-axis.

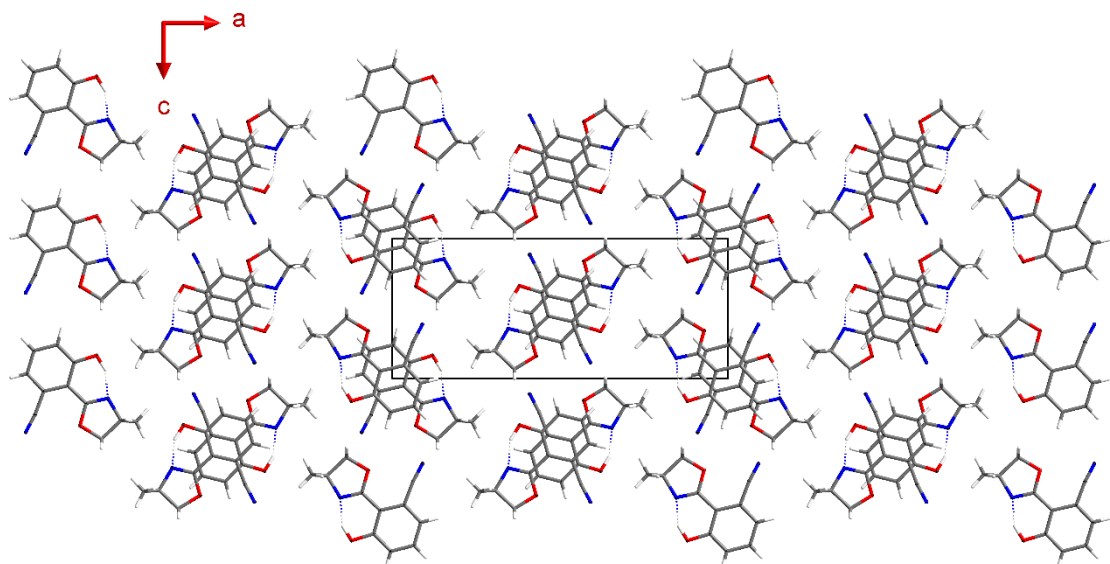


Figure S113: Unit cell (3x3x3) packing view of a **1-CN** crystal along the *b*-axis.

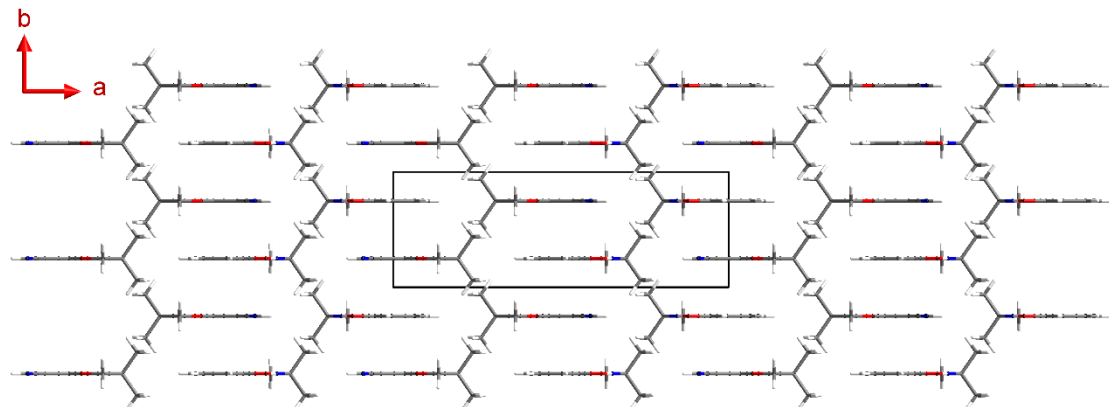


Figure S114: Unit cell (3x3x3) packing view of a **1-CN** crystal along the *c*-axis.

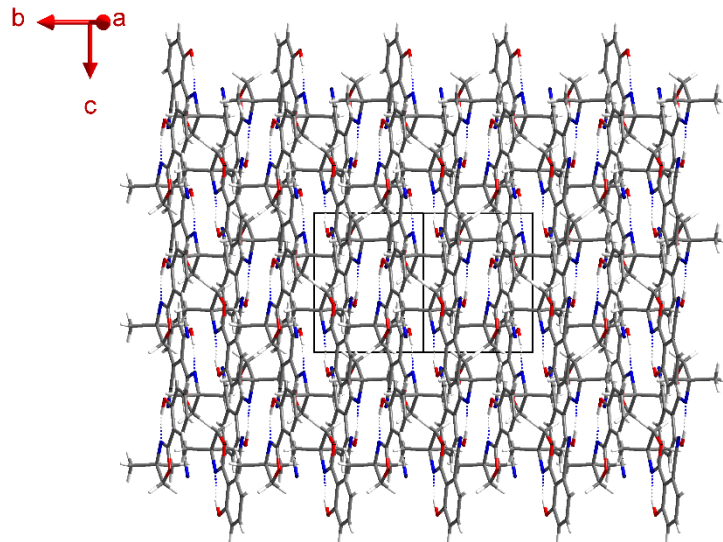


Figure S115: Unit cells ($3 \times 3 \times 3$) packing view of a **1-CN** crystal along the $1\bar{1}0$ -axis.

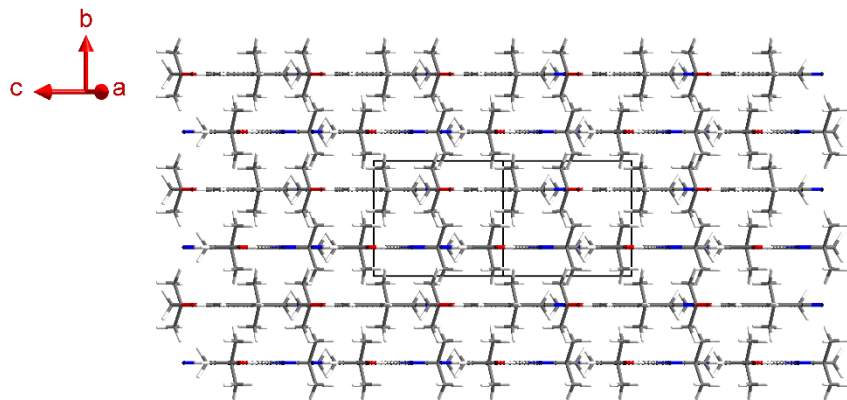


Figure S116: Unit cells ($3 \times 3 \times 3$) packing view of a **1-CN** crystal along the $1\bar{0}1$ -axis.

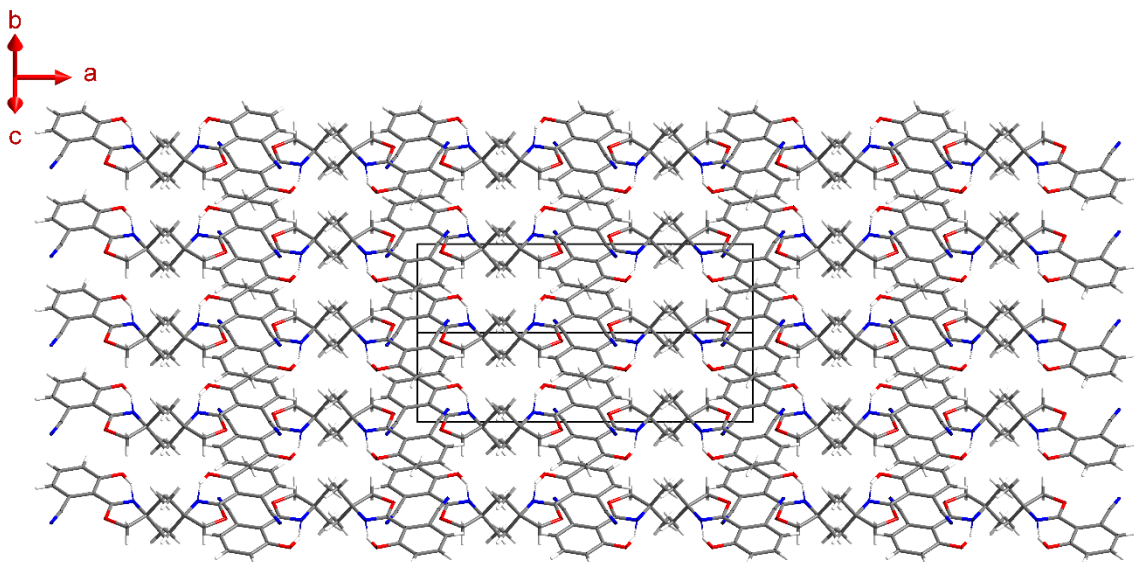


Figure S117: Unit cells ($3 \times 3 \times 3$) packing view of a **1-CN** crystal along the $0\bar{1}1$ -axis.

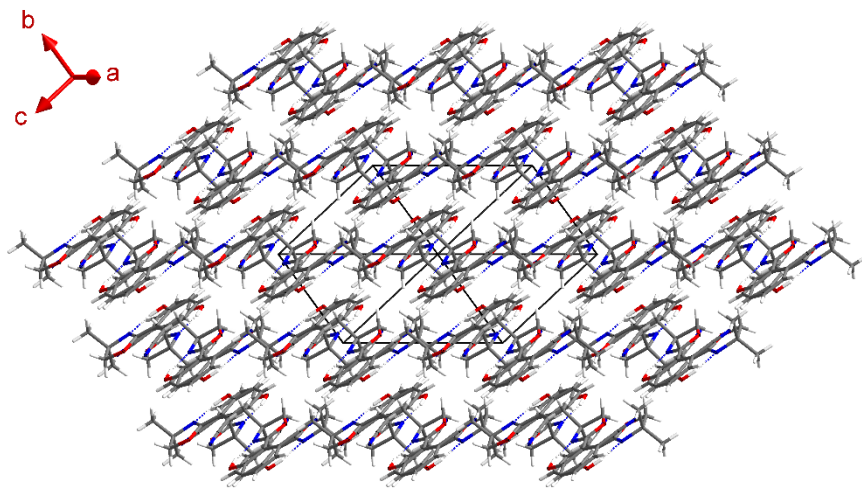


Figure S118: Unit cells (3x3x3) packing view of a **1-CN** crystal along the 111-axis.

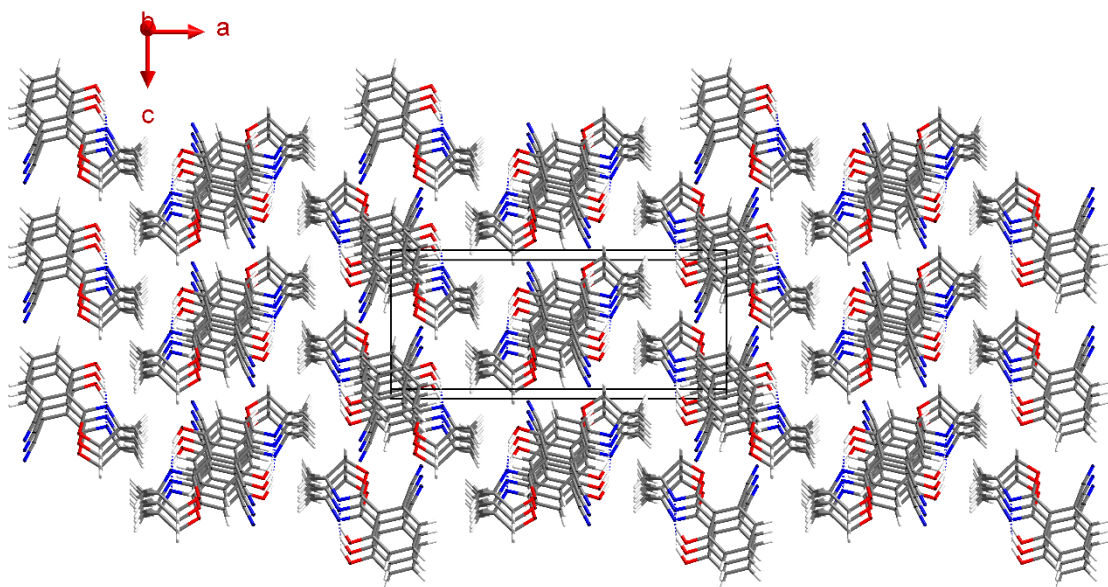


Figure S119: Unit cells (3x3x3) packing view of a **1-CN** crystal along the *b*-axis with 5° rotation around the *x*-axis.

4.1.3 Intermolecular Contacts in Crystal Lattice of 1-CN

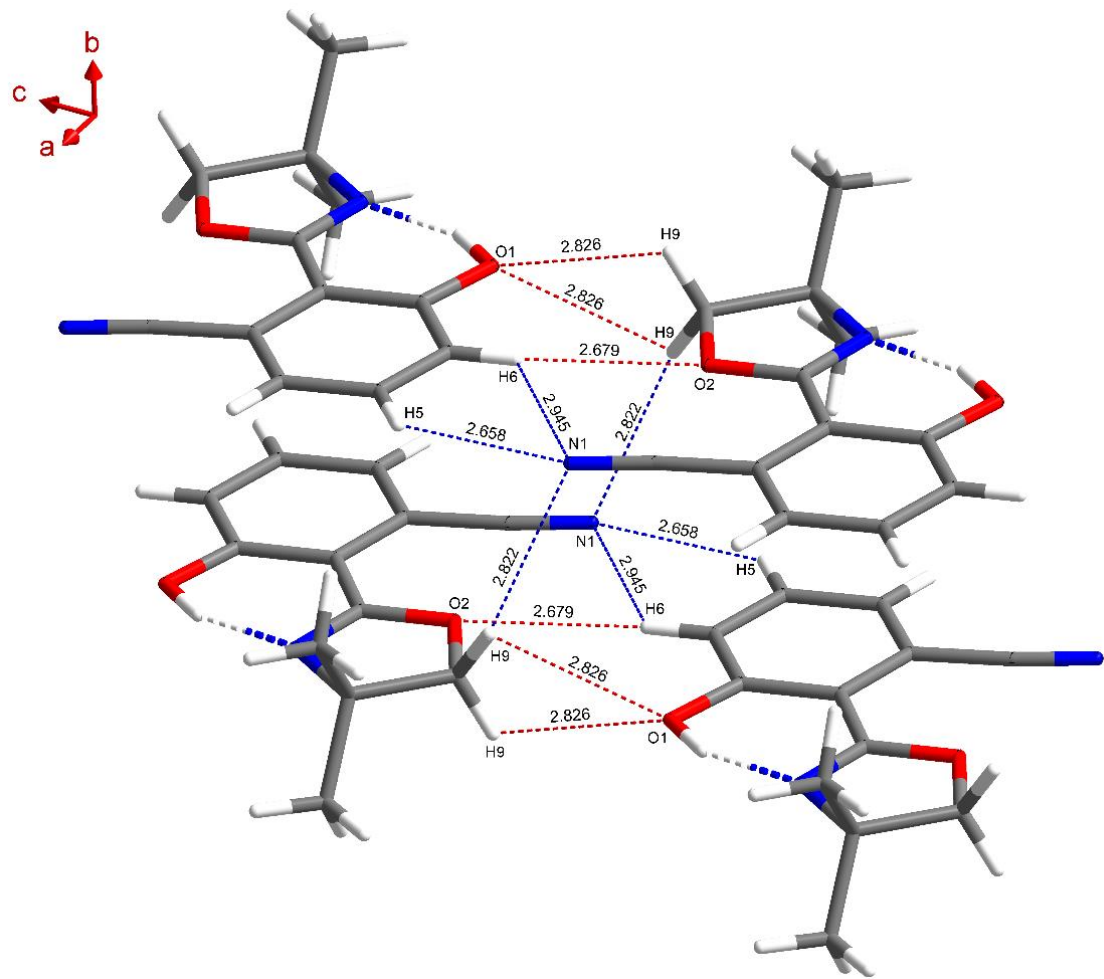


Figure S120: Various intermolecular interactions in 1-CN crystal lattice up to 3.000 Å distances, including C–H···O (red dotted lines) and C–H···N (blue dotted lines) interactions. All distances are given in Å.

4.1.4 Intermolecular π - π -Interactions in Crystal Lattice of 1-CN

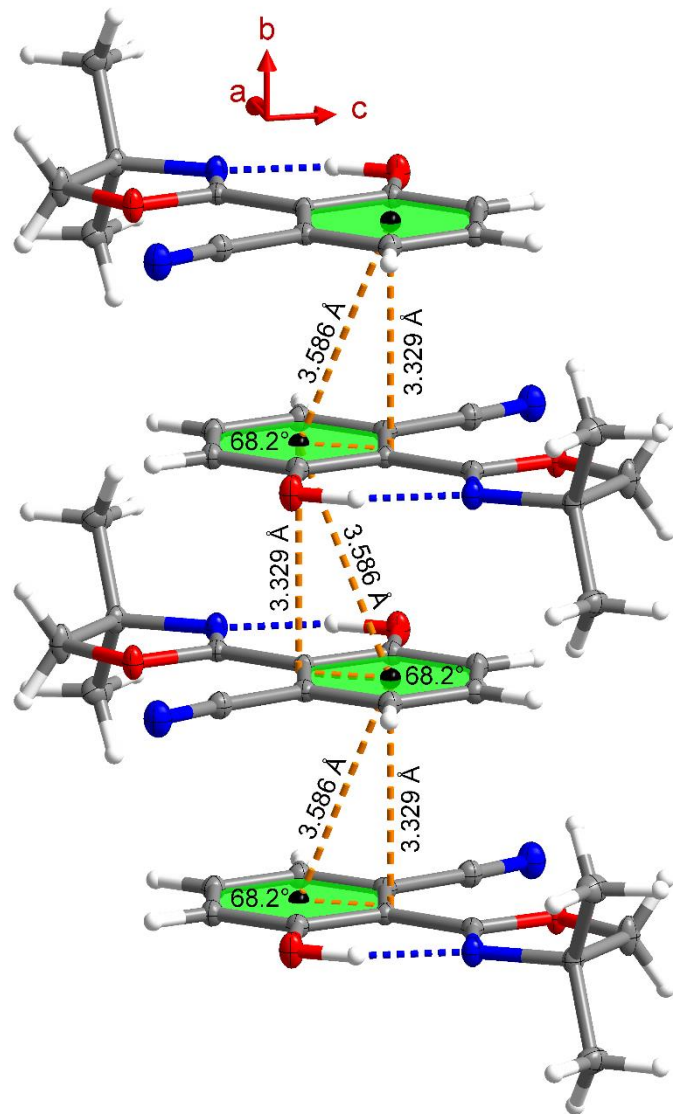


Figure S121: Intermolecular π - π -interactions of four adjacent molecules in **1-CN** crystal lattice with plane distance (orange dashed line) and corresponding centroid-centroid distance (orange dashed line between black spheres). All distances are given in Å.

4.2 3-(4,4-Dimethyl-4,5-dihydrooxazol-2-yl)-4-hydroxybenzonitrile (2-CN)

4.2.1 Crystal Data for 2-CN.

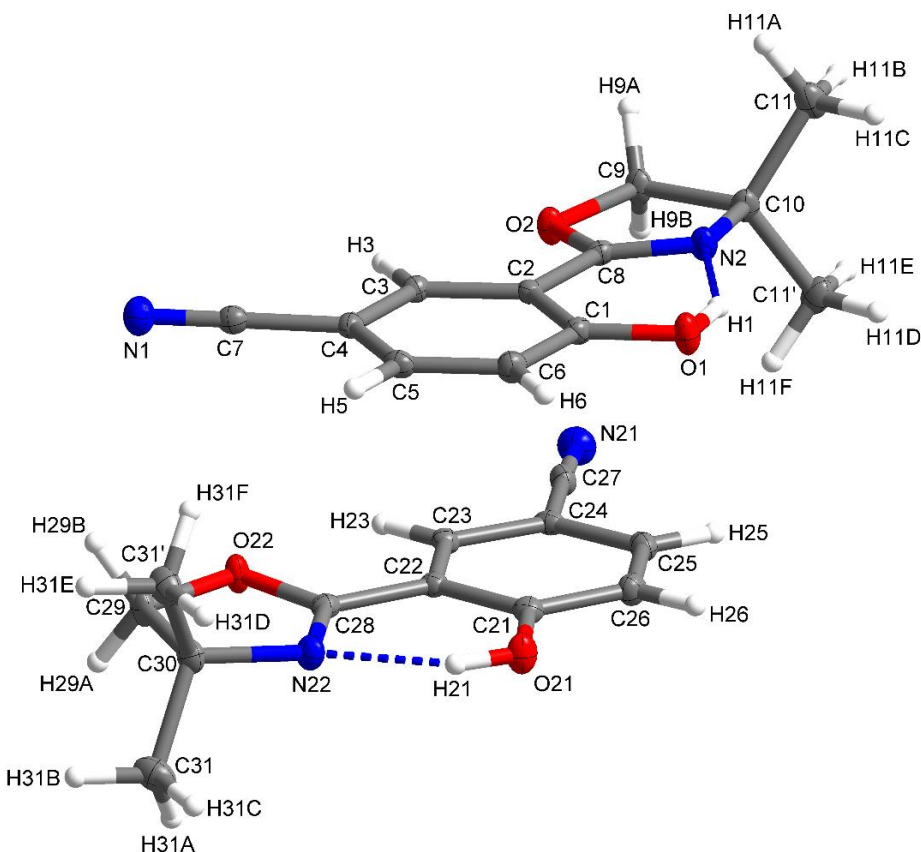


Figure S122: Asymmetric unit of 2-CN with atom labels.

Table S8: Crystal data and structure refinement for 2-CN.

Empirical formula	C ₁₂ H ₁₂ N ₂ O ₂
Formula weight, g mol ⁻¹	216.24
Crystal system	Triclinic
Crystal size, mm ³	0.28 × 0.15 × 0.11
Space group	P-1
a/Å	6.7920(3)
b/Å	12.0885(5)
c/Å	14.1497(5)
α/°	112.3500(10)
β/°	93.1240(10)
γ/°	95.396(2)
Volume/Å ³	1064.57(8)

Z	4
ρ_{calc} , g/cm ³	1.349
μ/mm^{-1}	0.094
F(000)	456.0
2 Θ range for data collection/ $^{\circ}$	5.672 to 52.99
	-7 \leq h \leq 8
Index ranges	-15 \leq k \leq 15
	-17 \leq l \leq 17
No. of reflections collected	26149
No of independent reflections	4419 [$R_{\text{int}} = 0.0570$, $R_{\text{sigma}} = 0.0354$]
Data/restraints/parameters	4419/0/295
Goodness-of-fit on F ²	1.073
Final R indexes [I $\geq 2\sigma$ (I)]	$R_1 = 0.0539$, wR ₂ = 0.1407
Final R indexes [all data]	$R_1 = 0.0735$, wR ₂ = 0.1545
Largest diff. peak/hole / e Å ⁻³	0.52/-0.35
CCDC number	1970921

Table S9: Fractional Atomic Coordinates ($\times 10^4$) and Equivalent Isotropic Displacement Parameters (Å² $\times 10^3$) for **2-CN**. U_{eq} is defined as 1/3 of the trace of the orthogonalized U_{II} tensor.

Atom	x	y	z	U(eq)
O1	6995(2)	5330.2(12)	944.8(10)	19.1(3)
N1	8883(3)	9141.9(15)	5877.0(13)	19.6(4)
C1	7333(3)	6127.3(16)	1918.2(14)	13.4(4)
O2	7687(2)	9042.7(11)	1631.0(10)	15.3(3)
N2	7423(2)	7164.4(14)	398.5(12)	15.0(4)
C2	7637(3)	7381.6(16)	2176.3(13)	11.3(4)
C3	8009(3)	8167.6(16)	3200.2(14)	12.2(4)
C4	8079(3)	7713.6(16)	3966.1(14)	12.7(4)
C5	7777(3)	6465.6(17)	3709.4(14)	14.4(4)
C6	7404(3)	5686.2(17)	2698.0(14)	15.7(4)
C7	8523(3)	8524.4(16)	5028.9(14)	14.2(4)
C8	7580(3)	7833.2(16)	1350.8(14)	12.5(4)
C9	7676(3)	9231.0(16)	673.6(14)	15.7(4)

C10	7354(3)	7952.9(16)	-186.1(14)	14.6(4)
C11	9001(3)	7738.0(17)	-902.5(15)	19.4(4)
C11'	5322(3)	7675.2(18)	-794.7(15)	20.2(4)
C21	2444(3)	6099.1(16)	2650.7(14)	13.2(4)
O21	2269(2)	5140.7(11)	2910.3(10)	18.4(3)
N21	2877(3)	9796.0(16)	1413.2(13)	22.1(4)
N22	2870(2)	6640.5(14)	4814.0(12)	15.8(4)
C22	2858(3)	7292.5(16)	3395.7(14)	11.7(4)
O22	3642(2)	8624.3(11)	5166.6(10)	16.6(3)
C23	2991(3)	8255.2(16)	3078.9(14)	12.0(4)
C24	2723(3)	8041.2(17)	2042.2(14)	12.8(4)
C25	2347(3)	6857.3(17)	1305.3(14)	14.8(4)
C26	2213(3)	5902.8(17)	1613.1(14)	15.9(4)
C27	2816(3)	9030.8(17)	1706.8(14)	14.3(4)
C28	3106(3)	7485.6(16)	4479.5(14)	12.4(4)
C29	3753(3)	8544.7(17)	6172.3(14)	17.3(4)
C30	3322(3)	7181.8(17)	5945.1(14)	15.7(4)
C31	1525(3)	6900(2)	6452.9(16)	22.4(5)
C31'	5137(3)	6678.7(19)	6230.1(15)	20.0(4)

Table S10: Bond Lengths for **2-CN**.

Atom	Atom	Length/Å	Atom	Atom	Length/Å
O1	C1	1.339(2)	C21	O21	1.339(2)
N1	C7	1.144(2)	C21	C22	1.416(3)
C1	C2	1.410(3)	C21	C26	1.393(3)
C1	C6	1.397(3)	N21	C27	1.148(2)
O2	C8	1.355(2)	N22	C28	1.280(2)
O2	C9	1.456(2)	N22	C30	1.482(2)
N2	C8	1.273(2)	C22	C23	1.395(2)
N2	C10	1.483(2)	C22	C28	1.458(3)
C2	C3	1.391(2)	O22	C28	1.350(2)
C2	C8	1.465(2)	O22	C29	1.461(2)

C3	C4	1.389(3)	C23	C24	1.388(3)
C4	C5	1.403(3)	C24	C25	1.403(3)
C4	C7	1.445(3)	C24	C27	1.443(2)
C5	C6	1.375(3)	C25	C26	1.377(3)
C9	C10	1.547(3)	C29	C30	1.549(3)
C10	C11	1.525(3)	C30	C31	1.526(3)
C10	C11'	1.524(3)	C30	C31'	1.525(3)

Table S11: Bond Angles for **2-CN**.

Atom	Atom	Atom	Angle/ [°]	Atom	Atom	Atom	Angle/ [°]
O1	C1	C2	122.42(16)	O21	C21	C22	122.05(16)
O1	C1	C6	118.13(16)	O21	C21	C26	118.34(17)
C6	C1	C2	119.44(17)	C26	C21	C22	119.61(17)
C8	O2	C9	105.26(13)	C28	N22	C30	108.09(15)
C8	N2	C10	107.92(15)	C21	C22	C28	119.07(16)
C1	C2	C8	118.94(16)	C23	C22	C21	119.41(17)
C3	C2	C1	119.95(16)	C23	C22	C28	121.52(16)
C3	C2	C8	121.10(16)	C28	O22	C29	105.61(14)
C4	C3	C2	119.86(16)	C24	C23	C22	120.08(17)
C3	C4	C5	120.20(17)	C23	C24	C25	120.36(17)
C3	C4	C7	120.08(16)	C23	C24	C27	120.57(17)
C5	C4	C7	119.70(17)	C25	C24	C27	119.06(17)
C6	C5	C4	120.09(17)	C26	C25	C24	119.83(17)
C5	C6	C1	120.46(17)	C25	C26	C21	120.69(18)
N1	C7	C4	178.23(19)	N21	C27	C24	178.1(2)
O2	C8	C2	117.16(15)	N22	C28	C22	123.96(17)
N2	C8	O2	118.57(16)	N22	C28	O22	118.32(16)
N2	C8	C2	124.26(16)	O22	C28	C22	117.71(16)
O2	C9	C10	105.29(14)	O22	C29	C30	105.16(14)
N2	C10	C9	102.63(14)	N22	C30	C29	102.67(14)
N2	C10	C11	109.93(15)	N22	C30	C31	109.64(16)
N2	C10	C11'	108.62(15)	N22	C30	C31'	108.67(15)

C11	C10	C9	112.25(15)	C31	C30	C29	112.08(16)
C11'	C10	C9	112.38(16)	C31'	C30	C29	112.19(17)
C11'	C10	C11	110.68(16)	C31'	C30	C31	111.20(16)

Table S12: Torsion Angles for **2-CN**.

A	B	C	D	Angle/ [°]	A	B	C	D	Angle/ [°]
O1	C1	C2	C3	-179.11(17)	C21	C22	C23	C24	-0.1(3)
O1	C1	C2	C8	0.0(3)	C21	C22	C28	N22	-3.8(3)
O1	C1	C6	C5	178.98(18)	C21	C22	C28	O22	175.27(16)
C1	C2	C3	C4	-0.1(3)	O21	C21	C22	C23	-178.98(17)
C1	C2	C8	O2	173.84(16)	O21	C21	C22	C28	0.1(3)
C1	C2	C8	N2	-5.6(3)	O21	C21	C26	C25	178.96(17)
O2	C9	C10	N2	-5.60(19)	C22	C21	C26	C25	-1.2(3)
O2	C9	C10	C11	-123.57(17)	C22	C23	C24	C25	-1.0(3)
O2	C9	C10	C11'	110.90(17)	C22	C23	C24	C27	178.69(17)
C2	C1	C6	C5	-0.4(3)	O22	C29	C30	N22	-3.81(19)
C2	C3	C4	C5	0.0(3)	O22	C29	C30	C31	-121.39(17)
C2	C3	C4	C7	178.21(17)	O22	C29	C30	C31'	112.67(17)
C3	C2	C8	O2	-7.0(3)	C23	C22	C28	N22	175.24(18)
C3	C2	C8	N2	173.49(18)	C23	C22	C28	O22	-5.7(3)
C3	C4	C5	C6	-0.2(3)	C23	C24	C25	C26	1.0(3)
C4	C5	C6	C1	0.4(3)	C24	C25	C26	C21	0.1(3)
C6	C1	C2	C3	0.2(3)	C26	C21	C22	C23	1.2(3)
C6	C1	C2	C8	179.38(17)	C26	C21	C22	C28	-179.69(17)
C7	C4	C5	C6	-178.38(18)	C27	C24	C25	C26	-178.69(17)
C8	O2	C9	C10	5.03(19)	C28	N22	C30	C29	3.1(2)
C8	N2	C10	C9	4.3(2)	C28	N22	C30	C31	122.38(17)
C8	N2	C10	C11	123.86(17)	C28	N22	C30	C31'	-115.90(18)
C8	N2	C10	C11'	-114.90(18)	C28	C22	C23	C24	-179.21(17)
C8	C2	C3	C4	-179.18(17)	C28	O22	C29	C30	3.28(19)
C9	O2	C8	N2	-2.6(2)	C29	O22	C28	N22	-1.5(2)
C9	O2	C8	C2	177.87(16)	C29	O22	C28	C22	179.37(16)

C10	N2	C8	O2	-1.2(2)	C30	N22	C28	C22	177.92(17)
C10	N2	C8	C2	178.22(17)	C30	N22	C28	O22	-1.2(2)

Table S13: Hydrogen Atom Coordinates ($\text{\AA} \times 10^4$) and Isotropic Displacement Parameters ($\text{\AA}^2 \times 10^3$) for **2-CN**.

Atom	x	y	z	U(eq)
H1	7044.46	5697.54	546.46	29
H3	8214.96	9013.21	3375.56	15
H5	7830.33	6158.37	4235.23	17
H6	7192.24	4841.83	2528.32	19
H9A	8955	9672.18	637.47	19
H9B	6587.59	9697.61	613.11	19
H11A	10292.67	7904.47	-499.02	29
H11B	8964.52	8273.98	-1275.4	29
H11C	8806.08	6897.51	-1393.54	29
H11D	5105.91	6823.02	-1258.61	30
H11E	5266.04	8178.63	-1196.64	30
H11F	4287.27	7845.4	-320.32	30
H21	2402.21	5373.81	3552.83	28
H23	3265.84	9058.58	3573.54	14
H25	2184.85	6714.51	595.72	18
H26	1960.99	5101.92	1112.34	19
H29A	2752.9	8995.05	6593.25	21
H29B	5090.02	8877.05	6543.3	21
H31A	383.99	7235.55	6259.48	34
H31B	1828	7258.08	7200.62	34
H31C	1206.82	6024.25	6224.77	34
H31D	4844.7	5802.44	6006.73	30
H31E	5468.51	7042.44	6975.97	30
H31F	6265.25	6867.89	5890.71	30

4.2.2 Crystal Packing Views of 2-CN

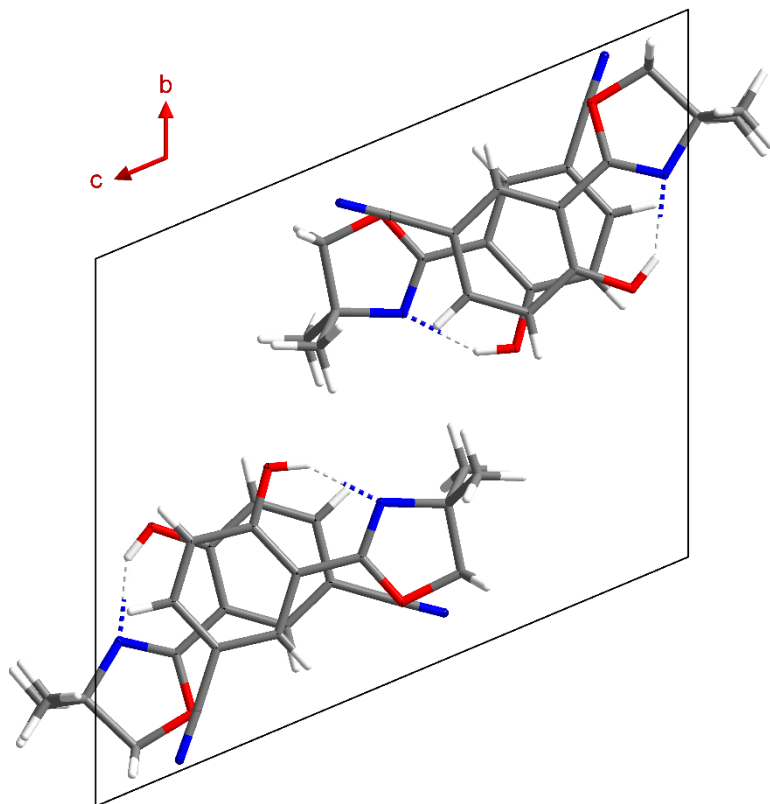


Figure S123: Unit cell packing view of a **2-CN** crystal along the *a*-axis.

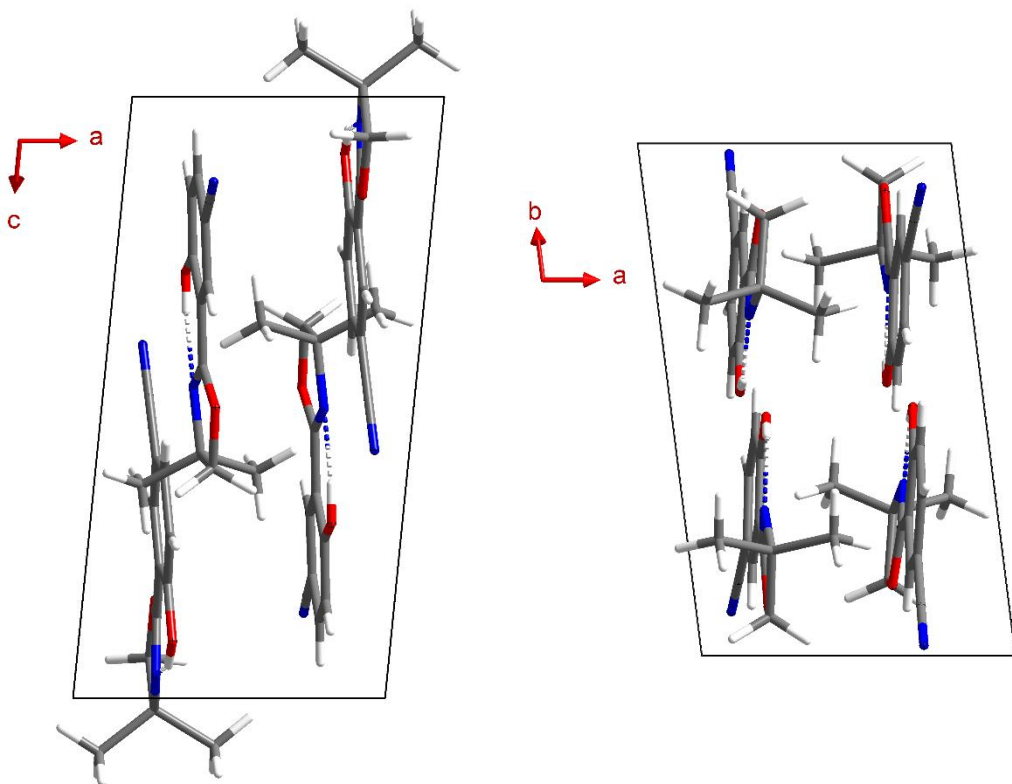


Figure S124: Unit cell packing view of a **2-CN** crystal along the *b*-axis (left) and along the *c*-axis (right).

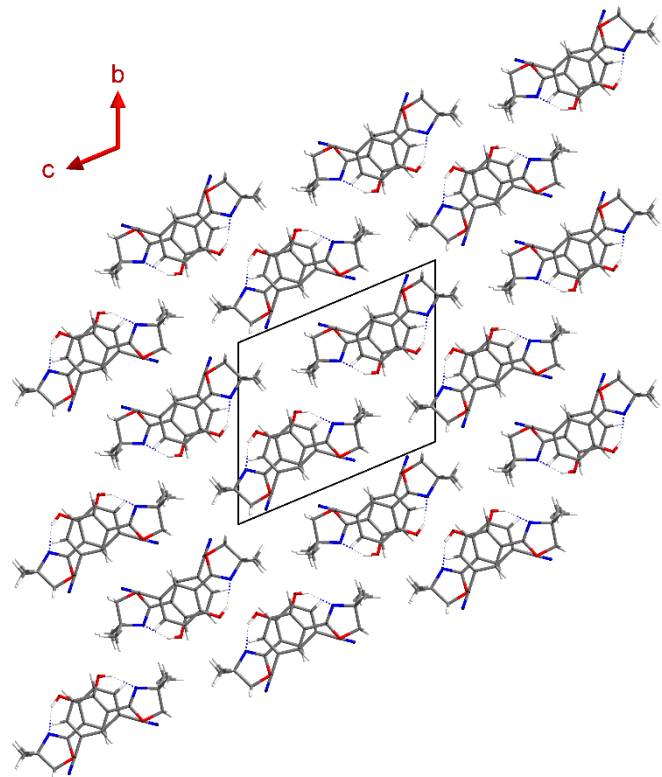


Figure S125: Unit cell (3x3x3) packing view of a 2-CN crystal along the *a*-axis.

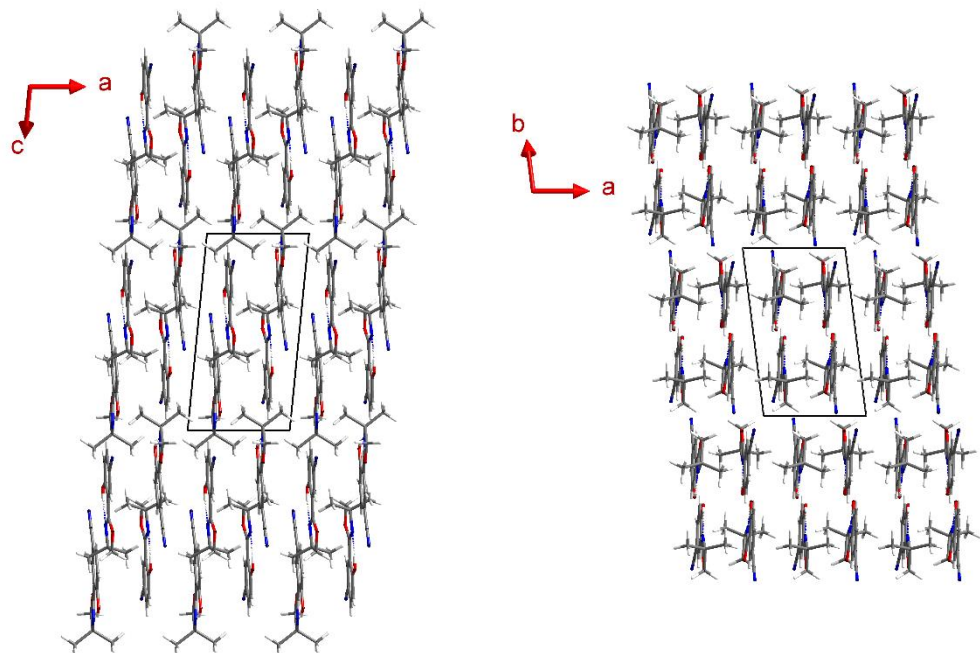


Figure S126: Unit cell (3x3x3) packing view of a 2-CN crystal along the *b*-axis (left) and along the *c*-axis (right).

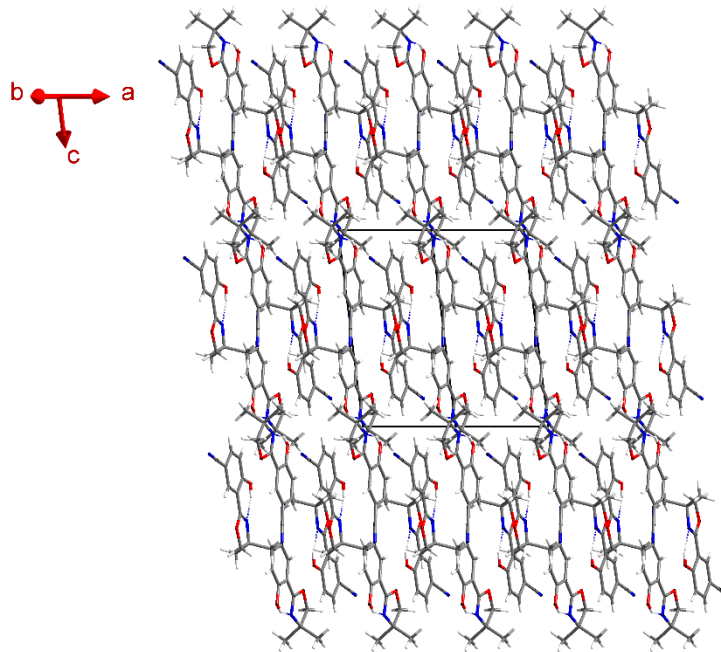


Figure S127: Unit cell ($3 \times 3 \times 3$) packing view of a **2-CN** crystal along the 110 -axis.

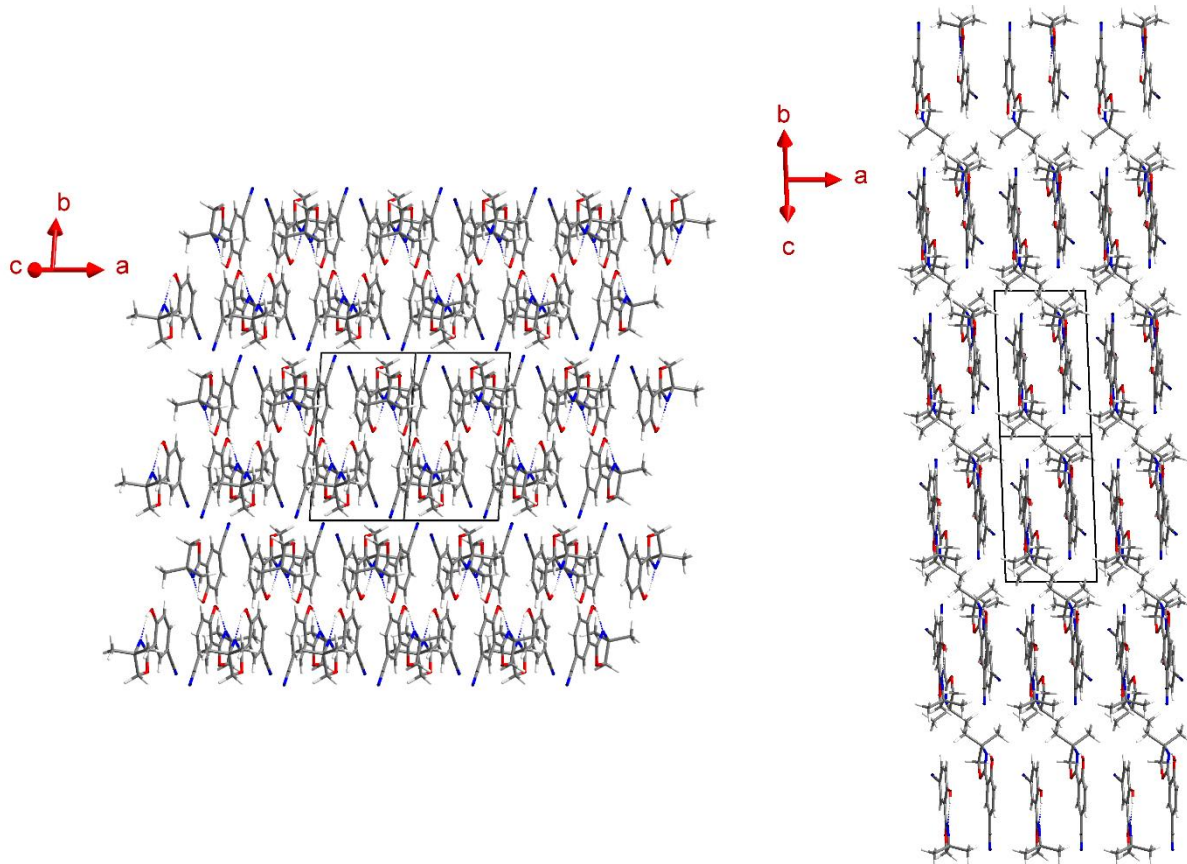


Figure S128: Unit cell ($3 \times 3 \times 3$) packing view of a **2-CN** crystal along the 101 -axis (left) and along the 011 -axis (right).

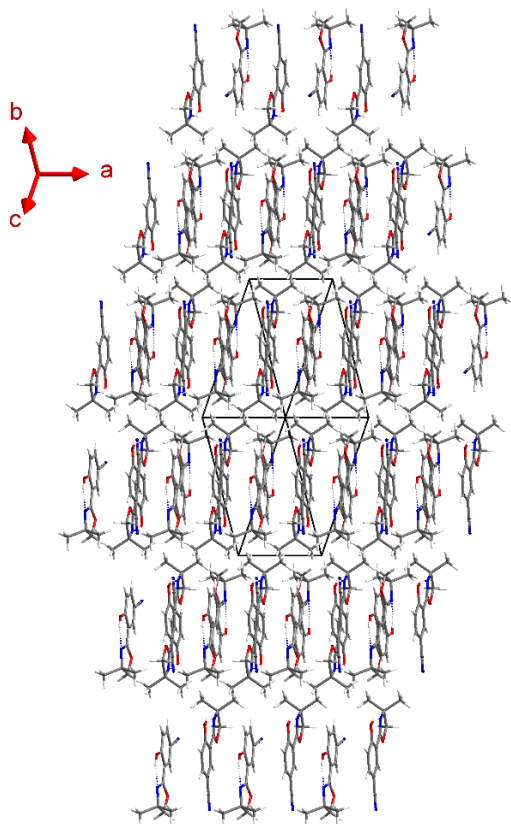


Figure S129: Unit cells (3x3x3) packing view of a 2-CN crystal along the 111-axis.

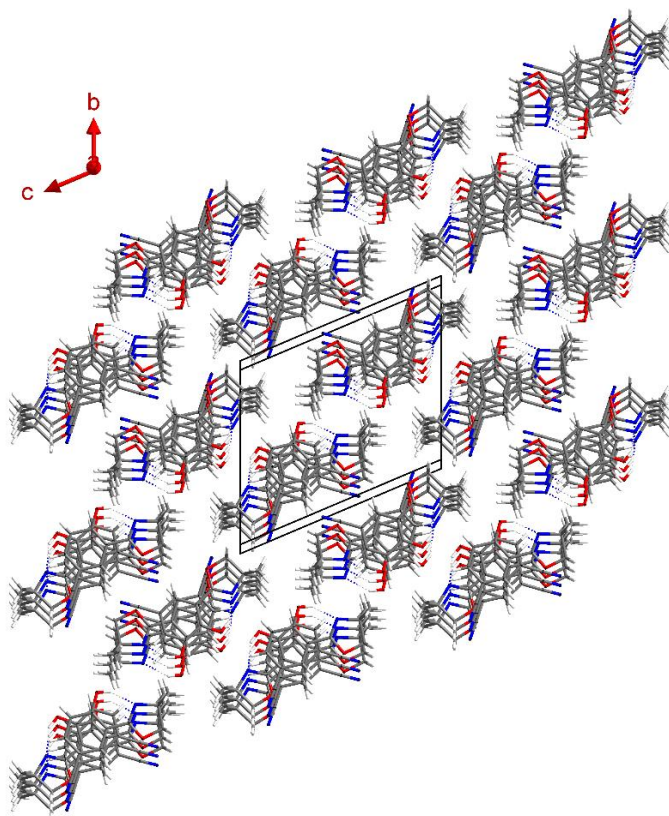


Figure S130: Unit cells (3x3x3) packing view of a 2-CN crystal along the *a*-axis with 5° rotation around the *x*-axis.

4.2.3 Intermolecular Contacts in Crystal Lattice of 2-CN

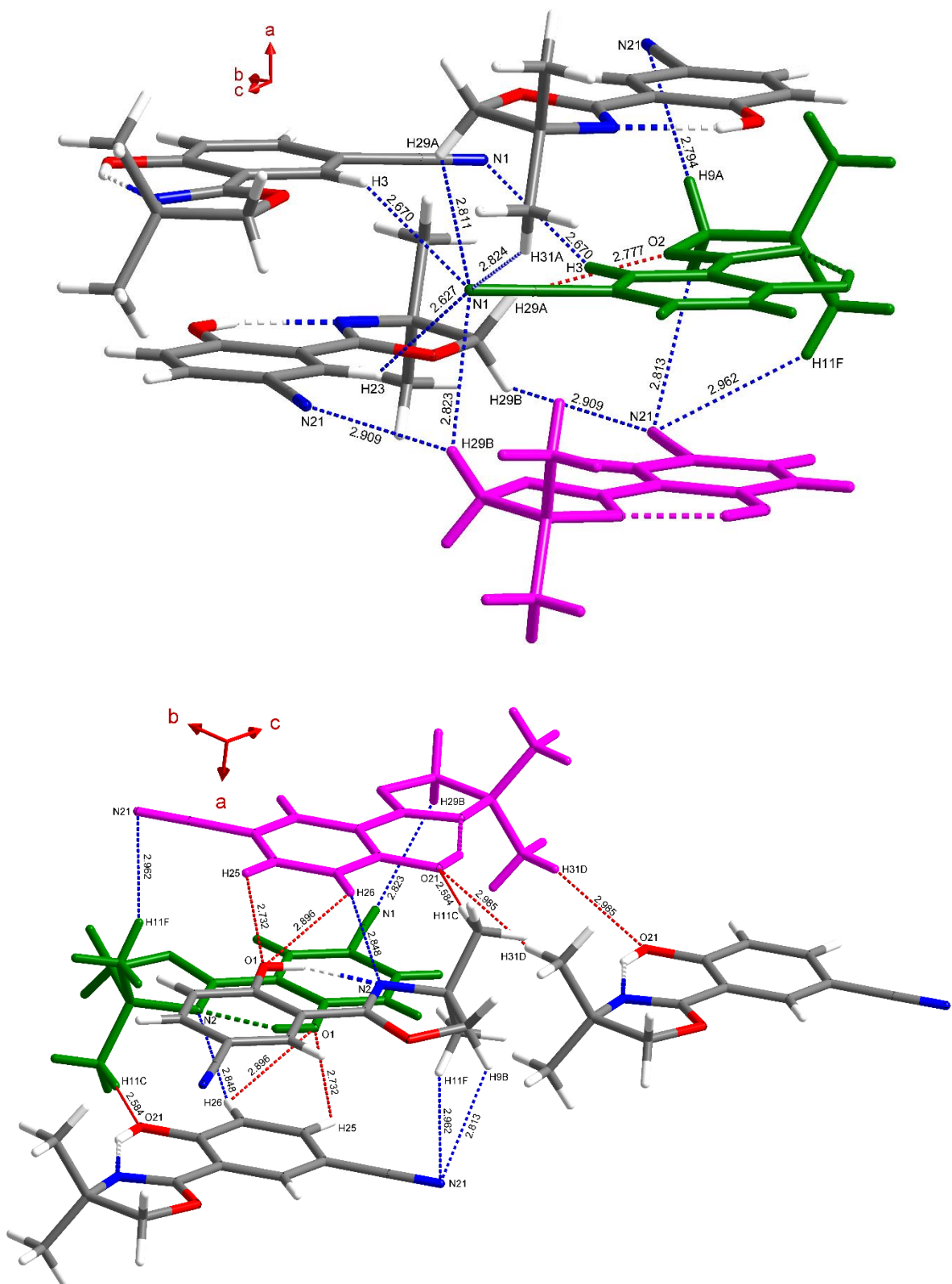


Figure S131: Various intermolecular interactions in 2-CN crystal lattice up to 3.000 Å distances, including C–H...O (red dotted lines) and C–H...N (blue dotted lines) interactions. All distances are given in Å. For a better overview, two definite molecules are colored green and pink, respectively.

4.2.4 Intermolecular π - π -Interactions in Crystal Lattice of 2-CN

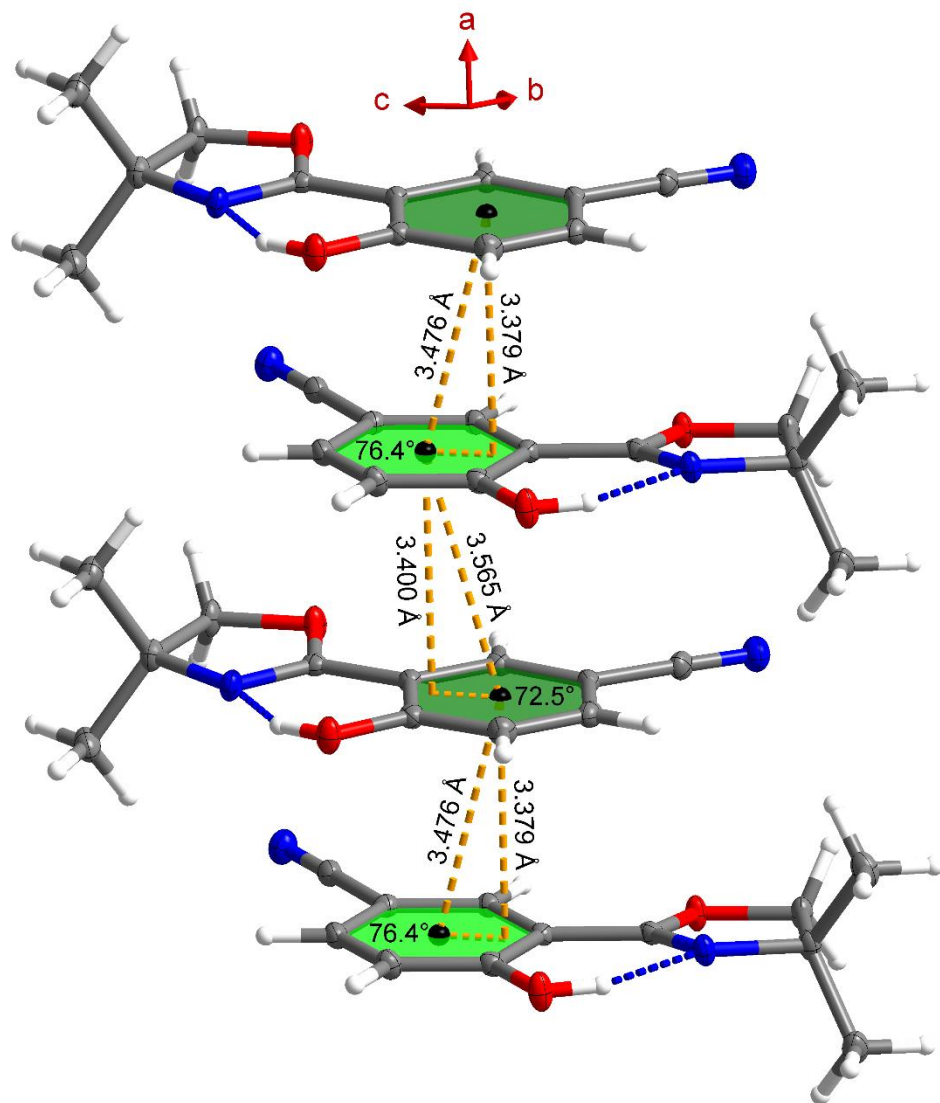


Figure S132: Intermolecular π - π -interactions of four adjacent molecules in **2-CN** crystal lattice with plane distance (orange dashed line) and corresponding centroid-centroid distance (orange dashed line between black spheres). All distances are given in Å.

4.3 4-(4,4-Dimethyl-4,5-dihydrooxazol-2-yl)-3-hydroxybenzonitrile (3-CN)

4.3.1 Crystal Data for 3-CN

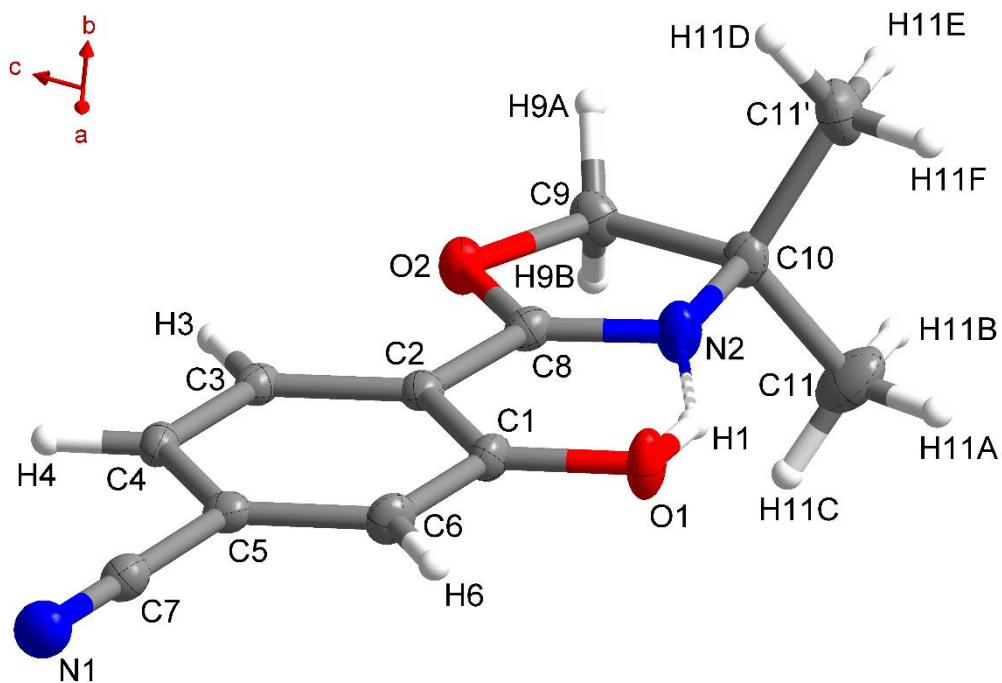


Figure S133: Asymmetric unit of 3-CN with atom labels.

Table S14: Crystal data and structure refinement for 3-CN.

Empirical formula	C ₁₂ H ₁₂ N ₂ O ₂
Formula weight, g mol ⁻¹	216.24
Crystal system	Monoclinic
Crystal size, mm ³	0.24 × 0.13 × 0.11
Space group	P2 ₁ /c
a/Å	12.9061(12)
b/Å	6.6510(6)
c/Å	13.8072(12)
α/°	90
β/°	110.888(3)
γ/°	90
Volume/Å ³	1107.30(17)
Z	4
ρ _{calc} , g/cm ³	1.297
μ/mm ⁻¹	0.090

F(000)	456.0
2Θ range for data collection/ $^\circ$	6.316 to 55.496
	$-16 \leq h \leq 16$
Index ranges	$-8 \leq k \leq 8$
	$-18 \leq l \leq 18$
No. of reflections collected	27844
No of independent reflections	2600 [$R_{\text{int}} = 0.0390$, $R_{\text{sigma}} = 0.0210$]
Data/restraints/parameters	2600/0/148
Goodness-of-fit on F^2	1.080
Final R indexes [$I \geq 2\sigma(I)$]	$R_I = 0.0405$, $wR_2 = 0.1044$
Final R indexes [all data]	$R_I = 0.0521$, $wR_2 = 0.1109$
Largest diff. peak/hole / e \AA^{-3}	0.36/−0.25
CCDC number	1970920

Table S15: Fractional Atomic Coordinates ($\times 10^4$) and Equivalent Isotropic Displacement Parameters ($\text{\AA}^2 \times 10^3$) for **3-CN**. U_{eq} is defined as 1/3 of the trace of the orthogonalized U_{II} tensor.

Atom	x	y	z	U(eq)
O1	4893.9(7)	3126.6(16)	2434.6(7)	25.7(2)
N1	8643.4(9)	2353.6(17)	6310.9(9)	25.9(3)
C1	5153.8(10)	2873.5(18)	3458.3(9)	17.3(3)
C2	4340.5(9)	2700.5(16)	3918.5(9)	14.6(2)
N2	2838.1(8)	2962.3(17)	2261.4(8)	22.1(2)
O2	2400.6(7)	2584.8(13)	3693.6(6)	19.2(2)
C3	4660.9(10)	2477.0(16)	4989.8(9)	15.3(2)
C4	5768.7(10)	2404.9(17)	5614.2(9)	16.1(2)
C5	6565.9(9)	2551.4(17)	5148.3(9)	16.2(3)
C6	6269.7(10)	2789.3(19)	4082.8(9)	18.8(3)
C7	7728.4(10)	2448.2(18)	5791.6(9)	19.3(3)
C8	3169.7(9)	2760.6(17)	3244.6(9)	16.2(2)
C9	1327.0(10)	2643.1(19)	2841.9(9)	20.3(3)
C10	1607.6(9)	2952(2)	1851.6(9)	19.6(3)
C11	1194.4(11)	1224(2)	1082.0(11)	35.0(4)

C11'	1191.1(11)	4965(2)	1332.5(10)	26.7(3)
------	------------	---------	------------	---------

Table S16: Bond Lengths for **3-CN**.

Atom	Atom	Length/Å	Atom	Atom	Length/Å
O1	C1	1.3418(14)	O2	C9	1.4637(14)
N1	C7	1.1441(16)	C3	C4	1.3823(16)
C1	C2	1.4122(16)	C4	C5	1.3978(16)
C1	C6	1.3912(16)	C5	C6	1.3909(17)
C2	C3	1.3947(16)	C5	C7	1.4471(16)
C2	C8	1.4656(16)	C9	C10	1.5480(17)
N2	C8	1.2766(16)	C10	C11	1.5266(18)
N2	C10	1.4837(15)	C10	C11'	1.5230(18)
O2	C8	1.3500(14)			

Table S17: Bond Angles for **3-CN**.

Atom	Atom	Atom	Angle/°	Atom	Atom	Atom	Angle/°
O1	C1	C2	122.51(11)	C5	C6	C1	119.58(10)
O1	C1	C6	118.21(10)	N1	C7	C5	179.02(13)
C6	C1	C2	119.28(11)	N2	C8	C2	123.84(11)
C1	C2	C8	118.39(10)	N2	C8	O2	118.35(10)
C3	C2	C1	119.94(11)	O2	C8	C2	117.81(10)
C3	C2	C8	121.66(10)	O2	C9	C10	105.11(9)
C8	N2	C10	108.22(10)	N2	C10	C9	102.67(9)
C8	O2	C9	105.62(9)	N2	C10	C11	109.25(10)
C4	C3	C2	120.98(10)	N2	C10	C11'	109.01(10)
C3	C4	C5	118.55(10)	C11	C10	C9	112.40(11)
C4	C5	C7	119.11(11)	C11'	C10	C9	112.21(10)
C6	C5	C4	121.66(11)	C11'	C10	C11	110.92(11)
C6	C5	C7	119.23(10)				

Table S18: Torsion Angles for **3-CN**.

A	B	C	D	Angle/°	A	B	C	D	Angle/°
O1	C1	C2	C3	-178.80(11)	C3	C4	C5	C7	-179.09(10)
O1	C1	C2	C8	1.26(17)	C4	C5	C6	C1	-0.37(18)
O1	C1	C6	C5	179.26(11)	C6	C1	C2	C3	0.91(17)
C1	C2	C3	C4	-0.53(17)	C6	C1	C2	C8	-179.03(11)
C1	C2	C8	N2	-0.05(17)	C7	C5	C6	C1	179.48(11)
C1	C2	C8	O2	179.71(10)	C8	C2	C3	C4	179.42(10)
C2	C1	C6	C5	-0.47(17)	C8	N2	C10	C9	-1.33(13)
C2	C3	C4	C5	-0.30(16)	C8	N2	C10	C11	-120.82(12)
O2	C9	C10	N2	1.95(12)	C8	N2	C10	C11'	117.83(11)
O2	C9	C10	C11	119.22(11)	C8	O2	C9	C10	-1.91(12)
O2	C9	C10	C11'	-114.95(11)	C9	O2	C8	C2	-178.57(10)
C3	C2	C8	N2	-179.99(11)	C9	O2	C8	N2	1.21(14)
C3	C2	C8	O2	-0.23(16)	C10	N2	C8	C2	179.90(11)
C3	C4	C5	C6	0.76(17)	C10	N2	C8	O2	0.14(15)

Table S19: Hydrogen Atom Coordinates ($\text{\AA} \times 10^4$) and Isotropic Displacement Parameters ($\text{\AA}^2 \times 10^3$) for **3-CN**.

Atom	x	y	z	U(eq)
H1	4201.03	3149.84	2141.43	39
H3	4109.53	2372.77	5295.04	18
H4	5983.56	2259.03	6344.05	19
H6	6825.89	2893.52	3783.4	23
H9A	868.45	3766.89	2935.44	24
H9B	918.68	1367.6	2803.21	24
H11A	1465.98	1403.58	509.18	52
H11B	381.66	1212.71	809.81	52
H11C	1470.22	-53.2	1433.07	52
H11D	1488.77	6053.26	1833.34	40
H11E	379	4991.14	1086.18	40
H11F	1437.65	5145.14	743.89	40

4.3.2 Crystal Packing Views of 3-CN

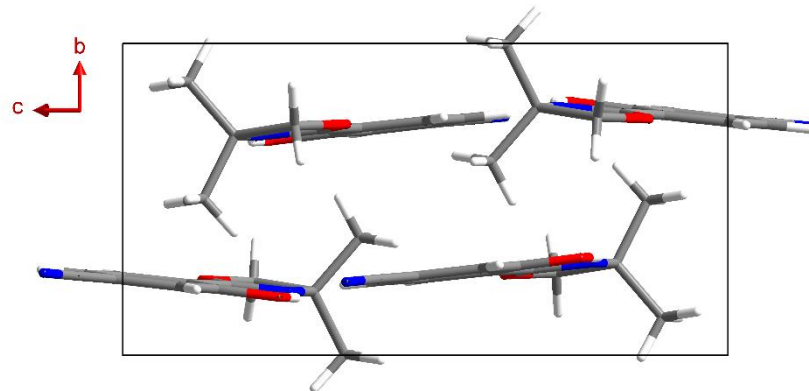


Figure S134: Unit cell packing view of a 3-CN crystal along the *a*-axis.

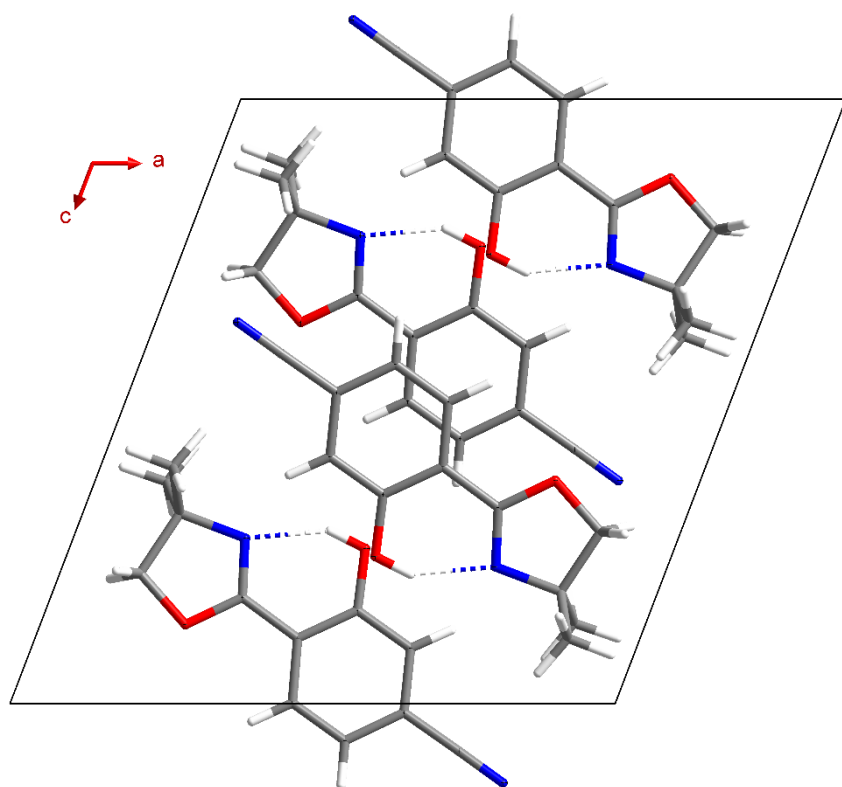


Figure S135: Unit cell packing view of a 3-CN crystal along the *b*-axis.

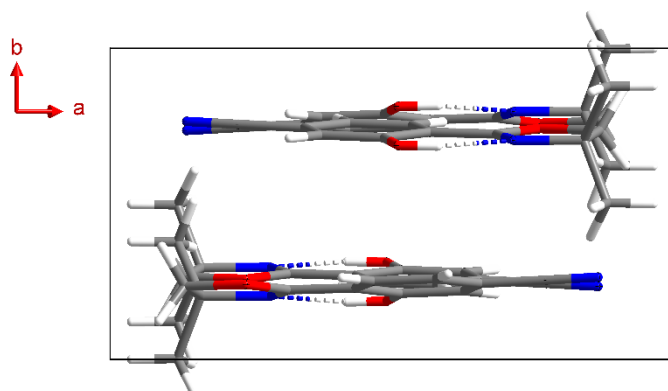


Figure S136: Unit cell packing view of a 3-CN crystal along the *c*-axis.

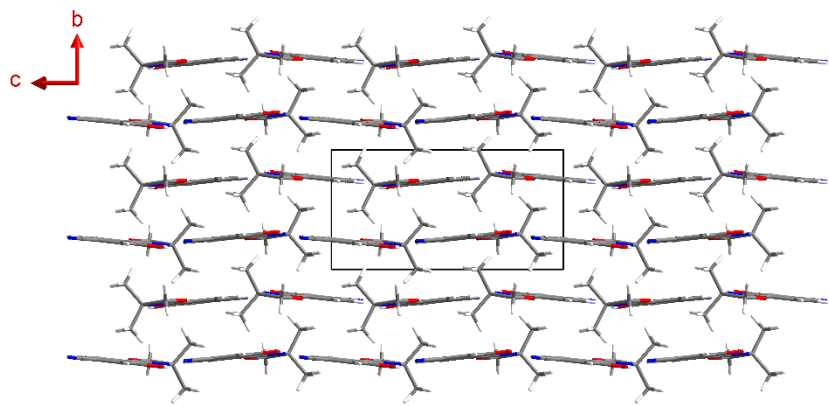


Figure S137: Unit cell (3x3x3) packing view of a 3-CN crystal along the *a*-axis.

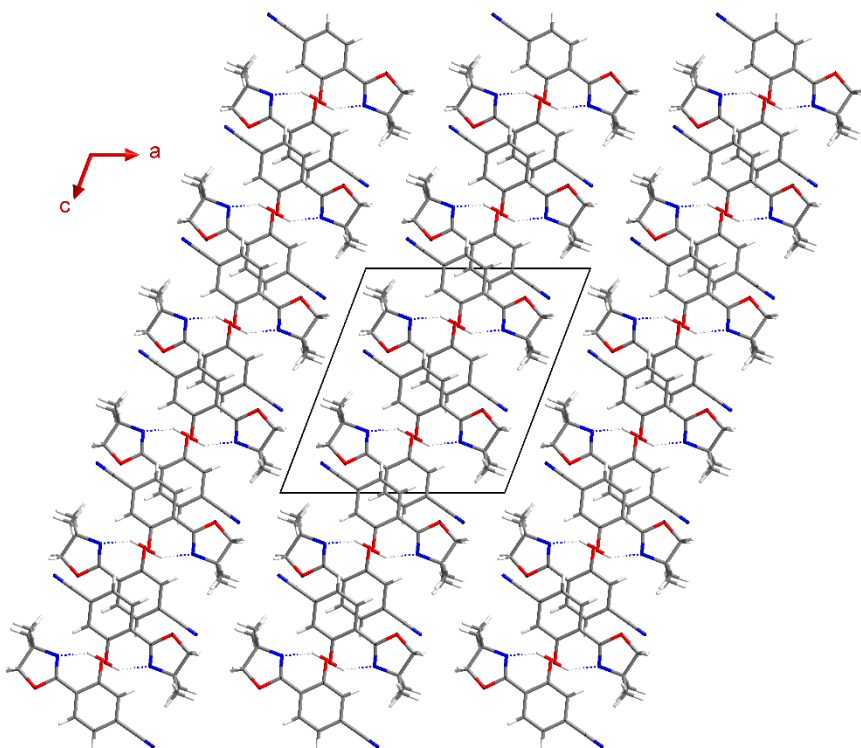


Figure S138: Unit cell (3x3x3) packing view of a 3-CN crystal along the *b*-axis.

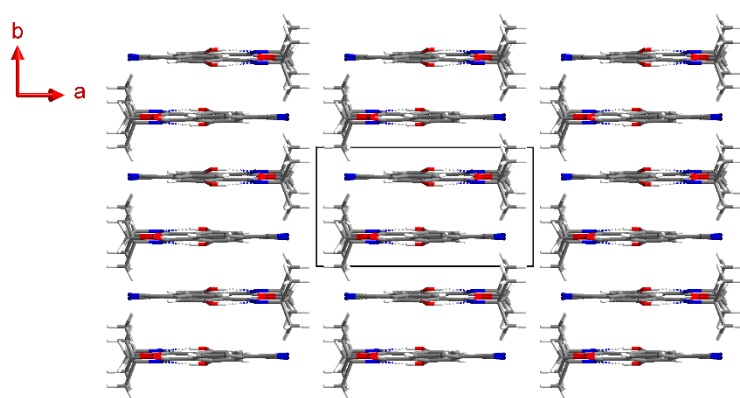


Figure S139: Unit cell (3x3x3) packing view of a 3-CN crystal along the *c*-axis.

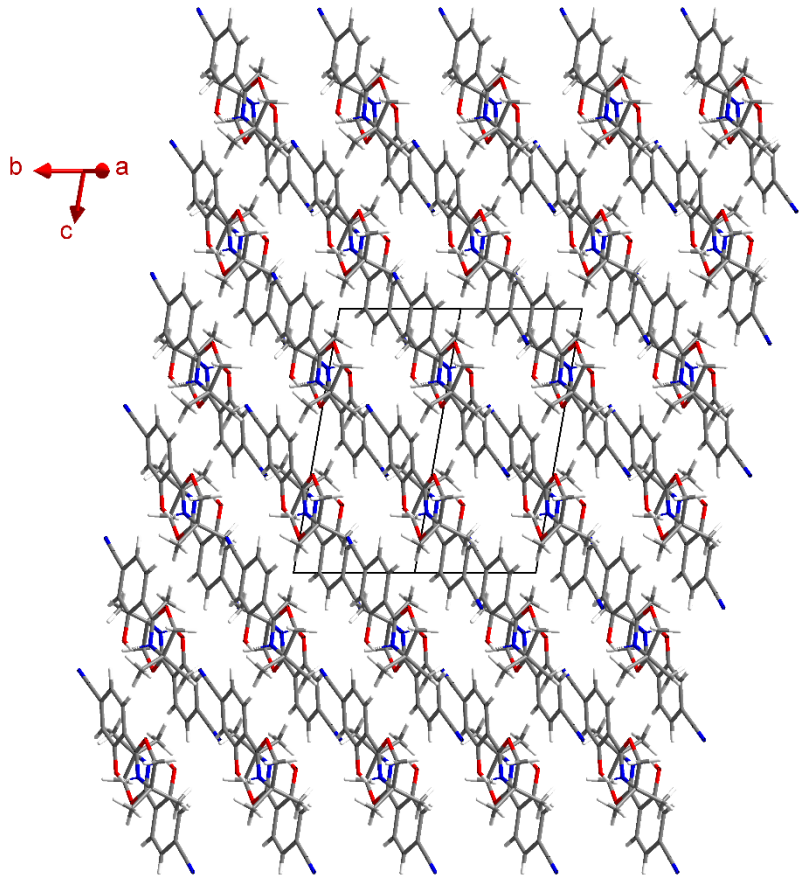


Figure S140: Unit cell (3x3x3) packing view of a 3-CN crystal along the 110-axis.

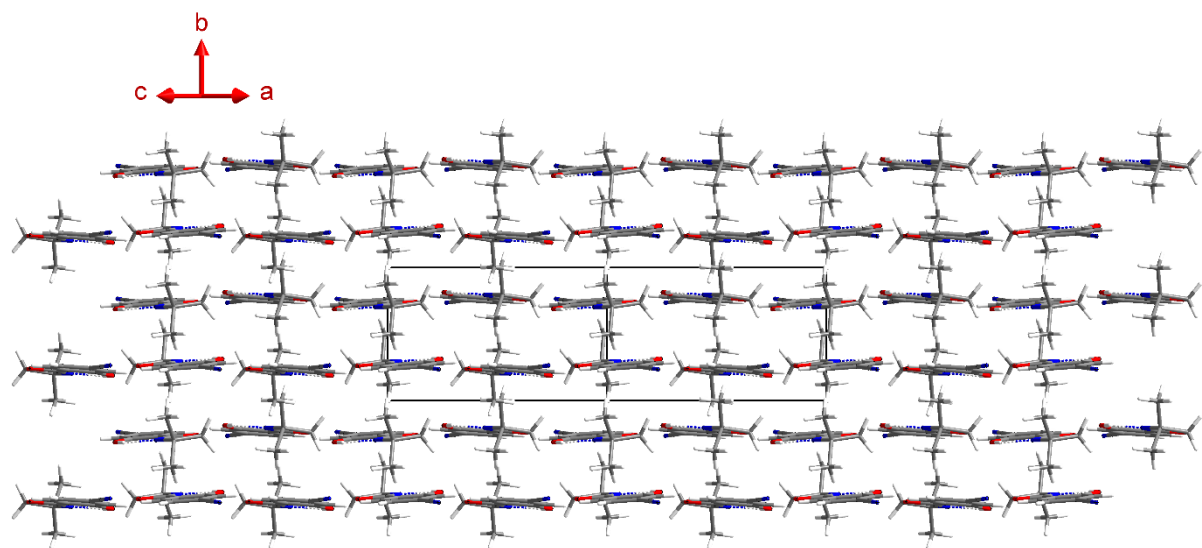


Figure S141: Unit cell (3x3x3) packing view of a 3-CN crystal along the 101-axis.

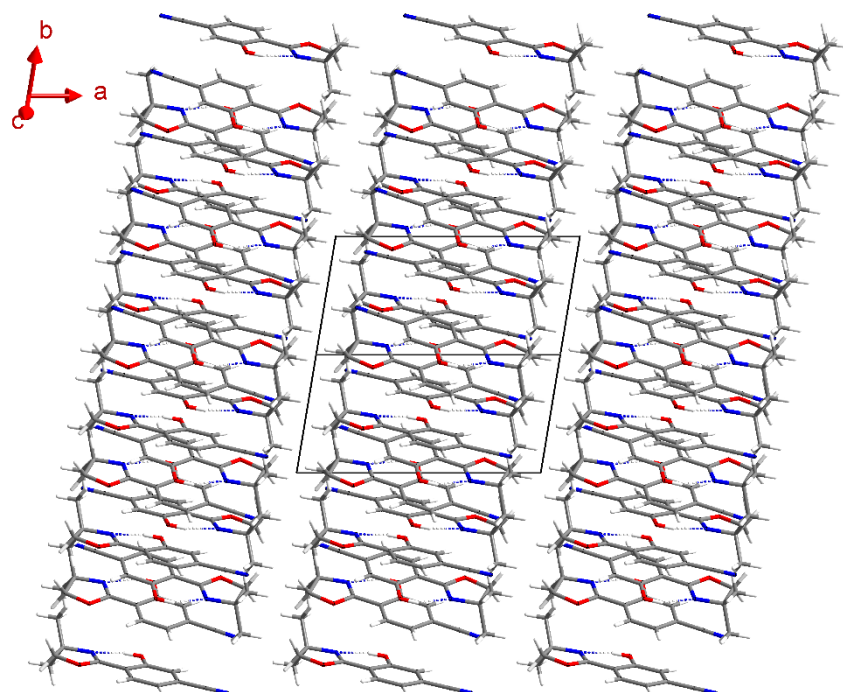


Figure S142: Unit cell ($3 \times 3 \times 3$) packing view of a **3-CN** crystal along the $0\bar{1}1$ -axis.

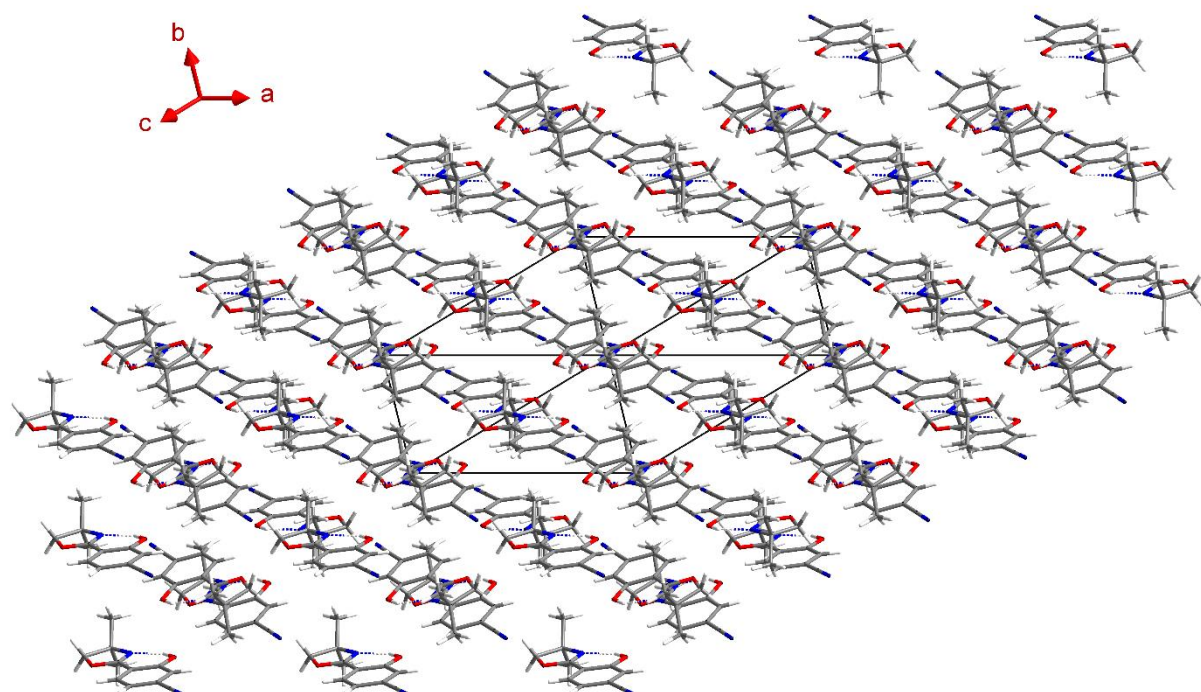


Figure S143: Unit cells ($3 \times 3 \times 3$) packing view of a **3-CN** crystal along the $1\bar{1}\bar{1}$ -axis.

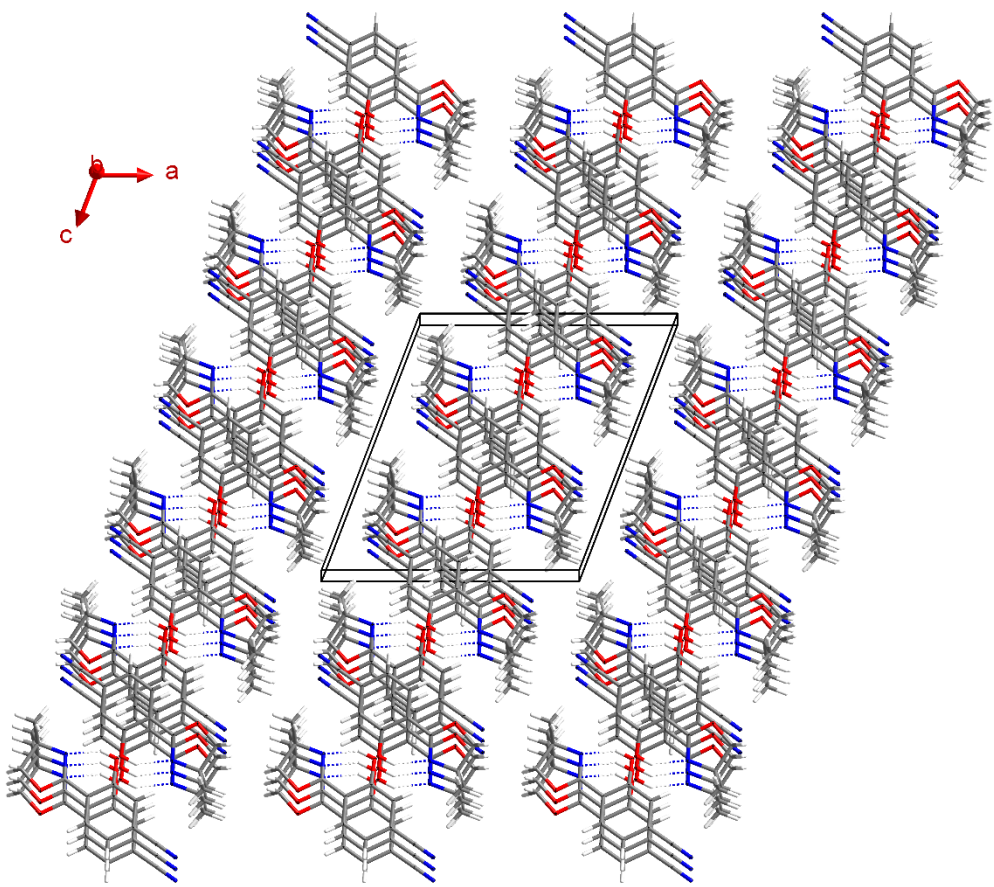


Figure S144: Unit cells ($3 \times 3 \times 3$) packing view of a **3-CN** crystal along the *b*-axis with 5° rotation around the *x*-axis.

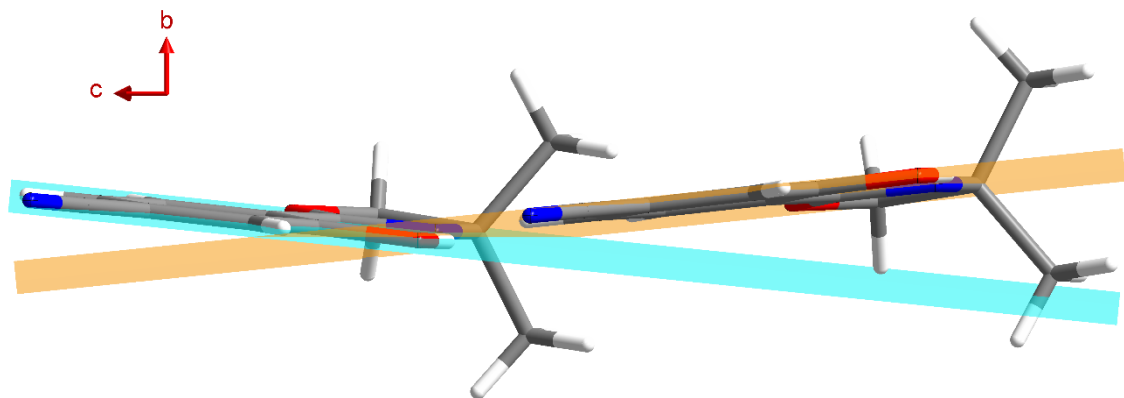


Figure S145: Out-of-plane distortion of **3-CN** within the unit cell results in a dihedral angle of 12.41° between the planes.

4.3.3 Intermolecular Contacts in Crystal Lattice of 3-CN

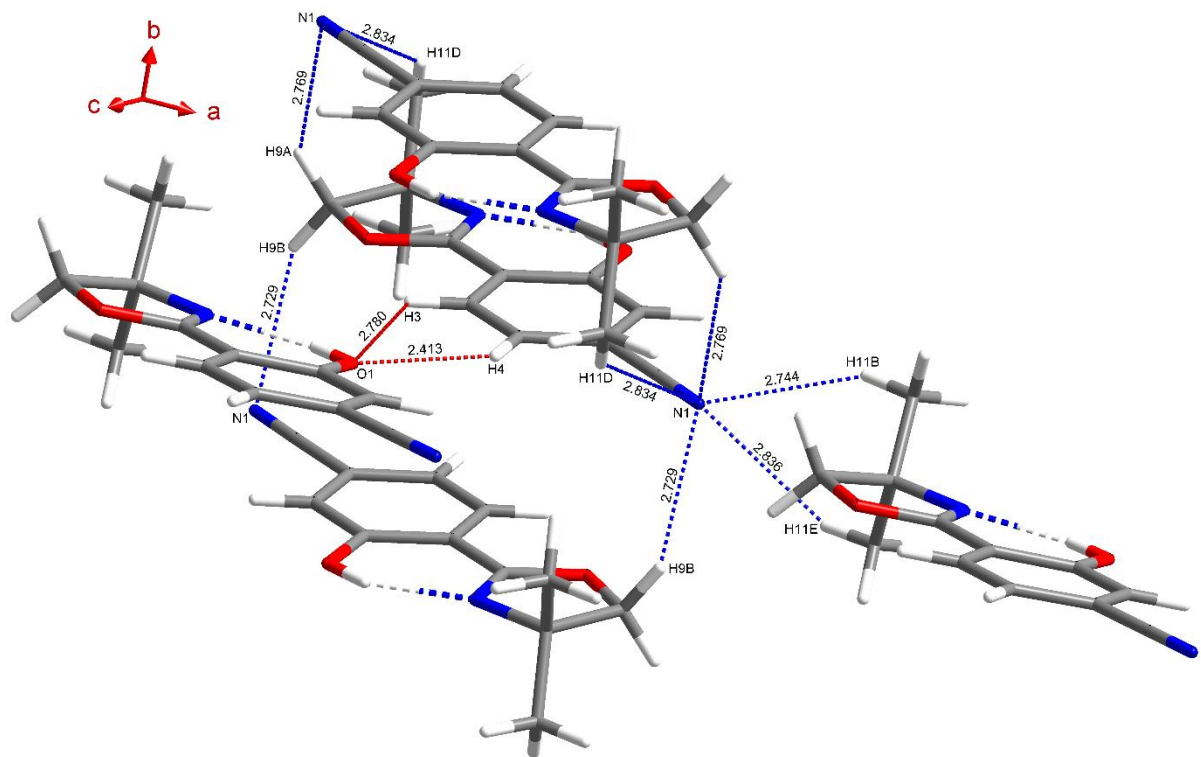


Figure S146: Various intermolecular interactions in 3-CN crystal lattice up to 3.000 Å distances, including C–H···O (red dotted lines) and C–H···N (blue dotted lines) interactions. All distances are given in Å.

4.3.4 Intermolecular π - π -Interactions in Crystal Lattice of 3-CN

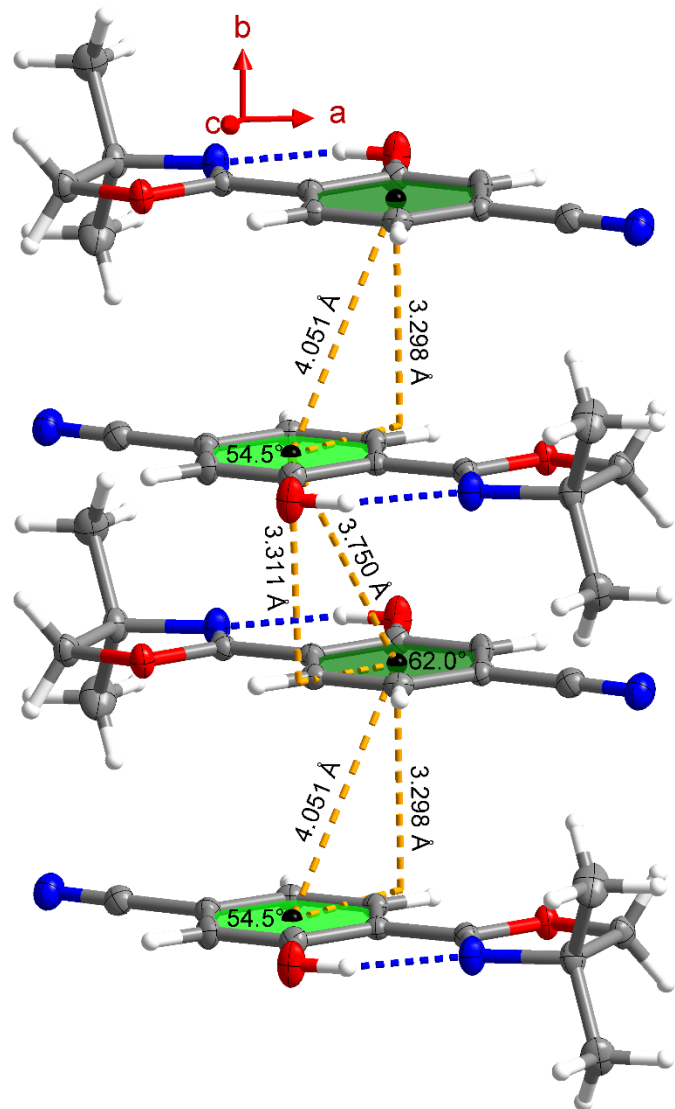


Figure S147: Intermolecular π - π -interactions of four adjacent molecules in **3-CN** crystal lattice with plane distance (orange dashed line) and corresponding centroid-centroid distance (orange dashed line between black spheres). All distances are given in Å.

5 Cartesian Coordinates of Optimized Structures

The data of the respective ketoform are given in xyz format with angstrom [Å] as unit.

1-CN (S_0)

C	-1.60580981911333	1.78334057263818	0.24058775375366
C	-0.29780554351065	1.27662709615545	0.01731797358653
C	-0.02933402029179	-0.07318924437290	0.06330506495191
C	-1.05949319973656	-1.04762651555925	0.34666638942660
C	-2.40833632551339	-0.51320848860947	0.56082215699769
C	-2.64827079378662	0.90245352788091	0.50721678639829
C	-3.42553538223256	-1.48570869926010	0.79639240428142
N	-3.16032983924005	-2.77810331162194	0.89766769608254
C	-4.39368973553942	-3.57965337690371	0.96368400740300
C	-5.41808313596657	-2.43534331000700	1.23048422052718
O	-4.72479345217506	-1.20058071714684	0.90963873459367
O	-0.78640329070850	-2.28908873751367	0.39873802144441
C	-4.64215351115604	-4.28187920128211	-0.38501631255768
C	-4.33632056447837	-4.59009988777091	2.11859681643446
H	-1.80122743890699	2.85626718969176	0.20741300367318
H	0.97664938414157	-0.46491222203259	-0.10667756189557
H	-2.11758537990183	-2.97740317676147	0.69929852952427
H	-5.72060477905211	-2.38001323466460	2.28925824644777
H	-6.31239234700949	-2.48703805470673	0.59368336377754
H	-4.70714879783210	-3.54793898490417	-1.20525955860718
H	-5.58374456305833	-4.85650498457362	-0.35273427464931
H	-3.82121858074661	-4.98148106755699	-0.61305304669936
H	-4.10991258225374	-4.08549019554611	3.07150672363872
H	-3.55632795137336	-5.34693329679325	1.93353973288857
H	-5.30116690576776	-5.11582443699218	2.21781035267429
H	0.51112238587375	1.98295279144804	-0.19372776451526
C	-3.94953925418961	1.47764992968733	0.73807631708608
N	-4.97214057647442	2.01008103707798	0.92070022333254

1-CN (S₁)

C	-1.64297195091764	1.79179924582550	0.11753538754238
C	-0.36902285291827	1.35644462068242	-0.18981463837522
C	-0.01687412681539	-0.01709154325006	-0.06480698773781
C	-0.97506666250807	-0.95123153857835	0.31296108109712
C	-2.34253499767317	-0.54695230410756	0.59266423694944
C	-2.63389558026640	0.86568149977671	0.53551938907038
C	-3.31714532687177	-1.53903740219661	0.86939640279453
N	-3.14320606301836	-2.84294738947958	1.24482736149417
C	-4.39982947319558	-3.59154713366745	1.03138865242024
C	-5.37377839846174	-2.40408703209985	1.22217131195710
O	-4.63014776270737	-1.24588932319961	0.79840463261562
O	-0.69745347171327	-2.23777368264570	0.40656800421888
C	-4.47313771366720	-4.17169633805192	-0.39461930637317
C	-4.57390949023304	-4.67893447962545	2.09765154951398
H	-1.90698718788149	2.84976877930469	0.06668043242228
H	0.98772187234542	-0.36899812770052	-0.30171447723129
H	-2.23969233481759	-3.28319365891924	1.08699007872870
H	-5.65350861085206	-2.27078261591985	2.28209868149199
H	-6.27929109347865	-2.46695062223900	0.60310780729407
H	-4.38797451015393	-3.37287519784610	-1.14987814089791
H	-5.43021171710378	-4.69788535797456	-0.55180095426058
H	-3.65708359490417	-4.89487826360279	-0.56207111447254
H	-4.46583396617349	-4.25738660754726	3.10950639870496
H	-3.82023068237738	-5.47444507788020	1.97093366564472
H	-5.56861576159630	-5.14778885362129	2.01258459315860
H	0.39628511764460	2.06988441683105	-0.50520096186163
C	-3.89314490100655	1.39606933718201	0.94545815712957
N	-4.89405775867734	1.90407865055058	1.27939375696142

2-CN (S₀)

C	-1.70322369660991	1.76645498701144	0.28547567608954
C	-0.36081588514619	1.30171981547153	0.07012879093039
C	-0.04593676701340	-0.03517144359416	0.10427399488755
C	-1.04485001584603	-1.05153817278825	0.36425367204905
C	-2.40680742786231	-0.54455661146631	0.57500867637093
C	-2.70730953503752	0.83679963899501	0.53371958946547
C	-3.41637958139905	-1.52017148316959	0.80741424444209
N	-3.16020320275042	-2.81437076504345	0.89234445928922
C	-4.39745962539907	-3.61027806829385	0.96251858068602
C	-5.40841400249032	-2.46109794136450	1.26225238625269
O	-4.71433326165972	-1.22526266423425	0.94029240464441
O	-0.75529569276635	-2.28481510614943	0.40363758779389
C	-4.67141734045802	-4.28686320223644	-0.39417341815116
C	-4.33351464974839	-4.63941668350886	2.10005332531234
H	0.97733864789442	-0.38084675441084	-0.06146734810221
H	-2.12858576570256	-3.02547030632064	0.69437627213661
H	-5.68766289549303	-2.41728392573618	2.32809982455419
H	-6.31596453794017	-2.50303882145980	0.64369296310939
H	-4.74181196257874	-3.53862670741691	-1.20093439053694
H	-5.61722040410362	-4.85410532881309	-0.35749437133737
H	-3.86024330443501	-4.98949515302544	-0.64610311106535
H	-4.08540999124813	-4.15351703699961	3.05725684343000
H	-3.56629385360009	-5.40251975445116	1.88958903473598
H	-5.30278127983950	-5.15538916416173	2.20619251326183
H	0.42019995631396	2.04208853130905	-0.12515121155667
H	-3.73482968335017	1.16901316959147	0.69904607439583
C	-1.99955466390540	3.16932103068157	0.24317119662356
N	-2.23472477482518	4.31360850758445	0.20895931328870

2-CN (S₁)

C	-1.71665874127175	1.74777919815510	0.18422939715753
C	-0.40472177827795	1.37114061573890	-0.11722293692012
C	-0.00789582620495	0.01918492846998	0.00150623005853
C	-0.92357757721262	-0.96207885975221	0.38655507197612
C	-2.30482977855291	-0.59937093479209	0.65940816553352
C	-2.65201664674098	0.77042489054768	0.58788468679350
C	-3.27485651072219	-1.59227940410509	0.97097275891863
N	-3.11691494336712	-2.92208675319900	1.27674403429541
C	-4.40324262016079	-3.61742882795181	1.04678752773085
C	-5.33736296638015	-2.42543779838522	1.36620292555461
O	-4.58883715449506	-1.25337850603520	0.99444059321615
O	-0.59977483631416	-2.22838966782927	0.50442574981524
C	-4.54236761159863	-4.07635113420154	-0.41824670375354
C	-4.57307187273050	-4.78298244561846	2.02702315162941
H	1.01304002952054	-0.28713179841078	-0.22959780432099
H	-2.24593566504285	-3.36787652378637	0.99493524887868
H	-5.56675573445404	-2.37025262366966	2.44566474595218
H	-6.27215627352514	-2.42939929891858	0.78782977384203
H	-4.45155529961339	-3.22167699207469	-1.10912452241347
H	-5.52132385922368	-4.55679520721128	-0.58702731009145
H	-3.75790310455147	-4.80994918904708	-0.67076603823288
H	-4.41368474473907	-4.44828444230365	3.06425595607932
H	-3.84810748172425	-5.58487097441596	1.80768417114728
H	-5.58369346375258	-5.21695161320034	1.94373194188994
H	0.32826212775843	2.12188954002172	-0.41858244092351
H	-3.66777344843040	1.06377832835745	0.85542475941537
C	-2.11840260691559	3.12338461175906	0.09954515872831
N	-2.45138761127672	4.24056088185839	0.03175070804336

3-CN (S₀)

C	-0.31029340523746	1.38192078019672	-0.07061821608991
C	1.02127672589534	0.88927461173528	-0.26303498185266
C	1.32446346325814	-0.46330287065487	-0.19469803604443
C	0.30522893049765	-1.44821728542526	0.08265133673097
C	-1.04440214705779	-0.91432873166391	0.26855604960239
C	-1.31819689794888	0.47842512684293	0.18958496484099
C	-2.06647093741635	-1.87393441468753	0.51088848001197
N	-1.81899959499414	-3.16715498455376	0.62744510934876
C	-3.06401292880945	-3.95136421333798	0.69004332842298
C	-4.07105926352706	-2.79054942486714	0.95582241316743
O	-3.36537170217658	-1.56563901467985	0.61815281007318
O	0.58007608349003	-2.68850756709918	0.15428730738600
C	-3.32087257577493	-4.64651913816635	-0.66084095713039
C	-3.02684403543483	-4.96460506122637	1.84292629895082
C	2.07579079541439	1.83573208256831	-0.53696696532745
N	2.92054422465096	2.61024162224008	-0.75677071411273
H	-0.50630894488387	2.45312048348340	-0.13213013370959
H	2.34429466322565	-0.82279597285408	-0.34505732168515
H	-2.34426029662337	0.82435842420845	0.33966011493660
H	-0.77444781621635	-3.37695469218736	0.44090011853278
H	-4.36195457521990	-2.72530609210193	2.01762743761823
H	-4.97209165939925	-2.83912873870773	0.32811619384070
H	-3.37485646610809	-3.90990292583643	-1.47949243999114
H	-4.26987536089034	-5.20887204072291	-0.63086859171115
H	-2.50896396591759	-5.35610446864383	-0.88972279033971
H	-2.79205909819147	-4.46669227439460	2.79729352759167
H	-2.26049927168363	-5.73479577852184	1.65669988876748
H	-4.00089894292080	-5.47344744094223	1.93950676817136

3-CN (S₁)

C	-0.34935366175476	1.34400471699498	-0.18544541962005
C	0.99401901739145	0.96634276614199	-0.38443677111932
C	1.39348801822688	-0.39484215040676	-0.18752128525696
C	0.46044663356133	-1.35086516712617	0.17814708137565
C	-0.93632376455439	-0.98456589693183	0.35016711160264
C	-1.28690518345393	0.39279479410891	0.18059372874144
C	-1.91617323698258	-1.95607624684861	0.64684608175055
N	-1.77942822399043	-3.28489010621896	0.93949373709694
C	-3.07568333900717	-3.96889061077930	0.75375565392178
C	-3.98965854014604	-2.75821900703498	1.05992214438849
O	-3.22275739978782	-1.60318122231230	0.66778071658296
O	0.76516539202646	-2.62021245346550	0.38509449776210
C	-3.24394012525542	-4.46344571771179	-0.69662562371114
C	-3.24270771579288	-5.10772508285140	1.76592199585226
C	1.96529188660972	1.93561350720134	-0.76598513180346
N	2.76384414806751	2.73318899542145	-1.08008694573240
H	-0.64420017665942	2.38687829588595	-0.31746197852778
H	2.43191460419027	-0.69333821629524	-0.33009087529512
H	-2.32766850170728	0.67557205859929	0.34667531668496
H	-0.90991344171810	-3.74671599059095	0.68339880798924
H	-4.21277598344114	-2.68133928667174	2.13899855369824
H	-4.92623434627729	-2.75370868480394	0.48487592056163
H	-3.15974132487887	-3.62766855283598	-1.41106668551192
H	-4.22899178485449	-4.94097343920123	-0.83455315550772
H	-2.46927021889470	-5.20888388296346	-0.94416493447316
H	-3.06282795699905	-4.74964815652491	2.79192126163031
H	-2.53104579974173	-5.92346173806454	1.55478076893510
H	-4.25963397417609	-5.53079352471428	1.70902642798473

4-CN (S₀)

C	-1.72352664121995	2.26023318083029	0.20569286841697
C	-0.40215877478765	1.79923719057867	-0.01033083673392
C	-0.07787953969522	0.44520244393071	0.02371036599252
C	-1.08900273054456	-0.57199256606294	0.29329874158125
C	-2.44177127072120	-0.04709400148082	0.50430758486448
C	-2.72780698515754	1.34170153819758	0.45807976510895
C	-3.45696797772732	-1.01440238820442	0.74142230702523
N	-3.21760952056676	-2.31239328854626	0.83255611054362
C	-4.46373645416511	-3.09359537814614	0.90120560059441
C	-5.45875292418579	-1.93262617252624	1.20529529478737
O	-4.75316381403688	-0.70593731270230	0.87436860315646
O	-0.80751767168724	-1.80319673302050	0.33658572879169
C	-4.74733617615280	-3.76234675506177	-0.45752849703533
C	-4.41105348852203	-4.12737463263418	2.03504644256792
H	-2.19439694606688	-2.54296669691348	0.63417201141857
H	-5.72888788058533	-1.88352726912735	2.27340799588603
H	-6.37164910233835	-1.96630109373574	0.59409289435478
H	-4.81124087360129	-3.01049770005653	-1.26149090852998
H	-5.69883981996352	-4.32002107946963	-0.42109233405233
H	-3.94378021936116	-4.47215212453381	-0.71354556684976
H	-4.15587796402692	-3.64799909696388	2.99367427890633
H	-3.65294532405838	-4.89846012927399	1.82089166238251
H	-5.38609662939707	-4.63254248476478	2.14025039377031
H	0.39483326162882	2.52110394553197	-0.21104603321884
H	-3.75621612376648	1.67294738592137	0.62659821776034
H	-1.94001890086923	3.32974554556015	0.17158533298634
C	1.27324758612825	0.01865022955475	-0.20577217796455
N	2.38051626644764	-0.29825088788067	-0.39858430651136

4-CN (S₁)

C	-1.60645413682175	1.73100220520470	0.27764668097066
C	-0.33390016543774	1.33921879359445	-0.08867974462280
C	0.04907410519703	-0.04571253436308	0.01002129607778
C	-0.87510490968567	-1.02088850040995	0.42949229216804
C	-2.23780728042005	-0.60970249856611	0.74300943796462
C	-2.54211562253920	0.76930103631314	0.71982794119389
C	-3.21770351544226	-1.59650077578516	1.05469556433654
N	-3.05405138780022	-2.91406824153781	1.38307350428617
C	-4.31165273328812	-3.63834276185372	1.08651292587291
C	-5.28512885479571	-2.45973941131294	1.33175811921838
O	-4.53277100199543	-1.27340830727634	1.00578196808968
O	-0.57471817234880	-2.28184003768580	0.53811959587689
C	-4.34943051984795	-4.12042384136263	-0.37701242918066
C	-4.51875807428966	-4.79370790433836	2.07181594085925
H	-2.14843981902076	-3.33157156414276	1.16261700281318
H	-5.59059295570897	-2.40020559602089	2.39179163246740
H	-6.17623169310953	-2.48288133113228	0.68857584888190
H	-4.22592346368392	-3.27495226370121	-1.07408097494757
H	-5.30876289566752	-4.61814326339947	-0.60009034804498
H	-3.53957383767604	-4.84488512561037	-0.56729229485040
H	-4.42684660168577	-4.44295497483056	3.11194105621846
H	-3.76814819751201	-5.58482993703598	1.90660935874837
H	-5.51506933216393	-5.24699297259299	1.93528387141929
H	0.41787041506911	2.05902958190241	-0.41720377980861
H	-3.52930732800881	1.08129177420266	1.06682876720961
H	-1.89052094756953	2.78536015637630	0.24605678093442
C	1.35962082714509	-0.46022856657813	-0.38015895273223
N	2.43819613510818	-0.77680850205709	-0.70134410942021

6 NBO Analysis

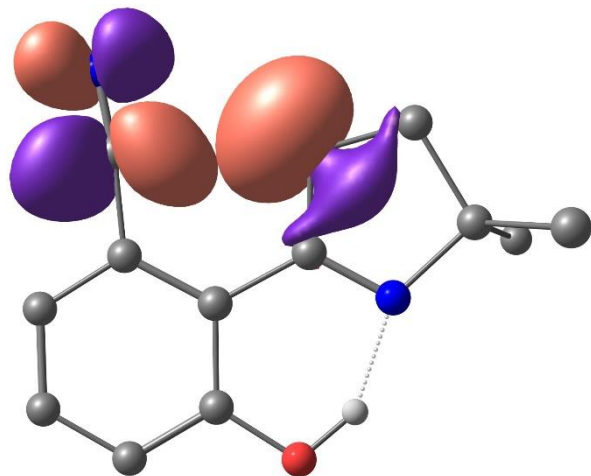


Figure S148: Visualized adjacent orbital interaction of the nonbonding orbital of oxazoline-oxygen and a π^* -orbital of the nitrile bond, which results in the bent nitrile bond of **1-CN**. The structure was optimized using B97/aug-cc-pVDZ level of theory and the RIJCOSX approximation with Gridx6 settings.

7 TGA and DSC

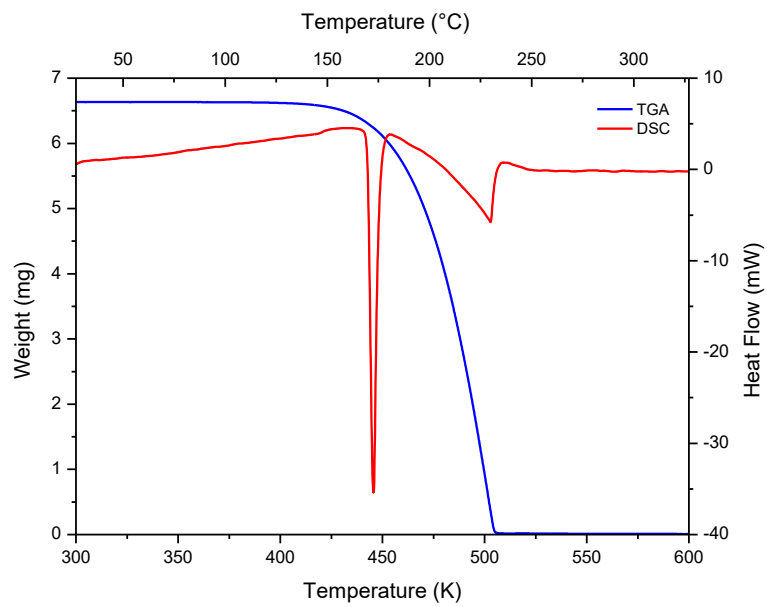


Figure S149: TGA (blue line) and DSC (red line) curve for **1-CN** (6.633 mg) at heating rate 10 K/min. For TGA curve, the onset is determined to 199 °C (472 K) and the endset to 233 °C (506 K). For DSC curve, the melting temperature (T_M) is proved to 172.4 °C and the decomposition temperature (T_{decomp}) is determined to 229.5 °C.

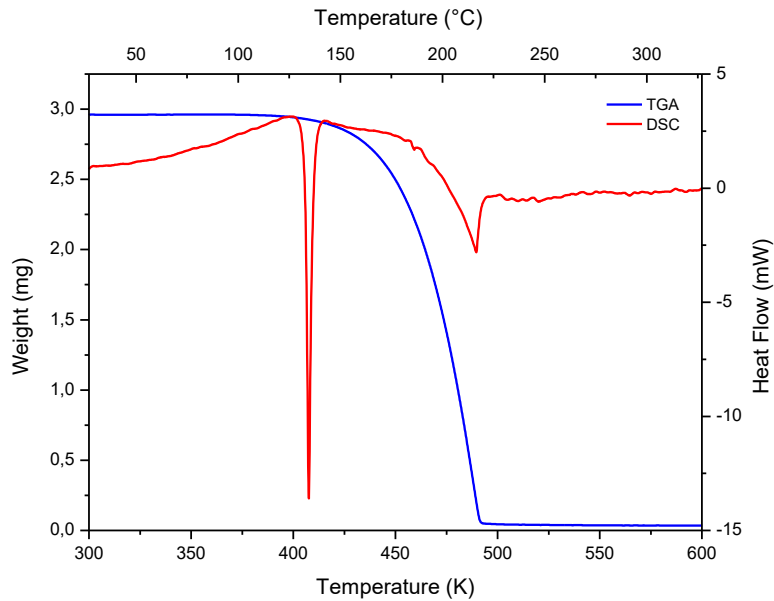


Figure S150: TGA (blue line) and DSC (red line) curve for **2-CN** (2.960 mg) at heating rate 10 K/min. For TGA curve, the onset is determined to 188 °C (461 K) and the endset to 220 °C (493 K). For DSC curve, the melting temperature (T_M) is proved to 134.5 °C and the decomposition temperature (T_{decomp}) is determined to 216.5 °C.

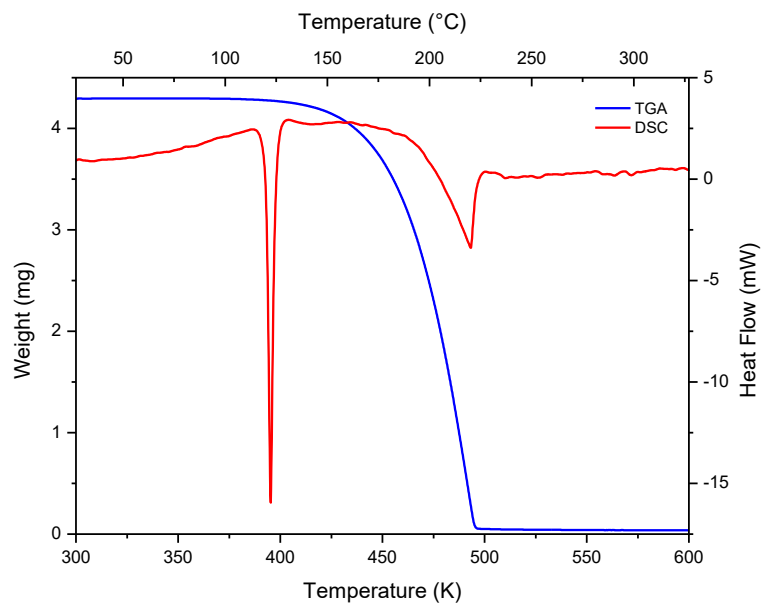


Figure S151: TGA (blue line) and DSC (red line) curve for **3-CN** (4.291 mg) at heating rate 10 K/min. For TGA curve, the onset is determined to 190 °C (463 K) and the endset to 224 °C (497 K). For DSC curve, the melting temperature (T_M) is proved to 122.2 °C and the decomposition temperature (T_{decomp}) is determined to 219.9 °C.

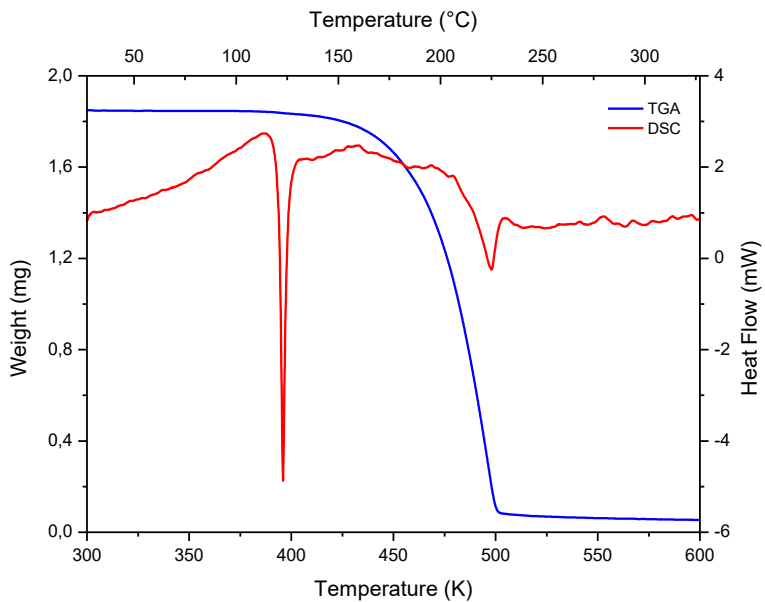


Figure S152: TGA (blue line) and DSC (red line) curve for **4-CN** (1.852 mg) at heating rate 10 K/min. For TGA curve, the onset is determined to 198 °C (471 K) and the endset to 229 °C (502 K). For DSC curve, the melting temperature (T_M) is proved to 122.8 °C and the decomposition temperature (T_{decomp}) is determined to 224.8 °C.

8 References

- 1 W. L. F. Armarego and C. L. L. Chai, *Purification of Laboratory Chemicals*, Elsevier/BH, Oxford, 6th edn., 2009.
- 2 a) O. V. Dolomanov, L. J. Bourhis, R. J. Gildea, J. A. K. Howard and H. Puschmann, *J. Appl. Cryst.*, 2009, **42**, 339; b) G. M. Sheldrick, *Acta Cryst. A*, 2008, **64**, 112;
- 3 F. Neese, *WIREs Comput. Mol. Sci.*, 2012, **2**, 73.
- 4 a) P. Hohenberg and W. Kohn, *Phys. Rev.*, 1964, **136**, B864-B871; b) W. Kohn and L. J. Sham, *Phys. Rev.*, 1965, **140**, A1133-A1138;
- 5 A. D. Becke, *J. Chem. Phys.*, 1997, **107**, 8554.
- 6 T. H. Dunning, *J. Chem. Phys.*, 1989, **90**, 1007.
- 7 R. Bauernschmitt and R. Ahlrichs, *Chem. Phys. Lett.*, 1996, **256**, 454.
- 8 F. Neese, F. Wennmohs, A. Hansen and U. Becker, *Chem. Phys.*, 2009, **356**, 98.
- 9 R. L. Martin, *J. Chem. Phys.*, 2003, **118**, 4775.
- 10 W. Humphrey, A. Dalke and K. Schulten, *J. Mol. Graphics*, 1996, **14**, 33.
- 11 A. Krasovskiy and P. Knochel, *Angew. Chem. Int. Ed.*, 2004, **43**, 3333.
- 12 F. Bodroux, *C. R. Chim.*, 1902, **135**, 1350.
- 13 A. Krasovskiy, V. Krasovskaya and P. Knochel, *Angew. Chem. Int. Ed.*, 2006, **45**, 2958.
- 14 L. P. Hammett, G. H. Walden and S. M. Edmonds, *J. Am. Chem. Soc.*, 1934, **56**, 1092.
- 15 K. Schwekendiek and F. Glorius, *Synthesis*, 2006, **2006**, 2996.
- 16 L. A. Bozzini, J. H.C. Batista, M. B.M. de Mello, R. Vessecchi and G. C. Clososki, *Tetrahedron Lett.*, 2017, **58**, 4186.
- 17 D. Haas, M. S. Hofmayer, T. Bresser and P. Knochel, *Chem. Commun.*, 2015, **51**, 6415.
- 18 D. Göbel, N. Clamor, E. Lork and B. J. Nachtsheim, *Org. Lett.*, 2019, **21**, 5373.

9 NMR-Spectra

